AD

USAAMRDL TECHNICAL REPORT 72-6

INVESTIGATION OF GEARBOX DESIGN MODIFICATIONS FOR REDUCING HELICOPTER GEARBOX NOISE

By

Robert H. Badgley
Thomas Chiang

March 1972

EUSTIS DIRECTORATE
U. S. ARMY AIR MOBILITY RESEARCH AND DEVELOPMENT LABORATORY
FORT EUSTIS, VIRGINIA

CONTRACT DAAJ02-70-C-0035
MECHANICAL TECHNOLOGY INCORPORATED
LATHAM, NEW YORK

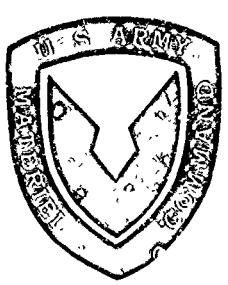

DISCLAIMERS

The findings in this report are not to be construed as an official Department of the Army position unless so designated by other authorized documents.

When Government drawings, specifications, or other data are used for any purpose other than in connection with a definitely related Government procurement operation, the United States Government thereby incurs no responsibility nor any obligation whatsoever; and the fact that the Government may have formulated, furnished, or in any way supplied the said drawings, specifications, or other data is not to be regarded by implication or otherwise as in any manner licensing the holder or any other person or corporation, or conveying any rights or permission, to manufacture, use, or sell any patented invention that may in any way be related thereto.

Trade names cited in this report do not constitute an official endorsement or approval of the use of such commercial hardware or software.

DISPOSITION INSTRUCTIONS

Destroy this report when no longer needed. Do not return it to the originator.

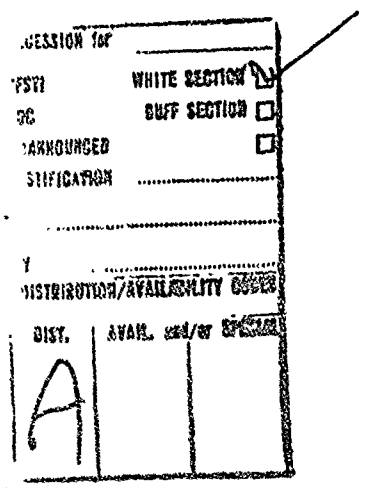

DEPARTMENT OF THE ARMY
U. S. ARMY AIR MOBILITY RESEARCH & DEVELOPMENT LABORATORY
EUSTIS DIRECTORATE
FORT EUSTIS, VIRGINIA 23604

This report presents a part of a continuing effort to understand and ultimately control the noise produced by helicopter power trains. The objective of this effort was directed toward the investigation of the dynamic behavior of the rotating components within the transmission and the manner in which the housing interacts with them.

This program is an extension of the work presented in USAAVLABS Technical Reports 68-41 and 70-12.

This Directorate concurs in the conclusions made by the contractor.

The technical monitor for this contract was Mr. E. R. Givens, Propulsion Division.

UNCLASSIFIED

Security Classification

DOCUMENT CONTROL DATA - R & D

(Security classification of title, body of abstract and indexing annotation must be entered when the overall report is classified)

1 ORIGINATING ACTIVITY *(Corporate author)*

Mechanical Technology Incorporated
Latham, New York

2a. REPORT SECURITY CLASSIFICATION

Unclassified

2b. GROUP

None

3. REPORT TITLE

INVESTIGATION OF GEARBOX DESIGN MODIFICATIONS FOR REDUCING HELICOPTER GEARBOX NOISE

4. DESCRIPTIVE NOTES *(Type of report and inclusive dates)*

Final Technical Report

5. AUTHOR(S) *(First name, middle initial, last name)*

Robert H. Badgley
Thomas Chiang

6 REPORT DATE	7a. TOTAL NO. OF PAGES	7b. NO. OF REFS
March 1972	170	7

8a. CONTRACT OR GRANT NO.	9a. ORIGINATOR'S REPORT NUMBER(S)
DAAJ02-70-C-0035	USAAMRDL Technical Report 72-6
b. PROJECT NO.	
c. Task 1G162207AA7201	9b. OTHER REPORT NO(S) *(Any other numbers that may be assigned this report)*
d.	MTI Report 71TR50

10 DISTRIBUTION STATEMENT

Approved for public release; distribution unlimited.

11 SUPPLEMENTARY NOTES	12 SPONSORING MILITARY ACTIVITY
	Eustis Directorate U.S. Army Air Mobility R&D Laboratory Fort Eustis, Virginia

13 ABSTRACT

Results presented were obtained in a continuing effort to control, through development of vibration and accustics technology, noise produced by helicopter geared power trains. The results achieved, while not all inclusive, represent a significant step in understanding the generation of gearbox noise. Efforts undertaken, directed at both the UH-1D main and CH-47 forward rotor-drive gearboxes, included predictions of lateral natural frequency and forced response vibration characteristics of the spiral bevel gear shafts, thin-shell predictions of natural frequency and forced-response vibration characteristics of the planetary ring gear casing, general and analytical modeling of gearbox mounts and adjoining airframe structure, and collection and evaluation of existing helicopter internal noise and vibration data from helicopter manufacturers and users.

This investigation's results demonstrate the strong dependence of major components of internal helicopter noise upon mechanical vibration characteristics of portions of the rotor-drive power train, particularly gear-carrying shafts and structural elements which are near the gears. Gear-mesh frequency vibration calculations have shown both logical reasons why noise is generated by the gearbox and also the effects of typical design changes to achieve lower noise levels.

Representative modifications which appear to have merit with regard to reducing the bevel mesh noise component, include changes to bevel-gear shaft dimensions, bearing stiffnesses, and materials. Stiffening of the ring gear appears to offer some promise for reducing the level of the noise component at the lower planetary mesh frequency.

DD FORM 1 NOV 65 1473

UNCLASSIFIED

Security Classification

14 KEY WORDS	LINK A		LINK B		LINK C	
	ROLE	WT	ROLE	WT	ROLE	WT
Helicopters						
Gearbox Vibration Calculations						
Gearbox Noise Calculations						
Gearbox Modifications						
Gearbox						
Noise						
Vibration						
Structural Vibration Response						
Structural Resonances						
Redesign for Noise Reduction						
Isolation						
Gear						
Torsional Vibrations						
Dynamic Tooth Forces						
Bevel Gearshaft						
Redesign						
Material Modifications						
Vibrations						
Planetary Gearing						
Ring Gear Vibrations						
Ring Gear Redesign						
Noise						
Prediction						
Reduction						
Vibration						
Prediction						
Reduction						
Isolation						

Task 1G162207AA7201
Contract DAAJ02-70-C-0035
USAAMRDL Technical Report 72-6
March 1972

INVESTIGATION OF GEARBOX DESIGN MODIFICATIONS FOR REDUCING HELICOPTER GEARBOX NOISE

MTI Report 71TR50

by

Robert H. Badgley
Thomas Chiang

Prepared by

Mechanical Technology Incorporated
Latham, New York

for the

EUSTIS DIRECTORATE
U.S. ARMY AIR MOBILITY RESEARCH AND DEVELOPMENT LABORATORY
FORT EUSTIS, VIRGINIA

SUMMARY

The results obtained in this investigation demonstrate the strong dependence of major components of internal helicopter noise upon the mechanical vibration characteristics of portions of the rotor-drive power train, particularly main transmission gear-carrying shafts and structural elements which are feasible for the gearbox designer to perform have shown both logical reasons why noise is generated by the gearbox and also the effects of typical design changes which might be considered during the development of future gearboxes in order to help achieve lower noise levels.

Modifications which were considered and which appear to have some merit with regard to reducing the level of the bevel mesh noise component include changes to bevel-gear shaft dimensions, bearing stiffnesses, and materials. Stiffening of the ring gear, the only modification considered for that element, appears to offer some promise for reducing the level of the noise component at the lower planetary mesh frequency. The modifications selected for examination are only representative of many. There are undoubtedly others which will exhibit greater noise reductions. The optimum configuration can only be determined by systematic study, and must ultimately be evaluated by a competent gearbox designer prior to implementation.

This study is part of a continuing effort to control, through the development and application of mechanical vibration and acoustics technology, the noise produced by helicopter geared power trains. While the results achieved by this study are not all inclusive, they represent a significant step forward in understanding the reasons for the generation of gearbox noise. The major aims of this study, which was directed at both the UH-1D main rotor-drive gearbox and the CH-47 forward rotor-drive gearbox, were as follows:

1. Theoretical predictions of lateral natural frequency and forced response vibration characteristics of the gearbox shafts which carry the spiral bevel gears, and the analytical demonstration of possible methods of reducing vibration, and therefore noise levels.

2. Theoretical predictions of natural frequency and forced-response vibration characteristics of the planetary ring-gear portions of the gearbox casings, considering the ring-gear structural supports as thin-shell elements, and the analytical demonstration of possible methods of reducing vibration, and therefore noise levels.

3. General analytical modeling of gearbox mounts and adjoining airframe structure, in sufficient detail that the transmissibility characteristics (with respect to acoustic-frequency vibrations) of various mount configurations might be examined.

4. Collection and evaluation of existing helicopter internal noise and.

vibration data from helicopter manufacturers and users, to improve the usability of a helicopter internal noise data bank. This data bank may be used to determine the precise nature of helicopter internal noise and its sources, and to assess the utility of gearbox modifications for noise reduction.

The objectives of this study have been achieved.

FOREWORD

This report was prepared by Dr. Robert H. Badgley and Dr. Thomas Chiang of Mechanical Technology Incorporated under Contract No. DAAJ02-70-C-0035 (Task 1G162207AA7201). The contract was carried out under the technical cognizance of Mr. E.R. Givens, Eustis Directorate, U.S. Army Air Mobility Research and Development Laboratory, Fort Eustis, Virginia.

Special credit is due to Mr. L. W. Winn of MTI, who performed the rolling element bearing stiffness calculations, and to Mrs. F. Gillham of MTI, who carried out the extensive calculations required for the achievement of the contract objectives.

TABLE OF CONTENTS

	Page
SUMMARY	iii
FOREWORD	v
LIST OF ILLUSTRATIONS	ix
LIST OF TABLES	xiii
INTRODUCTION	1
DESCRIPTION OF PROGRAM	3
Task I - Acoustic-Frequency Vibration Analysis of Bevel Gear Shafts	3
Task II - Acoustic-Frequency Vibration Analysis of Gearbox Ring-Gear Casings	3
Task III - Rotor-Drive Gearbox Mount Studies for Acoustic-Frequency Vibration Isolation	4
Task IV - Collection and Evaluation of Samples of Existing Gearbox Noise and Vibration Data	4
DYNAMIC FORCES IN CH-47 FORWARD ROTOR-DRIVE GEARBOX BEVEL GEAR SHAFT BEARINGS	5
Rolling-Element Bearing Radial Stiffness Calculation	5
Bevel Gear Shaft Lateral Natural Frequencies	6
Lateral Response of Shafts to Gear-Mesh-Induced Tooth Forces	10
Shaft-Bearing Modifications for Vibration and Noise Reduction	13
DYNAMIC FORCES IN UH-1D MAIN ROTOR-DRIVE GEARBOX BEVEL GEAR SHAFT BEARINGS	37
Rolling-Element Bearing Radial Stiffness Calculation	37
Bevel Gear Shaft Lateral Natural Frequencies	38
Lateral Response of Shafts to Gear-Mesh-Induced Tooth Forces	42
Shaft-Bearing Modifications for Vibration and Noise Reduction	45
DYNAMIC BEHAVIOR OF CH-47 FORWARD ROTOR-DRIVE GEARBOX RING-GEAR STRUCTURAL COMPONENTS	67
Introduction	67
Natural Frequencies of CH-47 Ring-Gear Casing	67
Dynamic Response of CH-47 Ring-Gear Casing	70

Page

Modification of CH-47 Ring-Gear Casing for Vibration and Noise Reduction 72

DYNAMIC BEHAVIOR OF UH-1D ROTOR-DRIVE GEARBOX RING-GEAR STRUCTURAL COMPONENTS. 93

Natural Frequencies of UH-1D Ring-Gear Casing 93
Dynamic Response of UH-1D Ring-Gear Casing. 95
Modifications of UH-1D Ring-Gear Casing for Vibration and Noise Reduction 101

VIBRATION ISOLATION ANALYSIS OF GEARBOX MOUNT COMPONENTS 119

DISCUSSION OF RESULTS. 125

CONCLUSIONS AND RECOMMENDATIONS. 132

LITERATURE CITED 134

APPENDIXES

I. DYNAMIC RESPONSE CALCULATIONS OF THE UH-1D MAIN ROTOR-DRIVE GEARBOX RING-GEAR CASING. 135

II. DYNAMIC RESPONSE CALCULATIONS OF THE CH-47 FORWARD ROTOR-DRIVE GEARBOX RING-GEAR CASING. 142

III. ACOUSTIC POWER GENERATED BY A VIBRATING SURFACE 148

IV. SUMMARY OF EXISTING HELICOPTER INTERNAL ACOUSTIC DATA. 151

DISTRIBUTION 157

LIST OF ILLUSTRATIONS

Figure		Page
1	CH-47 Forward Rotor-Drive Gearbox Bevel Gear Shaft-Bearing System	20
2	CH-47 Input Bevel Gear Shaft Dynamic Modeling Details	21
3	CH-47 Output Bevel Gear Shaft Dynamic Modeling Details	22
4	Critical Frequency Map for CH-47 Forward Rotor Gearbox Input Bevel Gear Shaft	23
5	Critical Frequency Map for CH-47 Forward Rotor Gearbox Output Bevel Gear Shaft	24
6	Calculated Vibration Amplitudes for CH-47 Nominal Configuration Input Bevel Gear Shaft	25
7	Calculated Vibration Amplitudes for CH-47 Nominal Configuration Output Bevel Gear Shaft	26
8	Calculated Dynamic Force Levels at Indicated Bearings With Constant Value Gear-Tooth Exciting Force for CH-47 Input Bevel Gear Shaft	27
9	Calculated Dynamic Force Levels at Indicated Bearings With Constant Value Gear-Tooth Exciting Force for CH-47 Output Bevel Gear Shaft	28
10	CH-47 Input Bevel Gear Shaft Vibration Amplitudes for Nominal and Modified Configurations	29
11	CH-47 Input Bevel Gear Shaft Vibration Amplitudes for Nominal and Modified Configurations	30
12	CH-47 Input Bevel Gear Shaft Vibration Amplitudes for Nominal and Modified Configurations	31
13	CH-47 Output Bevel Gear Shaft Vibration Amplitudes for Nominal and Modified Configurations	32
14	CH-47 Output Bevel Gear Shaft Vibration Amplitudes for Nominal and Modified Configurations	33
15	Effect of Bearing Stiffness Variations on Bearing Dynamic Forces for CH-47 Forward-Rotor-Drive Gearbox Input Bevel Gear Shaft - Stiffnesses Varied in Proportion to Each Other	34

Figure		Page
16	Calculated Dynamic Force Level With Stiffness Reduced by 50 Percent at Bearings No. 2 and 3 and Constant Value Gear-Tooth Exciting Force for CH-47 Input Bevel Gear Shaft	35
17	Calculated Dynamic Force Level at Indicated Bearings (Bearings No. 2 and 3 Removed) With Constant Value Gear-Tooth Exciting Force for CH-47 Input Bevel Gear Shaft . . .	36
18	UH-1D Input Bevel Gear Shaft Dynamic Modeling Details . . .	51
19	UH-1D Output Bevel Gear Shaft Dynamic Modeling Details . .	52
20	Critical Frequency Map for UH-1D Main Rotor Gearbox Input Bevel Gear Shaft	53
21	Critical Frequency Map for UH-1D Main Rotor Gearbox Output Bevel Gear Shaft	54
22	Calculated Vibration Amplitudes for UH-1D Input Bevel Gear Shaft - Nominal Configuration	55
23	Calculated Vibration Amplitudes for UH-1D Output Bevel Gear Shaft - Nominal Configuration	56
24	Calculated Dynamic Force Levels at Indicated Bearings With Constant Value Gear-Tooth Exciting Force for UH-1D Input Bevel Gear Shaft	57
25	Calculated Dynamic Force Levels at Indicated Bearings With Constant Value Gear-Tooth Exciting Force for UH-1D Output Bevel Gear Shaft	58
26	Calculated Vibration Amplitudes for UH-1D Input Bevel Gear Shaft for Nominal and Modified Configurations	59
27	Calculated Vibration Amplitudes for UH-1D Output Bevel Gear Shaft for Nominal and Modified Configurations	60
28	Calculated Vibration Amplitudes for UH-1D Output Bevel Gear Shaft for Nominal and Modified Configurations	61
29	Effect of Bearing Stiffness Variations on Bearing Dynamic Forces for UH-1D Rotor-Drive Gearbox Input Bevel Gear Shaft-Stiffnesses Varied in Proportion to Each Other	62
30	Calculated Vibration Amplitudes for UH-1D Input Bevel Gear Shaft for Nominal and Modified Bearing Stiffnesses . . .	63

Figure		Page
31	Calculated Vibration Amplitudes for UH-1D Output Bevel Gear Shaft for Nominal (Steel) and Titanium (C 130 AM) Configurations	64
32	Calculated Vibration Amplitudes for UH-1D Output Bevel Gear Shaft for Nominal and Modified Configurations	65
33	Calculated Vibration Amplitudes for UH-1D Input Bevel Gear Shaft for Nominal Configuration and With Damping	66
34	Model for CH-47 Ring-Gear-Casing Dynamic Analysis	83
35	Illustration of n=2 Circumferential Mode Shape	84
36	Illustration of CH-47 Ring-Gear-Casing Axial Mode Shapes	85
37	Frequency Diagram for CH-47 Ring-Gear Casing With Edges Simply Supported	86
38	CH-47 Frequency Diagram Illustrating the Effects of End Conditions on Ring-Gear-Casing Natural Frequencies for First Axial Mode Vibrations	87
39	Normal Displacement of CH-47 Ring-Gear Casing due to Lower Planetary Gear Forces at Mesh Frequency	88
40	CH-47 Ring-Gear-Casing Nominal Configuration	89
41	CH-47 Ring-Gear-Casing Modified Configuration	90
42	CH-47 Ring-Gear-Casing Vibration Amplitudes due to Forces From One Lower Planetary Gear at Mesh Frequency	91
43	Normal Displacement of CH-47 Modified Ring-Gear Casing due to Lower Planetary Gear Forces at Mesh Frequency	92
44	Model for UH-1D Ring-Gear-Casing Dynamic Analysis	108
45	Illustration of UH-1D Ring-Gear-Casing Axial Mode Shapes	109
46	Frequency Diagram for UH-1D Ring-Gear Casing With Edges Simply Supported	110
47	UH-1D Frequency Diagram Illustrating the Effects of End Conditions on Ring-Gear-Casing Natural Frequencies for First Axial Mode Vibrations	111
48	Normal Displacement of UH-1D Ring-Gear Casing due to Lower Planetary Gear Forces at Mesh Frequency	112

Figure		Page
49	UH-1D Ring-Gear-Casing Nominal Configuration	113
50	UH-1D Ring-Gear Casing With Center Section Modification . .	114
51	UH-1D Ring-Gear Casing With End Section Modifications . . .	115
52	UH-1D Ring-Gear Casing With Center and End Section Modifications	116
53	UH-1D Ring-Gear-Casing Vibration Amplitudes due to Forces From One Lower Planetary Gear at Mesh Frequency	117
54	Normal Displacement of UH-1D Ring-Gear Casing due to Lower Planetary Gear Forces at Mesh Frequency	118
55	Analytical Model for Analysis and Design of Gearbox-to-Airframe Isolators	120
56	Schematic Diagram and Coordinate System for the UH-1D Lower Planetary Gears	136
57	CH-47 Lower Planetary Gear Mesh Phasing Diagram	143
58	CH-47 Lower Planetary Gear Mesh Phasing Diagram Showing Gear-Tooth Positions	144
59	Measured Acoustic Spectrum Between Pilots in CH-47C Helicopter at Hover Condition With 235 RPM Rotor Speed (Courtesy Mr. R.T. Camp, Jr., U.S. Army Aeromedical Research Laboratory - Ref. 4).	153
60	Measured Acoustic Spectrum at Station 95 in CH-47C Helicopter at Hover Condition With 235 RPM Rotor Speed (Courtesy Mr. R.T. Camp, Jr., U.S. Army Aeromedical Research Laboratory - Ref. 4).	154
61	Measured Acoustic Spectrum at Station 320 in CH-47C Helicopter at Hover Condition With 235 RPM Rotor Speed (Courtesy Mr. R.T. Camp, Jr., U.S. Army Aeromedical Research Laboratory - Ref. 4).	155
62	Measured Acoustic Spectrum at Station 482 in CH-47C Helicopter at Hover Condition With 235 RPM Rotor Speed (Courtesy Mr. R.T. Camp, Jr., U.S. Army Aeromedical Research Laboratory - Ref. 4).	156

LIST OF TABLES

Table		Page
I	CH-47 Forward Rotor-Drive Gearbox Input Bevel Gear Shaft Dimensions and Properties Used in Dynamics Calculations. . . .	7
II	CH-47 Forward Rotor-Drive Gearbox Output Bevel Gear Shaft Dimensions and Properties Used in Dynamics Calculations. . . .	8
III	Summary of Results of Shaft-Bearing System Modifications for Reduction of Bevel Gear Mesh-Frequency Noise Component for CH-47 Main Rotor-Drive Gearbox	19
IV	UH-1D Main Rotor-Drive Gearbox Input Bevel Gear Shaft Dimensions and Properties Used in Dynamics Calculations. . . .	39
V	UH-1D Main Rotor-Drive Gearbox Output Bevel Gear Shaft Dimensions and Properties Used in Dynamics Calculations. . . .	40
VI	Summary of Results of Shaft-Bearing System Modifications for Reduction of Bevel Gear Mesh Frequency Noise Component for UH-1D Main Rotor-Drive Gearbox	50
VII	Natural Frequencies of CH-47 Ring-Gear Casing.	69
VIII	Amplitude of Normal Displacement W (10^{-6} inches) due to Lower Planetary Dynamic Forces at Fundamental Frequency, CH-47 Ring-Gear Casing	73
IX	Temporal Phase Angle of Normal Displacement φ (degrees) due to Lower Planetary Dynamic Forces at Fundamental Frequency, CH-47 Ring-Gear Casing	75
X	Amplitude of Normal Displacement W (10^{-6} inches) due to Lower Planetary Dynamic Forces at Fundamental Frequency, CH-47 Modified Ring-Gear Casing.	79
XI	Temporal Phase Angle of Normal Displacement φ (degrees) due to Lower Planetary Dynamic Forces at Fundamental Frequency, CH-47 Modified Ring-Gear Casing	81
XII	Natural Frequencies (in Hz) of UH-1D Ring-Gear Casing.	94
XIII	Amplitude of Normal Displacement W (10^{-6} inches) due to Lower Planetary Dynamic Forces at Fundamental Frequency, UH-1D Ring-Gear Casing	97
XIV	Temporal Phase Angle of Normal Displacement φ (degrees) due to Lower Planetary Dynamic Forces at Fundamental Frequency, UH-1D Ring-Gear Casing.	99

Table		Page
XV	Amplitude of Normal Displacement W (10^{-6} inches) due to Lower Planetary Dynamic Forces at Fundamental Frequency, UH-1D Modified Ring-Gear Casing	103
XVI	Temporal Phase Angle of Normal Displacement φ (degrees) due to Lower Planetary Dynamic Forces at Fundamental Frequency, UH-1D Modified Ring Gear-Casing.	105

INTRODUCTION

Helicopter internal noise is increasingly being recognized as one of the major problems which must be overcome if helicopters are to be a safe and comfortable mode of transportation in the future. Internal noise has often been considered inherent to the helicopter, primarily because of the weight penalty associated with the use of insulation and blanketing, together with limitations on the lift which can be achieved with this type of aircraft.

Internal noise levels have apparently not always been considered to bear strongly upon helicopter crew and passenger safety. There is increasing concern, however, for the legal aspects of hearing damage to both passengers and crew in military helicopters. There are also apparently some indications that certain noise components produced by the CH-47 rotor-drive gearbox may be interfering significantly with internal communications within operating CH-47 aircraft. Crew helmets do not and cannot alleviate this problem, since the noise impinges upon the microphones, as do the spoken words of the crew. Noise fatigue of both passengers and crew is undoubtedly another important element for consideration.

The continuing trends to higher and higher power levels, and the ever-present lift-to-weight ratio requirements, result in both higher drive-train mechanical force levels and higher mechanical vibration levels. Since one of the most important by-products of acoustic-frequency mechanical vibration is noise, noise levels can be expected to increase drastically as well. The inability of the aircraft designer to assign weight allowances to sound-absorption devices or materials means that the gearbox designer is faced with the problem of reducing or limiting internal noise levels during the design of the power train components, utilizing methods which incorporate new criteria.

The requirement to reduce noise levels in existing helicopters, wherever possible, and to achieve quieter future helicopters through design-level efforts has been recognized by the U.S. Army. Consequently, the Eustis Directorate, U.S. Army Air Mobility Research and Development Laboratory, Fort Eustis, Virginia (formerly the U.S. Army Aviation Materiel Laboratories) has embarked upon a program to understand the sources of internal helicopter noise, to modify existing hardware to reduce the noise levels emitted by these sources, and to transmit the information learned by these investigations to helicopter manufacturers for incorporation into the design process.

Rotor-drive gearboxes have long been recognized as one of the major sources, and perhaps the prime source, of the noise which is found in operational helicopters. Even before the use of sophisticated measuring equipment, the layman's ear could distinguish the gearbox as the probable source of the noise levels being experienced. During the past decade, better sound-recording apparatus, together with full-octave and one-third-octave analysis techniques, has enabled the internal sound spectrum to be studied in more detail. The results of these studies showed that in larger helicopters, such as the CH-47, the internal noise levels were due

primarily to very high narrow-band signals which were located in the frequency bands which contained the mesh frequencies of some of the speed reduction gears [1]*, [2], [3]. More recently, narrow-band analyses of similar recordings [4] have shown that these noise spikes are located precisely at several of the gear mesh frequencies. In smaller helicopters, such as the UH-1D, the studies indicated that accessory systems, such as hydraulic pumps and oil cooler fans, were in several cases of equal importance to the gearbox as sources of noise.

As a result of the information uncovered by the full-octave and one-third-octave analyses, which identified the gears as the probable prime sources of noise, an analytical effort was undertaken to formulate equations which would describe the type and amount of disturbance [1] introduced into the drive train, at the mesh frequency and its higher multiples, as a result of the normal meshing action of the gears. At the same time, an effort was undertaken to develop a torsional response analysis which could predict the dynamic gear tooth forces in the drive train under the forcing action of the gear mesh disturbances. These analyses, together with an empirical method for computing noise levels based on their results [1], [2], yielded encouraging results which formed the basis of the current study.

The production of certain components of noise by a power train gearbox requires the vibration of portions of the gearbox casing or of the supporting structure (which depends upon the transmissibility of the mounts), or both. These vibrations may be caused by the application of dynamic forces to the casing at the gear mesh frequencies (or their multiples). This condition exists in the usual rotor-drive gearbox design, in which an input shaft, usually mounted on three or four rolling-element bearings, supports a single bevel gear. While the drive force acting on the gear mesh frequency (or a multiple thereof) because of the torsional vibrations of the drive train, which are caused by the characteristics of the mesh itself. These variations in the rolling-element bearings which support the gear-carrying shaft; hence, the application of dynamic forces to the gearbox casing. A similar situation exists for the output bevel-gear shaft and for the ring-gear portion of the gearbox casing.

While the foregoing helps to explain one gearbox-related mechanism which may produce high internal noise levels, the gearbox designer should also be aware of another phenomenon which may occur. While the lateral natural frequencies of the bevel-gear-carrying shafts are usually far above rotational frequencies, they are often very nearly the same as the mesh frequency or one of its multiples. Thus, the very real possibility exists for forcing one or more of the shafts at a <u>lateral</u> resonance frequency.

*Numbers in brackets refer to literature cited at the end of this report.

DESCRIPTION OF PROGRAM

This study of helicopter power train acoustic-frequency vibrations and resulting noise was conducted in four tasks, the individual efforts of which are summarized below.

In the vibrations analysis of any system, several distinct types of calculations are required for a complete understanding of the behavior of the system. First, the natural frequency (free-vibration) aspects of the problem must be considered, taking into account the actual support masses and stiffnesses. This analysis yields the natural frequencies of the system, together with the vibration mode shapes which may be expected. The analyst learns from these results the frequency ranges upon which he must concentrate during the second portion of the study, which is an investigation of the response of the system to specific forcing functions. From this part of the analysis, information is gained about the vibration amplitudes which may be expected. The third portion of the study is then usually an analysis of the sensitivity of the system to various changes in such parameters as the amplitude or location of the dynamic forces, the bearing stiffnesses, or the dimensions of the shaft.

TASK I — ACOUSTIC-FREQUENCY VIBRATION ANALYSIS OF BEVEL GEAR SHAFTS

As a result of the studies in [1] and [2], dynamic forces acting at the various gear meshes were available. Following rolling-element bearing stiffness calculations, gear lateral vibration natural frequency calculations were undertaken for the input and output bevel gear shafts of the CH-47 and UH-1D rotor-drive gearboxes. Following these studies, calculations were performed to show the response of the shafts, including dynamic bearing forces, to the dynamic forces generated at the gear teeth as a result of the gear-tooth mesh characteristics. Thus, the path for the transmission of acoustic-frequency vibration energy, from its point of origin in the gear mesh to its appearance as mechanical vibrations at the gearbox casing walls, has been rigorously studied by means of digital computer dynamic simulation.

The vibration responses of various modified shaft-bearing systems were calculated to illustrate the utility of several noise and vibration reduction techniques.

TASK II — ACOUSTIC-FREQUENCY VIBRATION ANALYSIS OF GEARBOX RING-GEAR CASINGS

This phase of the report was divided into two parts: the first part was devoted to the UH-1D ring-gear casing, and the second part to the CH-47 ring-gear casing.

For the UH-1D helicopter, the ring-gear casing was modeled for dynamic analysis. The structural natural frequencies of the casing were then determined for various modes of vibration using an existing MTI shell vibration computer

program. The natural frequencies thus obtained were compared with the gear mesh frequencies.

The dynamic tooth forces acting on the ring gear as reported in [1] and [2] were used as input data for the computation of dynamic responses. From the dynamic responses, the acoustic power was calculated, giving an indication of the noise level generated by the casing due to gear-mesh-induced vibrations.

The ring-gear casings were then modified in an effort to reduce the noise and vibration levels. The acoustic power generated by the modified casings was compared with the existing (nominal design) ring-gear casings.

TASK III — ROTOR-DRIVE GEARBOX MOUNT STUDIES FOR ACOUSTIC-FREQUENCY VIBRATION ISOLATION

The dynamic excitations originating at the gear-tooth mesh locations may cause the ring-gear casing to vibrate and thus emit noise. At the same time, however, dynamic forces and vibrational motion are transmitted through the joints to the aircraft structure, inducing vibrational stresses and generating noise. The isolation of the gearbox structure from these vibrations is therefore important from both the stress and noise points of view, although the major concern here is noise.

The possible use of a vibration isolator between the gearbox and the structure was analyzed by using a simple model. Two quantities are known to be significant in determining the effectiveness of vibration isolation: motion transmissibility and force transmissibility. The isolation analysis shows that the two transmissibilities can be expressed in terms of the mechanical impedances of the gearbox mount structure, the isolator and the aircraft structure.

TASK IV — COLLECTION AND EVALUATION OF SAMPLES OF EXISTING GEARBOX NOISE AND VIBRATION DATA

Visits to the U.S. Army Aeromedical Research Laboratory, Fort Rucker, Alabama; Vertol Division - The Boeing Company, Philadelphia, Pennsylvania; The Bell Helicopter Company, Fort Worth, Texas; and the Sikorsky Division of United Aircraft Corporation, Stratford, Connecticut, were undertaken to obtain and evaluate samples of existing helicopter gearbox noise and vibration measurements from the standpoints of completeness and usability in future helicopter internal noise reduction efforts.

DYNAMIC FORCES IN CH-47
FORWARD ROTOR-DRIVE GEARBOX BEVEL GEAR SHAFT BEARINGS

ROLLING-ELEMENT BEARING RADIAL STIFFNESS CALCULATION

The first quantities required for a lateral vibrations analysis are the actual stiffnesses of the elements which support the vibrating system relative to a fixed reference plane. These calculations were undertaken for the bearings supporting both the input and output bevel gear shafts in the CH-47 forward rotor-drive gearbox. For the purposes of the analysis, coordinate axes were assigned as follows:

	x-axis	y-axis	z-axis
Input Shaft	Horizontal (Fore-Aft, Along Shaft) Positive Forward	Vertical (Perp. to Shaft) Positive Down	Horizontal (Perp. to Shaft) Positive to Port Side
Output Shaft	Vertical (Along Shaft) Positive Down	Horizontal (Fore-Aft, Perp. to Shaft) Positive Forward	Horizontal (Perp. to Shaft and y-axis) Positive to Starboard

Simple calculations indicated the gearbox casing rolling-element support structure to be reasonably rigid compared to anticipated bearing radial stiffness values. Consequently, the assumption was made throughout the present studies that bearing support stiffness could be neglected and that the radial stiffness of the bearings was the controlling stiffness. Such an assumption is not always valid, however, and the gearbox designer is cautioned to obtain guidance in this area prior to undertaking calculations of this type. (The opposite is true for turbine engines, for instance, where the bearing supports are usually quite soft compared to the bearings themselves. This is often the case because the internal forces in turbine engines are usually much lower than those in helicopter gearboxes.)

For the analyses, the following aircraft operating parameters were assumed:

Aircraft Flight Condition	Hover
Aircraft Horsepower (Total)	3750
Forward Gearbox Horsepower	1500
Gearbox Input Shaft Speed	7059 rpm
Bevel Gear Tangential Drive Force	3764 lb

Under these operating characteristics, the steady-state forces (sign convention is with respect to the axes previously described) acting on the bevel gears are as follows:

	$F_{s,x}$ (lb)	$F_{s,y}$ (lb)	$F_{s,z}$ (lb)
Input Bevel Gear	-2371	678	3764
Output Bevel Gear	- 903	2296	3764

Utilizing these values, the shaft dimensions and their tolerances, and the ball and roller bearing dimensions and their tolerances, the following radial stiffness values were calculated by means of a computer program developed by Mr. A.B. Jones, Newington, Connecticut, Consultant to MTI, for the bevel gear shaft bearings (bearings are numbered in the direction of power flow, and this numbering will be maintained throughout this study):

Bearing	Shaft	K_y (lb/in. x 10^{-6})	K_z (lb/in. x 10^{-6})
1	Input	1.21	0.72
2	Input	3.42	2.08
3	Input	5.51	4.67
4	Input	3.17	5.91
5	Output	2.91	2.99
6	Output	3.60	3.76
7	Output	3.57	5.98

BEVEL GEAR SHAFT LATERAL NATURAL FREQUENCIES

Vertol assembly drawing 114D1001, Transmission, Mechanical, Forward Rotary Wing Drive, and subordinate drawings were used to model the input and output bevel gear shafts. Figure 1 is a simplified drawing of the components under consideration. Figures 2 and 3 show details of the analytical modeling which was performed for the vibration analysis. Tables I and II present details of the dimensions and other shaft properties used in the analysis.

The first step in a shaft lateral vibrations analysis should be the construction of a natural frequency map [5] on which are plotted the natural frequencies of the shaft-bearing system. Such a map shows the regime in which a particular shaft-bearing arrangement is operating, through comparison of the natural frequencies with each other and with the exciting frequency (in this case the mesh frequency). It also shows the behavior of the natural frequencies with respect to bearing stiffness, a characteristic which will become important during later stages in the analysis in which system property changes are considered.

The map is most efficiently constructed by first assuming equal bearing radial stiffnesses for all the bearings in the system and then superimposing upon the map the actual bearing stiffness vs. speed characteristics. (See Chapter II of Reference 5 for a more detailed discussion of this method of analysis.) Varying assumed bearing stiffness from 10^5 to 10^7 (all bearings assumed equal) yields the natural frequency maps shown in Figures 4 and 5 for the input and output spiral bevel shafts, respectively, for the CH-47 forward gearbox. The vertical lines (bearing stiffness is typically insensitive to vibration frequency changes at constant speed) represent the calculated bearing stiffnesses discussed earlier.

Figure 4 gives the following general information:

TABLE I. CH-47 FORWARD ROTOR-DRIVE GEARBOX INPUT BEVEL GEAR SHAFT DIMENSIONS AND PROPERTIES USED IN DYNAMICS CALCULATIONS

Shaft Station Number	Concentrated Weight (lb)	Conc. Polar Mom. of Inertia (lb-in.^{2})	Conc. Transverse Mom. of Inertia (lb-in.^{2})	Shaft Section Length to Next Station (in.)	Stiffness Outer Diameter (in.)	Mass Outer Diameter (in.)	Stiffness and Mass Inner Diameter (in.)
1	3.0	0.0	0.0	0.45	7.10	4.20	4.20
2	2.2	22.1	14.4	0.35	4.20	2.80	2.80
3	1.1	0.0	0.0	0.35	2.90	2.10	2.10
4	0.0	0.0	0.0	0.70	2.00	2.50	1.15
5	0.0	0.0	0.0	1.00	2.00	2.50	1.15
6	0.0	0.0	0.0	0.70	2.00	2.50	1.15
7	0.0	0.0	0.0	0.20	2.00	2.00	1.15
8	0.0	0.0	0.0	0.80	2.32	2.32	1.15
9	0.0	0.0	0.0	0.15	2.32	2.32	1.40
10	0.0	0.0	0.0	0.35	2.50	2.50	1.60
11	0.0	0.0	0.0	0.40	4.60	4.40	2.10
12	0.0	0.0	0.0	0.40	4.32	4.32	3.75
13	0.0	0.0	0.0	0.70	4.32	4.75	3.75
14	0.0	0.0	0.0	0.70	4.32	4.75	3.75
15	0.0	0.0	0.0	1.00	4.32	4.65	3.90
16	0.0	0.0	0.0	0.60	4.32	4.95	3.90
17	0.0	0.0	0.0	0.70	4.32	4.95	3.90
18	0.0	0.0	0.0	0.60	4.32	5.02	3.90
19	0.0	0.0	0.0	0.60	4.32	5.02	3.90
20	0.0	0.0	0.0	1.00	4.32	4.80	3.90
21	0.0	0.0	0.0	0.70	4.32	5.60	3.90
22	0.0	0.0	0.0	0.70	4.32	5.60	3.90
23	0.0	0.0	0.0	0.45	5.22	5.22	3.94
24	0.0	0.0	0.0	0.40	6.50	6.50	4.20
25	0.0	0.0	0.0	0.75	7.00	7.00	5.20
26	0.0	0.0	0.0	0.50	6.20	6.20	5.25
27	0.0	0.0	0.0	0.80	5.40	5.40	4.50
28	0.0	0.0	0.0	0.00	1.00	0.0	0.0

Young's Modulus: 29×10^6 lb/in.^{2}

Density: 0.281 lb/in.^{3}

Poisson's Ratio: 0.333

TABLE II. CH-47 FORWARD ROTOR-DRIVE GEARBOX OUTPUT BEVEL GEAR SHAFT DIMENSIONS AND PROPERTIES USED IN DYNAMICS CALCULATIONS

Shaft Station Number	Concentrated Weight (lb)	Conc. Polar Mom. of Inertia ($lb\text{-}in.^2$)	Conc. Transverse Mom. of Inertia ($lb\text{-}in.^2$)	Shaft Section Length to Next Station (in.)	Stiffness Outer Diameter (in.)	Mass Outer Diameter (in.)	Stiffness and Mass Inner Diameter (in.)
1	0.0	0.0	0.0	1.77	5.56	5.56	4.22
2	0.0	0.0	0.0	0.30	4.65	4.65	4.22
3	0.0	0.0	0.0	0.38	4.65	4.65	4.22
4	0.0	0.0	0.0	0.38	5.10	5.10	4.65
5	0.0	0.0	0.0	0.38	5.60	5.60	4.80
6	0.0	0.0	0.0	0.45	6.46	6.46	4.90
7	0.0	0.0	0.0	0.45	6.46	4.64	4.90
8	0.0	0.0	0.0	0.43	6.00	6.00	4.90
9	0.0	0.0	0.0	0.43	6.00	6.00	4.90
10	0.0	0.0	0.0	0.16	6.00	8.13	4.05
11	16.1	453.0	227.3	0.16	6.00	8.13	3.97
12	0.0	0.0	0.0	0.88	4.65	4.65	3.62
13	0.0	0.0	0.0	0.88	4.22	4.22	3.23
14	0.0	0.0	0.0	0.88	3.83	3.83	2.95
15	0.0	0.0	0.0	0.88	3.55	3.56	2.70
16	0.0	0.0	0.0	0.65	3.30	3.85	2.25
17	2.1	16.4	8.2	0.78	3.30	3.85	2.25
18	0.0	0.0	0.0	0.47	3.30	3.30	2.25
19	0.0	0.0	0.0	0.47	3.00	3.30	2.25
20	0.0	0.0	0.0	0.47	3.00	3.30	2.25
21	0.0	0.0	0.0	0.86	3.00	3.30	2.48
22	0.0	0.0	0.0	0.86	2.90	3.30	2.48
23	0.0	0.0	0.0	0.0	1.00	0.0	0.0

Young's Modulus: 29×10^6 $lb/in.^2$

Density: 0.281 $lb/in.^3$

Poisson's Ratio: 0.333

1. The input bevel gear shaft is being forced at the bevel mesh frequency only slightly above its third (bending) natural frequency. As the speed of the shaft increases, during run-up, the input bevel gear shaft will probably pass through three natural frequencies of which the first two will be of the rigid-body vibration type. (The first two criticals are very nearly straight lines between stiffnesses of 7×10^5 and 6×10^6 pounds/inch, and thus are almost directly dependent on bearing stiffness, a characteristic of a rigid-body critical.) The vertical axis of the map is vibration frequency, rather than shaft speed. The bearing radial stiffnesses would not, in general, be straight vertical lines on a speed vs. stiffness map.

2. Bearing radial stiffnesses lower than those calculated and shown in Figure 4 will result in a lower value for the third critical frequency (decreases to the left with lower stiffness), and thus a further separation between it and the mesh frequency.

When the above calculations are repeated with the radial bearing stiffness values as calculated (rather than assumed equal) in the vertical and horizontal directions separately, the natural frequencies are as follows:

Radial Stiffnesses	First Critical (cpm (Hz))	Second Critical (cpm (Hz))	Third Critical (cpm (Hz))
Vertical (y-axis)	33,500 (558)	82,100 (1370)	146,300 (2440)
Horizontal (z-axis)	32,000 (533)	93,800 (1565)	137,400 (2290)

Figure 5 gives the following information:

1. The output bevel gear shaft is being forced at the bevel mesh frequency only slightly below its third (bending) natural frequency. As the speed of the shaft increases, it will probably pass through two natural frequencies, of which the first will be a rigid-body vibration type. The discussion for the input shaft applies here as well.

2. Bearing radial stiffnesses lower than those calculated and shown in Figure 5 will result in a lower value for the third critical frequency, and thus less separation between it and the mesh frequency.

When the above calculations are repeated with the radial bearing stiffnesses as calculated (rather than assumed equal) in the vertical and horizontal directions separately, the following natural frequencies are obtained:

Radial Stiffnesses	First Critical (cpm (Hz))	Second Critical (cpm (Hz))	Third Critical (cpm (Hz))
Fore-Aft (y-axis)	64,200 (1070)	125,400 (2090)	380,000 (4670)
Horizontal (z-axis)	61,700 (1030)	122,500 (2040)	

The fact that the bearing radial stiffnesses are closer together in Figure

5 for the output shaft than in Figure 4 for the input shaft causes the points at which the critical frequency curves intersect the bearing stiffness curves to be closer together. This makes the results shown in Figure 5 somewhat easier to interpret than those in Figure 4. Both clearly indicate that the two shafts are operating in bending regimes, and in close proximity to their third critical frequencies.

LATERAL RESPONSE OF SHAFTS TO GEAR-MESH-INDUCED TOOTH FORCES

Figures 4 and 5 show that both bevel gear shafts are operating with the bevel gear mesh frequency in close proximity to their third critical frequencies. This portion of the analysis, which includes bearing radial stiffnesses along both the y and z axes, as well as the dynamic forces calculated in [2], is designed to indicate more exactly the relationship between system critical frequencies and the mesh frequency. Vibration amplitudes, together with the levels of the dynamic forces transmitted across the rolling-element bearings (which are a primary indicator of noise level), will also be obtained.

From [2], the dynamic forces (peak values) acting at the bevel gear mesh point at the mesh frequency are as follows:

	$F_{d,y}$ (lb)	$F_{d,z}$ (lb)
Input Bevel Gear	78	431
Output Bevel Gear	405	431

When these dynamic forces are applied at the bevel gear mesh frequency of 3412 Hz (equivalent to 230 rpm rotor speed), the input and output shafts vibrate (at 3412 Hz) in the mode shapes shown in Figures 6 and 7, respectively.

With respect to the input bevel gear shaft, Figure 6 shows several very important items:

1. The shaft is experiencing bending, and since the vibrations are not at the rotational speed, it is flexing.

2. In general, the levels of vibration are fairly low, on the order of 60×10^{-6} inch or less. With bearing radial stiffnesses on the order of 7×10^5 to 6×10^6 lb/in., however, dynamic forces on the order of 50 to 350 pounds are indicated. If these forces are transmitted directly to the casing, as it appears they are, it becomes apparent why measurable casing vibrations occur at the bevel mesh frequency, and thus why noise is produced at this frequency.

3. Both roller bearings experience about the same vibration amplitudes, and should therefore exhibit roughly the same lifetime degradation, (if any) due to this cause, other factors being equal.

4. The ball bearings exhibit higher vibration levels than the roller bearings. Since these bearings are relatively unconstrained radially, wear may be expected in or along the axially restraining shoulders.

5. Some flexing of the input coupling is indicated.

6. Little relative motion is predicted for the bevel teeth.

Maximum force levels in the bearings are predicted at an angle of about 10 degrees from the horizontal, measured counterclockwise as viewed from the aft end of the gearbox.

With respect to the output bevel gear shaft, Figure 7 shows several important items:

1. The shaft is experiencing bending, and since the vibrations are not at the rotational speed, it is flexing.

2. In general, the vibration levels are fairly low, on the order of 70×10^{-6} inch or less. With bearing radial stiffnesses on the order of 3×10^{6} to 6×10^{6} pounds/inch however, dynamic forces on the order of 200 to 400 pounds are indicated. Again, transmission of forces of this magnitude to the gearbox casing would appear likely to result in measurable casing vibration levels at this frequency.

3. The duplex ball bearings (numbers 5 and 6) experience considerably higher vibration levels than the roller bearing (number 7), apparently because of the translation inertia of the spur gear mounted just above the ball bearings. If other factors are equal, their lifetime may be anticipated to be shorter than the roller bearings.

4. The sun gear (upper end of the output bevel gear shaft) experiences more lateral vibration than that part of the shaft supported by the roller bearing. It may be anticipated that vibration sidebands* might be found at frequencies equal to the bevel mesh frequency plus and minus the lower planetary sun-planet mesh frequency; tha is, at $3412 \pm 1482 = 1930, 4894$ Hz.

In the effort to demonstrate the relationship of the shaft lateral natural frequencies to the bevel gear mesh frequency, the response calculations described above were repeated at other frequencies, while keeping the shaft rotational speed constant. Bearing stiffnesses and exciting forces were

*Recent CH-47 gearbox test cell noise and vibration measurements under U.S. Army Contract DAAJ02-71-C-0020 (Vertol-Division - the Boeing Company) appear to indicate the presence along the gearbox sidewalls of a significant signal at about 2000 Hz, which does not appear to be explainable by any other physical mechanism at the present time.

kept constant. This latter assumption is adequate with regard to the bearing properties. There is a strong likelihood that the dynamic forces would be different at any other frequency, if there was a source of excitation at each frequency considered. The vibration amplitudes and forces are therefore strictly correct (analytically) at the bevel mesh frequency of 3412 Hz. The utility of such a frequency sweep is that it immediately identifies the location of system critical frequencies (through locations of force and amplitude peaks) and it gives an indication of the relative severity of each critical frequency should a source of vibration be present at that frequency. Figures 8 and 9 present the results of frequency sweeps for the input and output bevel gear shafts, respectively.

Figure 8 shows several important results for the input shaft:

1. There is a significant peak in the bearing transmitted forces for all four bearings very close to the normal operating range of the bevel gear mesh frequency. This peak probably corresponds to the third critical frequency identified in Figure 4, although it is somewhat higher than that frequency.

2. There is a significant transmitted force peak near 1500 Hz, which also happens to be approximately the lower planetary mesh frequency. Thus, excitations from that source must be considered as a potential means for exciting what appears to be the shaft's second critical frequency. The smaller peak at about 1700 Hz would appear to be a lesser second critical frequency due possibly to dissimilar horizontal and vertical bearing stiffness values.

3. There is a lesser critical frequency at about 400 Hz, which apparently corresponds to the first critical frequency identified in Figure 4.

4. The calculated bearing dynamic force levels at the bevel gear mesh frequency (3412 Hz) are on the order of 100 to 250 pounds peak.

While very high dynamic forces are shown in Figures 8 and 9, this is calculated data which assumes both rigid supports and no damping. Both flexible supports and the presence of damping would obviously act to reduce these force levels. Of prime concern is the location of the third critical frequency peak relative to the mesh frequency. Figure 4 indicates that this peak is somewhat below the mesh frequency, while Figure 6 indicates that the peak is slightly above the mesh frequency.

It is likely that the actual supporting structure will exhibit lower stiffness than those levels assumed for these calculations, and that the mesh frequency will therefore very likely be above the third critical frequency in actual operation. The effects of changes to various bearing stiffness properties will be explored in the next section.

With the anticipated location of the force peak below the mesh frequency, it is likely that the bevel gear noise component will intensify at slightly lower gearbox shaft speeds.

Figure 9 also exhibits several interesting results:

1. A force peak is found at or slightly above the bevel mesh frequency. This peak apparently corresponds to the third system critical frequency shown in Figure 5.

2. There are distinct critical frequencies at about 1300 Hz (78,000 cpm) and 850 Hz (51,000 cpm), which appear to correspond to the second and first critical frequencies, respectively, shown in Figure 5.

3. The dynamic forces at the bevel gear mesh frequency (3412 Hz) are on the order of 200 to 400 pounds amplitude.

The comments made earlier relative to the calculated peak values and the likelihood of their attenuation by increased support flexibility and damping apply here as well.

SHAFT-BEARING MODIFICATIONS FOR VIBRATION AND NOISE REDUCTION

While it is impossible under this investigation to consider each of the many system modifications which could be used to reduce vibration, and therefore noise levels, it is both instructive and useful to demonstrate the type of modifications which should be considered. The ease of considering these modifications analytically, before proceeding to the test cell, will become apparent as the range of modifications is explored. The relative cost savings which may be achieved by ruling out marginal changes prior to testing will also become obvious. In each modification, the criteria against which the modification will be judged are the relative reductions in shaft-to-bearing vibration amplitude, and thus in bearing transmitted force, compared to the nominally calculated vibration amplitudes (recall that amplitude and force are proportional).

Structural Changes to the Shafts

Several changes to noncritical (i.e., inner or nonbearing surface) diameters were made to demonstrate the reduction in shaft bending which can be achieved by stiffening the bevel gear shafts. Figures 10 through 12 show the results of these changes for the input bevel gear shaft, while Figures 13 and 14 present results for the output bevel gear shaft.

In Figure 10, an additional wall thickness of 0.15 inch was added to the coupling end of the input shaft, together with a slightly steeper taper to the larger diameter, as shown by the shaded area. The calculated result of such a change is to stiffen the smaller diameter section, thereby decreasing the bending in that portion. The calculated effect is to reduce

the vibration amplitude in bearing 1 by 50 percent, in bearings 2 and 3 by about 30 percent, and in bearing 4 only by a slight amount. The vibration at the gear increases by about 50 percent. This modification should result in a quieter gearbox, on the whole.

In Figure 11, an additional wall thickness of 0.15 inch was added as shown, along with a somewhat steeper taper to the larger diameter. Somewhat less bending and lower vibration levels are achieved, but the marginal increase is small compared to that gained by the first change.

In Figure 12, additional material is added to the inner diameter beneath bearings 2-4, in addition to the first two changes. Little, if any, additional benefit is gained.

In Figure 13, the output bevel gear shaft is modified by the doubling of the wall thickness in the area shown. A reduction of about 30 percent is achieved in the vibration levels of the ball bearings, and a reduction of 50 percent is achieved in the lateral vibration of the small spur gear. Little if any change is noted at the bevel gear and roller bearing locations, while a 30-percent vibration reduction is noted at the sun gear location. This may be important in the reduction of sidebands which involve the bevel and sun gear mesh frequencies.

The shading in Figure 14 shows the calculated effects of tripling the original wall thickness. Again, some marginal improvements are noted.

Stiffening a shaft tends to <u>increase</u> its bending natural frequencies, in general, while the addition of mass has the opposite effect. The net result achieved will depend upon the relationship of the critical frequencies to the mesh frequency, and the relative importance of the stiffening compared to the effect of the added mass.

<u>Bearing Stiffness Modifications</u>

Several options are available to the designer with respect to modifications to the stiffness properties of the rolling element bearings. For instance, changes may be made to all bearings together, or to individual bearings if prior knowledge exists about the effects of such changes upon the bearing dynamic forces. When the problem is approached analytically, it is instructive to first make equal percentage changes to all bearings, in order to determine the effect of such changes upon the critical parameter, in this case the bearing dynamic forces. For the input bevel gear shaft, calculations were performed at both 50 percent and 200 percent of the nominal values presented earlier. The bearing dynamic forces resulting from these calculations are shown, together with the nominal values, in Figure 15.

Figure 15 shows that increases in the stiffnesses of bearings 1, 2, and 3 would result in lower dynamic forces, whereas the opposite is true for bearing 4.

Figure 8 shows that the shaft third critical frequency lies slightly above the bevel gear mesh frequency. Thus, the increase in bearing stiffnesses results generally in lower bearing dynamic forces because the third critical frequency is shifted upward, away from the mesh frequency.

The Vertol drawings indicate a further bearing (or bearing support) stiffness variation which should also be considered. On the input bevel gear shaft, outer races of bearings 2 and 3 (the ball bearings) are positioned axially with respect to the supporting structure by means of shoulders and shims. Radial restraint, however, depends strongly upon the axial force acting on the bearing and the coefficient of friction between the bearing outer race and its support. For high axial thrust levels, the outer race may be rather rigidly supported by the friction characteristics of the shoulder and shims, and the effective stiffness will be that of the bearing itself. For lower axial forces, however, relative motion may occur between the outer race and the shim, resulting in very low radial stiffnesses for bearings 2 and 3.

The further sets of calculations were made in order to investigate the effects of substantial reductions in the stiffnesses of bearings 2 and 3. In the first of these, the stiffnesses of bearings 2 and 3 were reduced to 50 percent of the nominal values reported earlier. In the second, the stiffness effects of bearings 2 and 3 were removed completely.

The results of these two sets of calculations are shown in Figures 16 and 17 respectively. These figures should be compared to Figure 8, in order to assess the effects of these bearing changes. In Figure 16, it may be seen that while the apparent severity of the third critical frequency has decreased, the critical frequency has shifted downward precisely into the middle of the bevel gear mesh frequency range. The critical frequency at about 1500 Hz has apparently experienced little change in either peak frequency or severity.

Figure 17, which shows the results of calculations with zero stiffness for bearings 2 and 3, indicates a further drop to about 3100 Hz for the third critical frequency, somewhat below the bevel mesh frequency range. Two distinct force peaks were noted near the second critical frequency between 1000 and 1500 Hz.

While it is difficult to estimate values of the radial stiffness which would be experienced during actual operation for bearings 2 and 3, it is very likely that they will generally be less than the nominal values discussed earlier. It is also likely that they will vary as the input shaft thrust load varies; that is, with variations in the levels of power which are transmitted to the rotor. Assuming an operating condition which results in the third critical frequency below the mesh frequency, as a result of lower radial support stiffness at bearings 2 and 3, then increased power levels would tend to stiffen the system by stiffening bearing 2 and 3 supports, and would raise the critical frequency into the mesh frequency range. This would result in higher dynamic force levels, and thus higher

noise levels, at the bevel mesh frequency. Further increases in power level would tend to further stiffen the system, pushing the critical frequency past the mesh frequency, resulting in lower dynamic force levels, and thus noise levels, at that frequency.

Thus, some of the apparently conflicting observations on the effects of certain aircraft operating parameters upon noise level may be explained.

A design which permits this apparent degree of variability of a critical frequency, particularly one so close to an important mesh frequency, should be modified to place the critical frequency 10 percent to 15 percent above the upper limit of the mesh frequency range. This may be accomplished by radially stiffening the thrust bearing supports, for instance.

Shaft Material Modifications

Modifications of this type should be considered as viable methods for altering the dynamic behavior of shaft-bearing systems of the type found in the CH-47 gearbox. In such a modification, the ratio of Young's modulus to material density is an important factor to consider. Higher ratios of these properties generally result in higher shaft natural frequencies, and thus a reduced tendency for the shaft to operate in or near a bending regime. Such an effect could be important for both input and output bevel gear shafts in the CH-47. The effects of modifications such as this are illustrated in a later section which deals with the UH-1D output bevel gear shaft. These very striking changes in vibration amplitude may be achieved by changing the shaft material from steel to titanium, for instance.

Damping Modifications

The addition of damping is another method which is often proposed for the reduction of vibration levels. This approach is certainly feasible to consider for the reduction of acoustic-frequency vibration amplitudes as well. The criterion for successful use of a damper is that the body or surface to be damped must vibrate with high velocity. When such is the case, then viscous dampers can generate high forces to oppose the motion, thereby reducing the vibration energy of the body or surface.

Maximum vibration velocity (assuming simple harmonic motion or circular motion with the vibration measured along a single axis) is given by the product $a\omega$, where a is the peak amplitude and ω is the frequency of vibration. For rotational-frequency vibrations, amplitudes on the order of 0.002 inch to 0.010 inch are common in general, and frequencies are on the order of 200 Hz (approximately 1200 rad/sec). Thus, values of vibration velocities of 2.5 to 12.0 in./sec are typical.

For acoustic-frequency vibrations, on the other hand, amplitudes on the order of 0.0001 or lower may be common at frequencies on the order of 3000 Hz (approximately 18000 rad/sec). Typical vibration velocities will

be on the order of 1.8 in./sec or lower. To be effective in reducing acoustic-frequency vibrations, therefore, dampers would have to possess from two to ten times the amount of damping normally available in typical low-frequency dampers.

The use of a damper was investigated for the CH-47 input bevel gear shaft in order to determine how much acoustic-frequency vibration could be reduced. A damper having a damping constant which was varied over the range 0.01 to 100 lb-sec/in. was positioned for calculation purposes between the input bevel gear shaft and the casing at the bevel gear location. Changes of only about three percent or less were observed in the bearing dynamic force levels, indicating that damping would not be effective in this location. The vibration mode shape observed in Figure 6 indicates that damping in the area of the thrust ball bearings or near the coupling pin might be more effective. The generally low overall vibration levels shown in Figure 6, however, indicate that damping may not be an important mechanism for the reduction of vibration and noise levels due to this particular shaft.

Summary of Results of Modifications

The potential usefulness of several system modifications for the reduction of acoustic-frequency vibrations has been demonstrated in the foregoing sections by means of digital computer dynamic simulation. In each case, the dynamic behavior of the modified shaft bearing system has been compared to the nominal behavior of that component, using as a basis for comparison the levels of both vibration amplitude and bearing dynamic force.

This type of information may be used in two ways:

1. It can be used, together with carefully conducted and documented test cell measurements, to confirm the regimes of operation of the gearbox interior shafts (bending versus rigid-body, for instance). Good correlation between calculated and measured mode shapes and levels of vibration provides a good indication of the relative importance of the several paths by which acoustic-frequency energy reaches the ear.

2. It can also be used to evaluate the usefulness of proposed gearbox modifications. It is far less costly to calculate the dynamic behavior of modified gearbox components than to build them and evaluate their performance in the test cell.

It is instructive to compare the modifications considered in this section with respect to the effective noise reduction, in db, which each could theoretically achieve. This comparison may be made by examining the changes in bearing dynamic forces which result from each modification. Under the assumption that the gearbox casing is relatively rigid compared to the bearing radial stiffness values, the dynamic forces were calculated for both the nominal and modified configurations.

Even though the casing is relatively rigid, it will undergo some vibration, probably of very low amplitude (the vibration which produces the noise generated by the casing). The levels of this vibration will be proportional to the bearing dynamic forces, assuming no local casing structural resonances. Hence, changes in dynamic force levels may be utilized to indicate changes in vibration amplitude, and thus in generated noise level.

Since the bearing dynamic forces act on a relatively small part of the casing (particularly in the case of the input bevel gear shaft) at the same frequency and in the same phase relationship to each other, it is convenient to sum their amplitudes, and to take the resulting number as an equivalent dynamic force acting on the inside of the casing. The changes in this equivalent force are then representative of noise level changes, which may be expressed by the relationship

$$\text{Equivalent Noise Level Change(db)} = 20 \log_{10} \frac{\sum (\text{new bearing dynamic force})}{\sum (\text{original bearing dynamic force})} \qquad (1)$$

The changes, expressed in this form, are shown in Table III for the several shaft-bearing system modifications discussed below.

While it appears that several physical changes to the drive train may be beneficial from the standpoint of noise reduction (and increased bearing lifetimes), these changes are only representative of many which may prove usable. There are very likely other shaft configurations, for example one which has very thick walls or one which carries solid sections at either end, which exhibit even greater noise-reduction capacities. The key is to place the vibration nodes precisely at the bearing locations, a condition which requires the examination of the results of vibration calculations for a sequence of trial design configurations. Such changes must ultimately be evaluated by a competent gearbox designer, who must be concerned with their implementation from the standpoints of practicality and safe operation.

TABLE III. SUMMARY OF RESULTS OF SHAFT-BEARING SYSTEM MODIFICATIONS FOR REDUCTION OF BEVEL GEAR MESH-FREQUENCY NOISE COMPONENT FOR CH-47 FORWARD ROTOR-DRIVE GEARBOX

Bevel Gear Shaft	Description of Modification	Peak Bearing Dynamic Force (lb) Bearing 1	Bearing 2	Bearing 3	Bearing 4	Equivalent Reduction in Bevel Gear Noise Component (db)
Input	Nominal Design	31.1	127.2	265.6	227.1	-
	Decrease of Inner Diameter (see Figure 10)	15.6	82.3	189.8	202.2	2.5
	Decrease of Inner Diameter (see Figure 11)	13.7	76.4	180.0	199.0	2.8
	Decrease of Inner Diameter (see Figure 12)	14.2	79.1	184.8	193.6	2.8
	50% Decrease of Bearing Stiffnesses of Bearings 1, 2, 3 and 4	83.8	312.4	471.4	77.0	(3.2) (increase)
	100% Increase of Bearing Stiffnesses of Bearings 1, 2, 3 and 4	10.8	50.5	140.5	314.1	2.0
	50% Decrease of Bearing Stiffnesses of Bearings 2 and 3	233.1	458.2	843.9	390.5	(9.4) (increase)
	100% Decrease of Bearing Stiffnesses of Bearings 2 and 3	32.3	-	-	78.9	15.4
		Bearing 5	Bearing 6	Bearing 7		
Output	Nominal Design	187.4	212.5	27.3		-
	Decrease of Inner Diameter (see Figure 13)	124.9	125.0	27.5		3.8
	Decrease of Inner Diameter (see Figure 14)	112.0	105.9	25.4		4.9

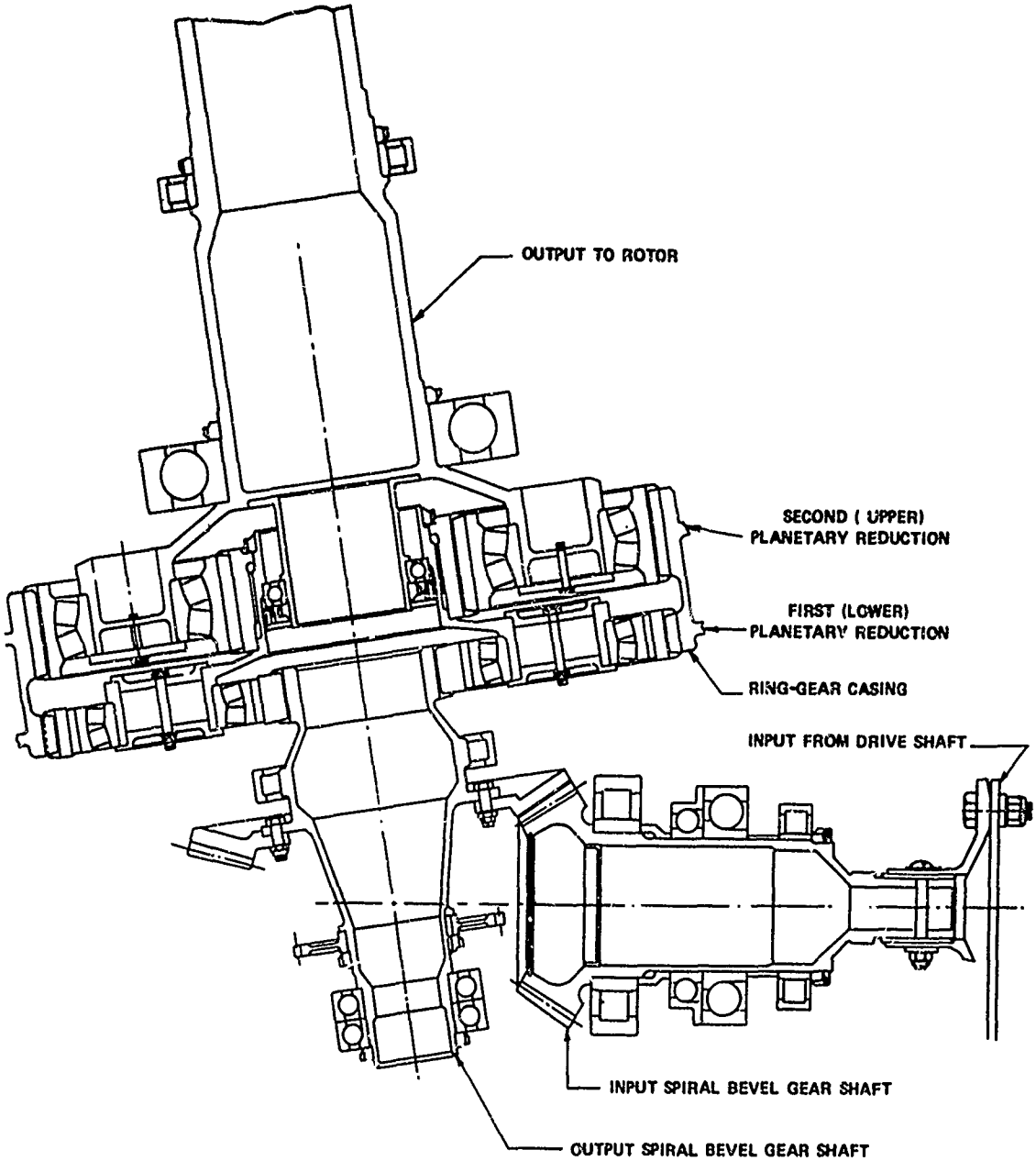

Figure 1. CH-47 Forward Rotor-Drive Gearbox Bevel Gear Shaft-Bearing System.

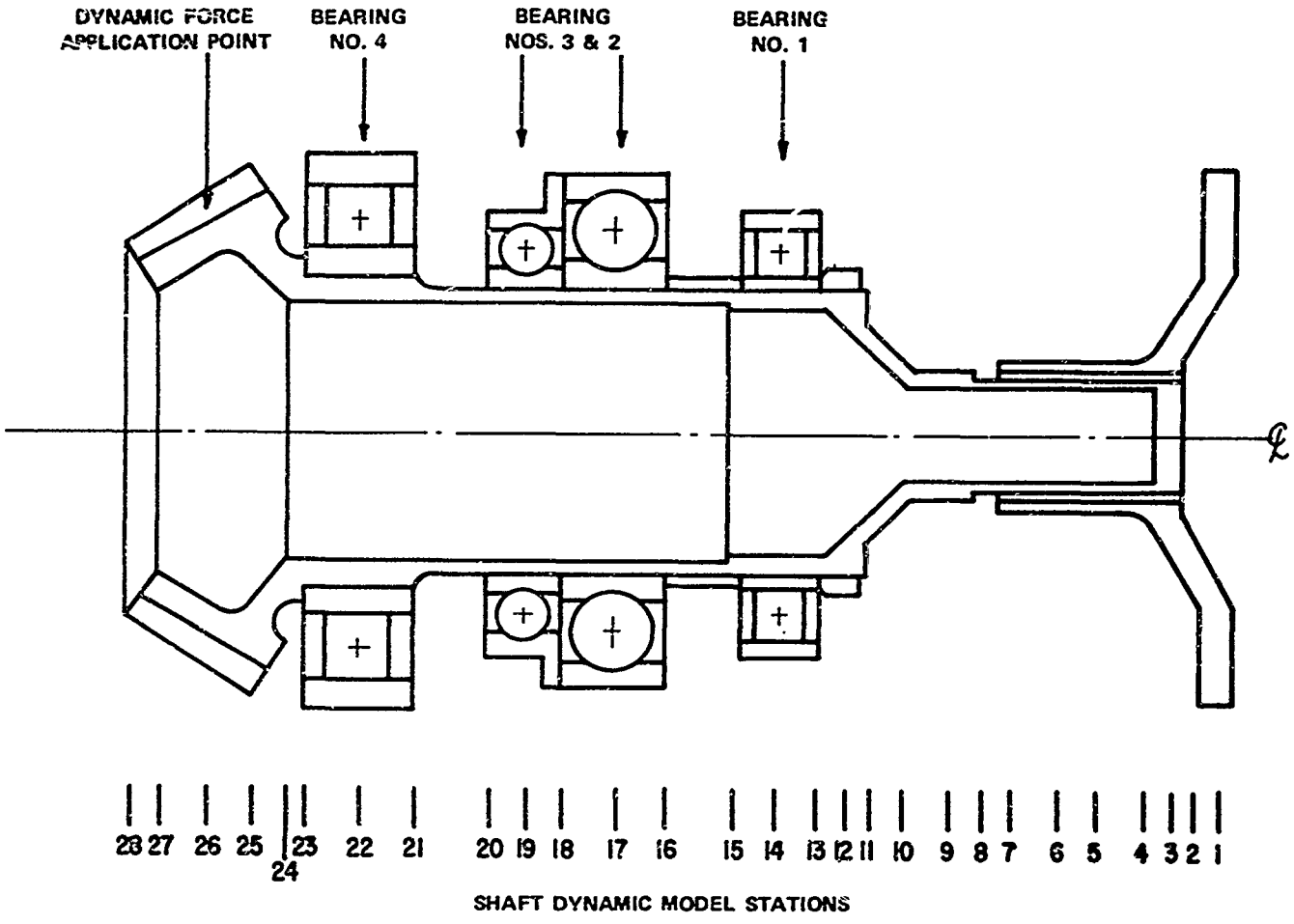

Figure 2. CH-47 Input Bevel Gear Shaft Dynamic Modeling Details.

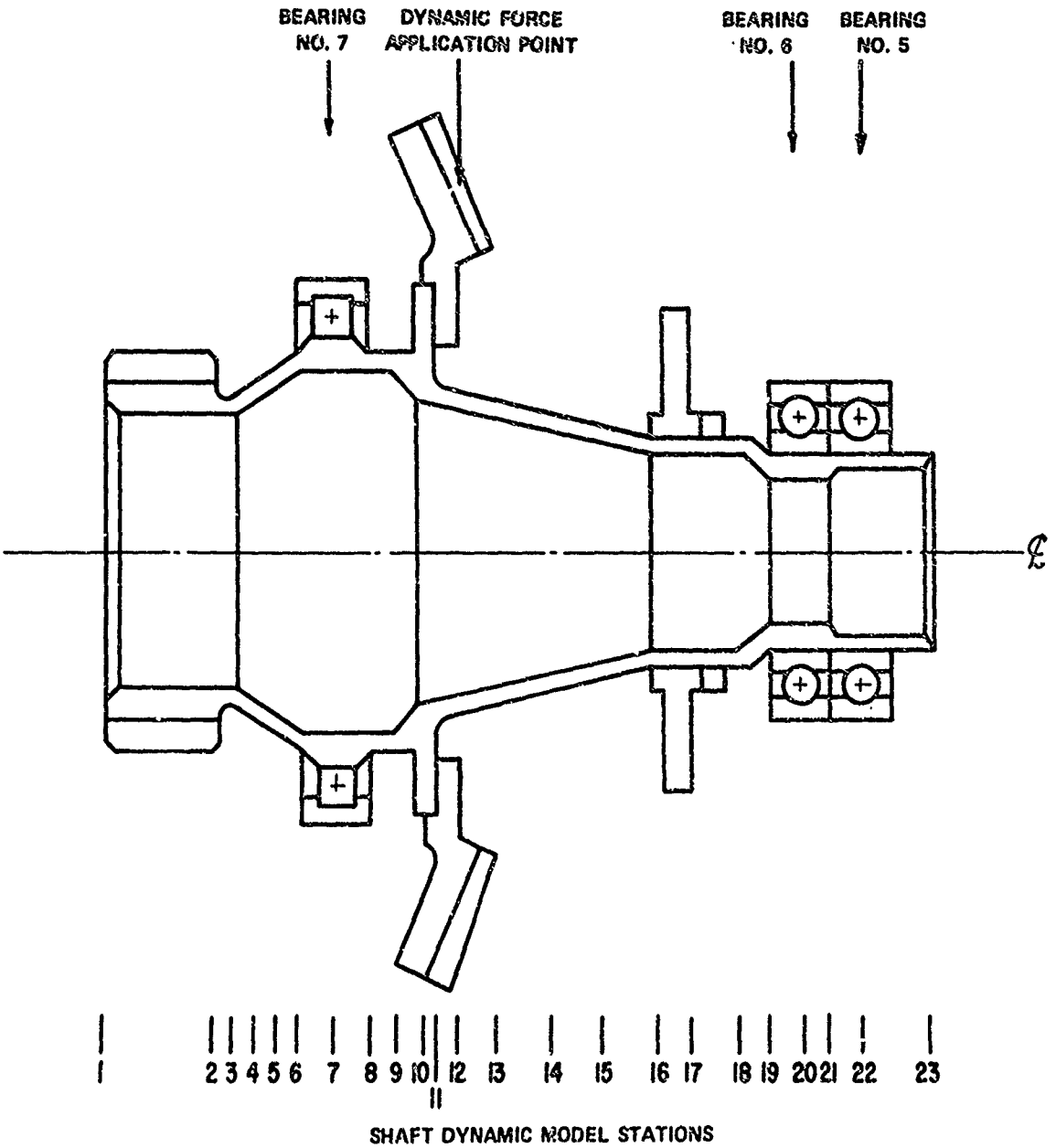

Figure 3. CH-47 Output Bevel Gear Shaft Dynamic Modeling Details.

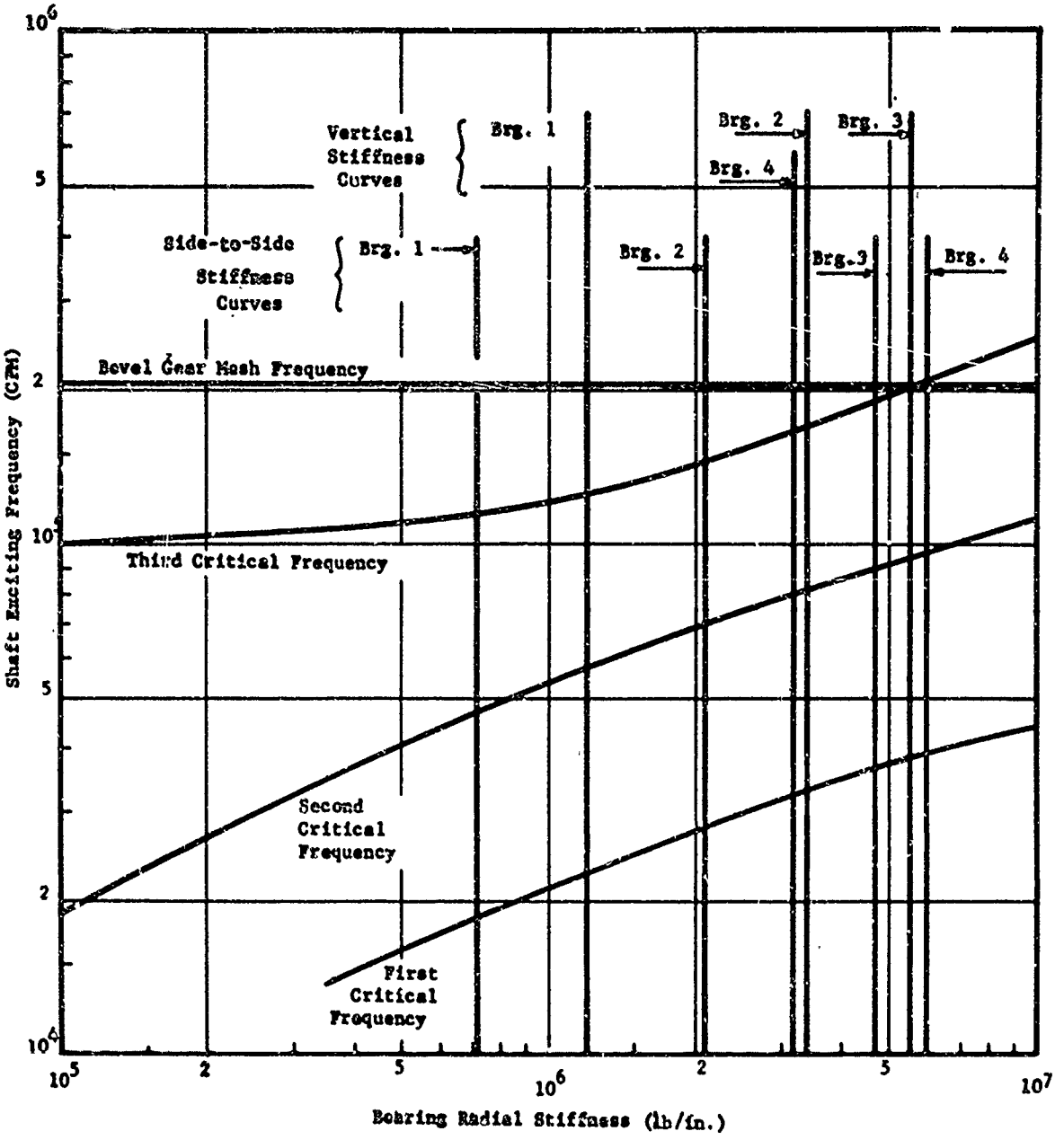

Figure 4. Critical Frequency Map for CH-47 Forward Rotor Gearbox Input Bevel Gear Shaft.

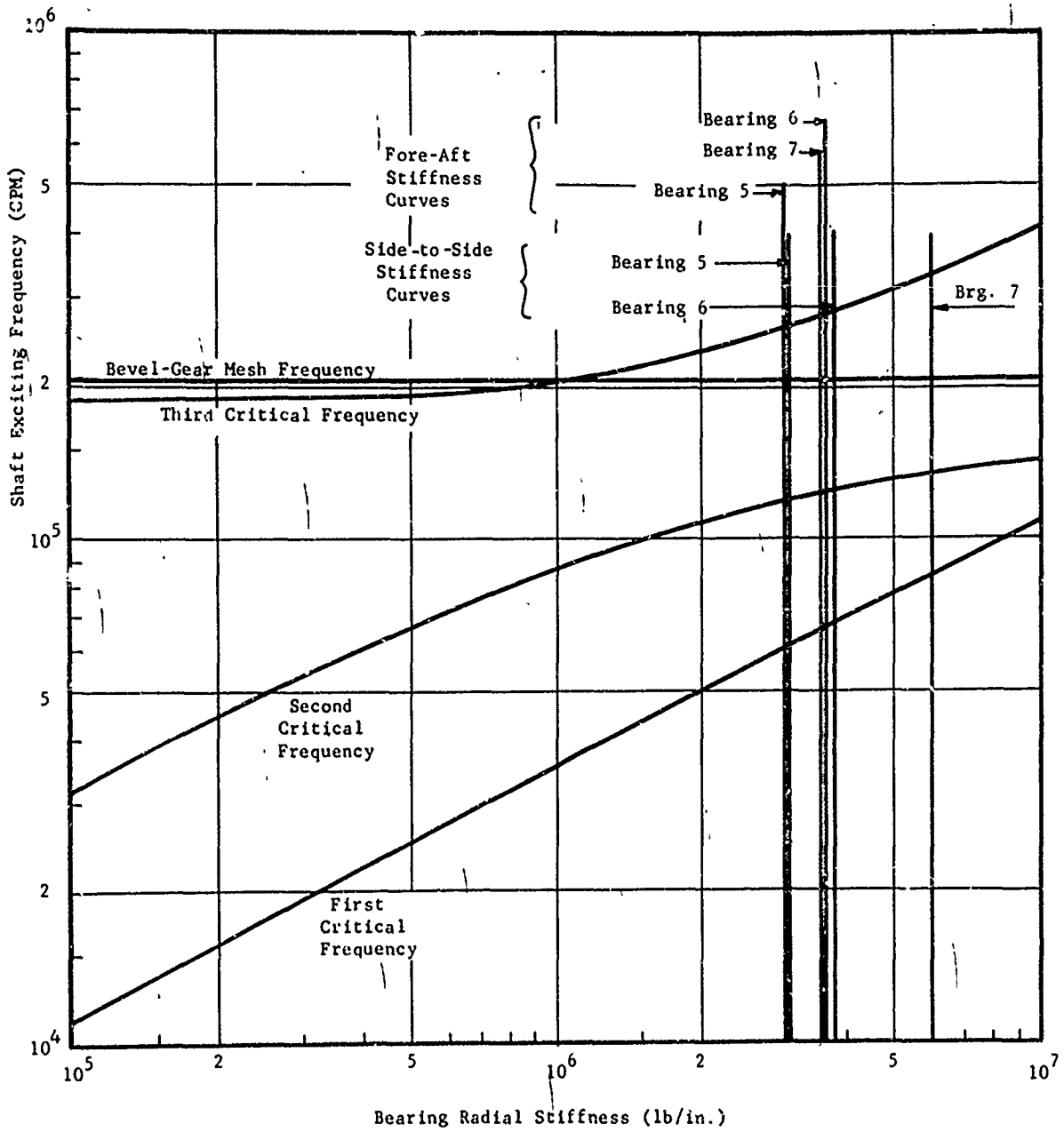

Figure 5. Critical Frequency Map for CH-47 Forward Rotor Gearbox Output Bevel Gear Shaft.

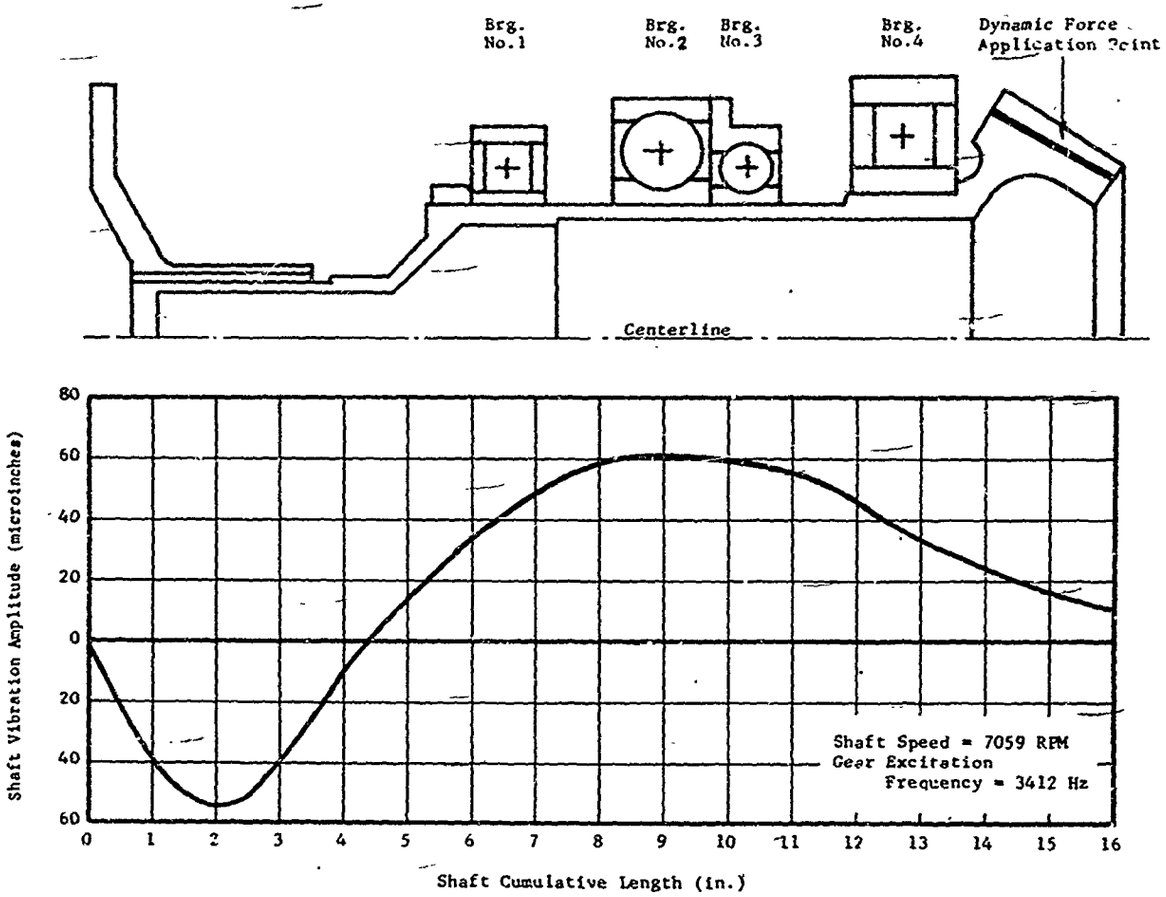

Figure 6. Calculated Vibration Amplitudes for CH-47 Nominal Configuration Input Bevel Gear Shaft.

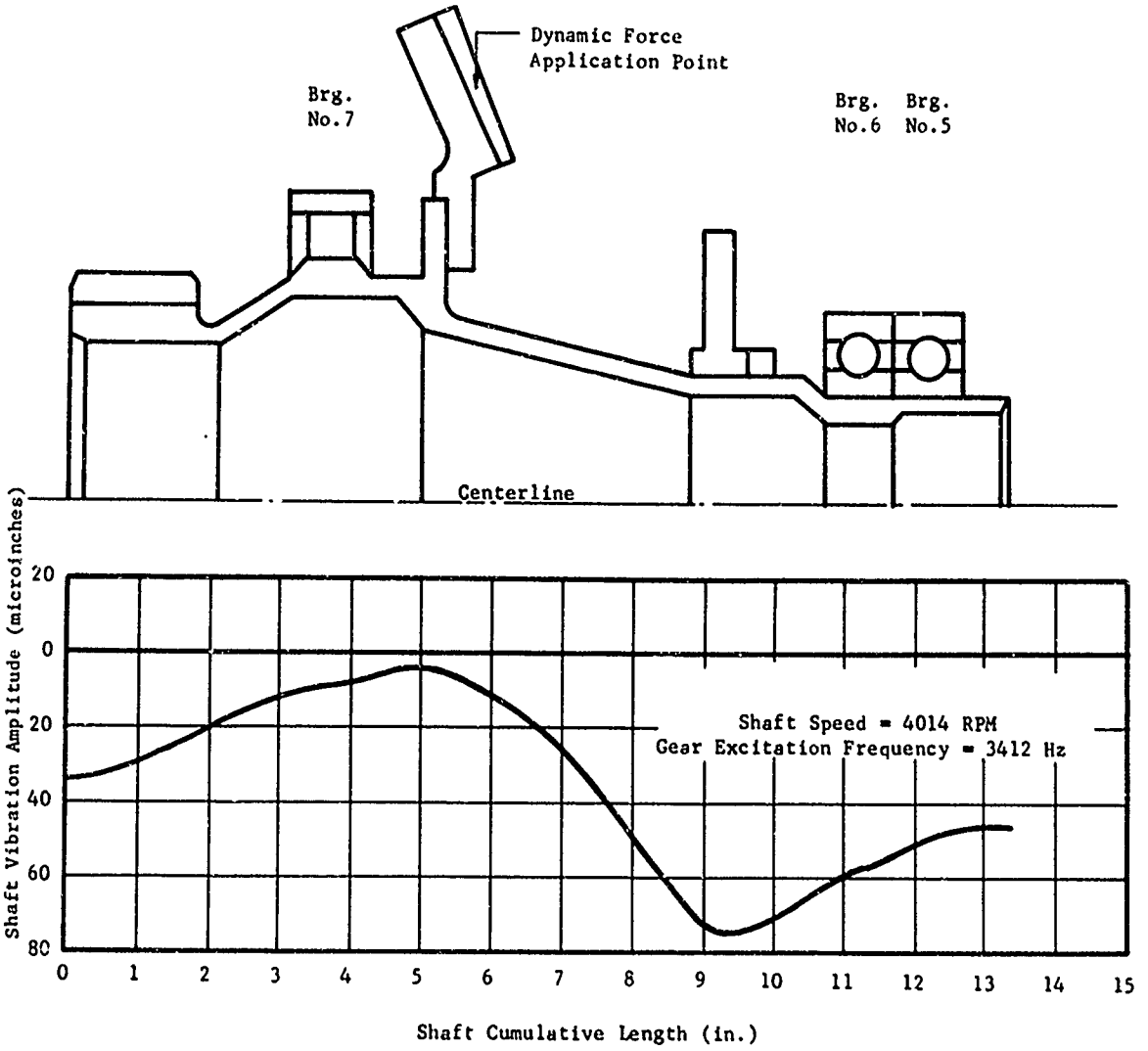

Figure 7. Calculated Vibration Amplitudes for CH-47 Nominal Configuration Output Bevel Gear Shaft.

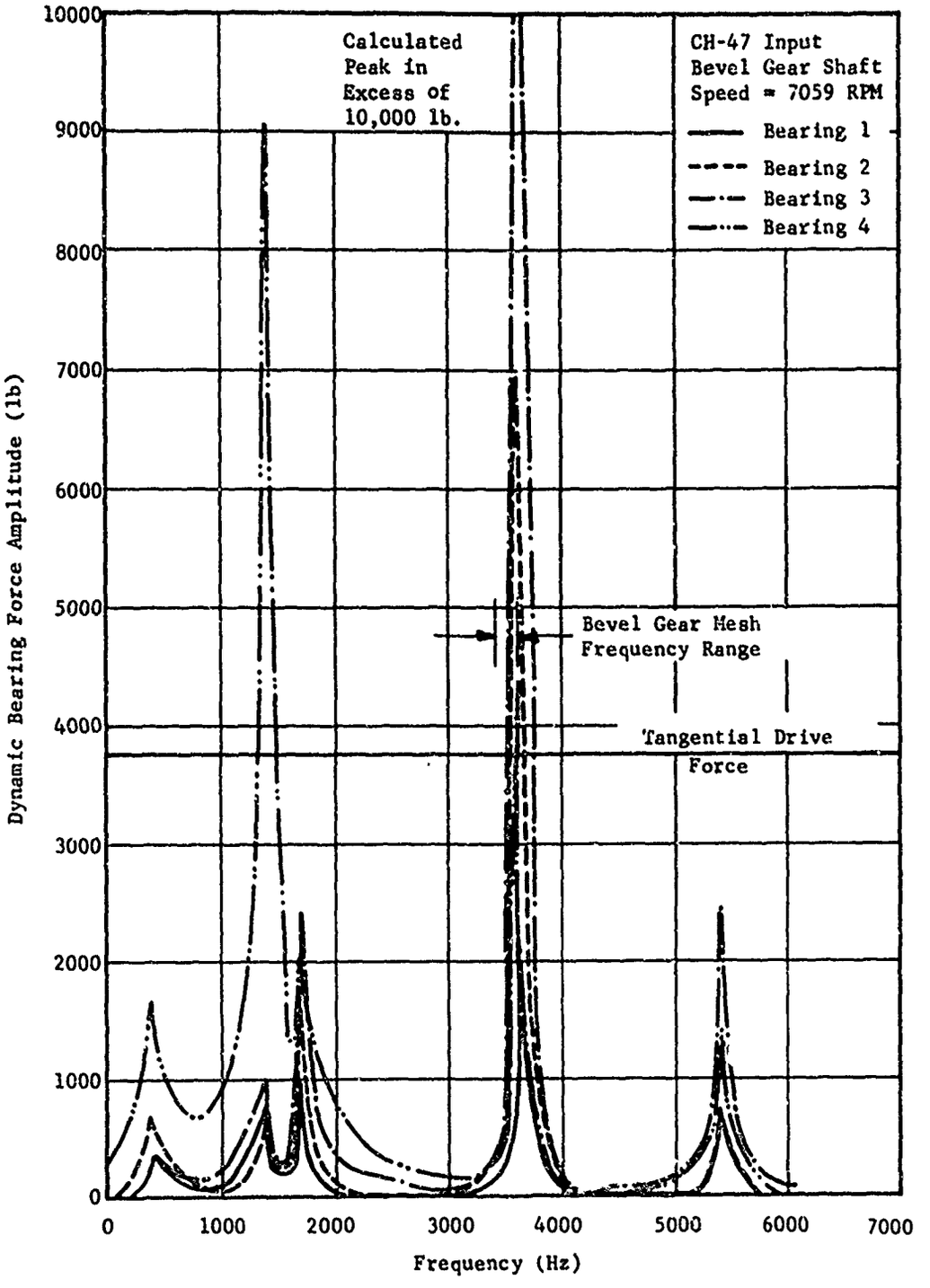

Figure 8. Calculated Dynamic Force Levels at Indicated Bearings With Constant Value Gear-Tooth Exciting Force for CH-47 Input Bevel Gear Shaft.

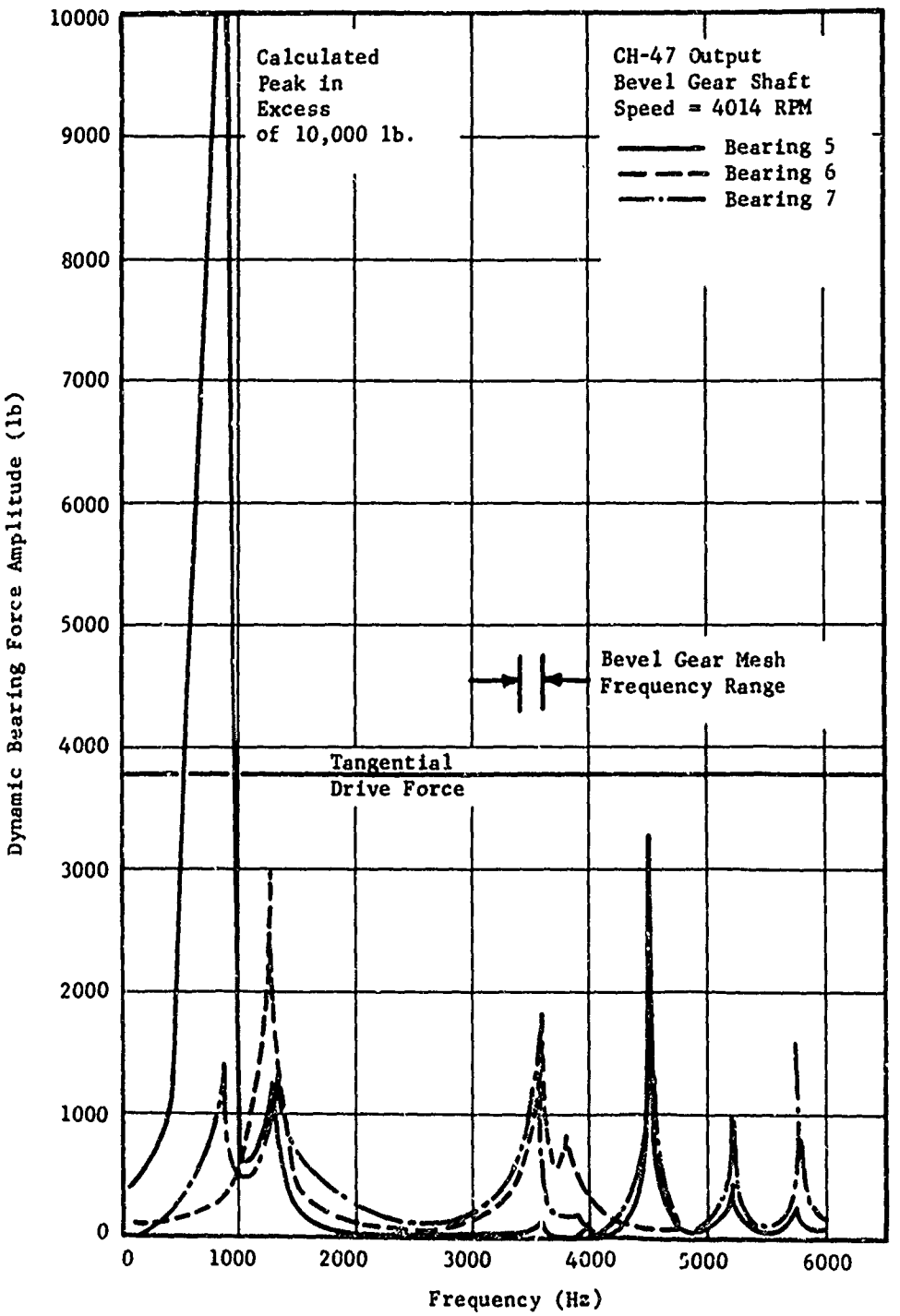

Figure 9. Calculated Dynamic Force Levels at Indicated Bearings With Constant Value Gear-Tooth Exciting Force for CH-47 Output Bevel Gear Shaft.

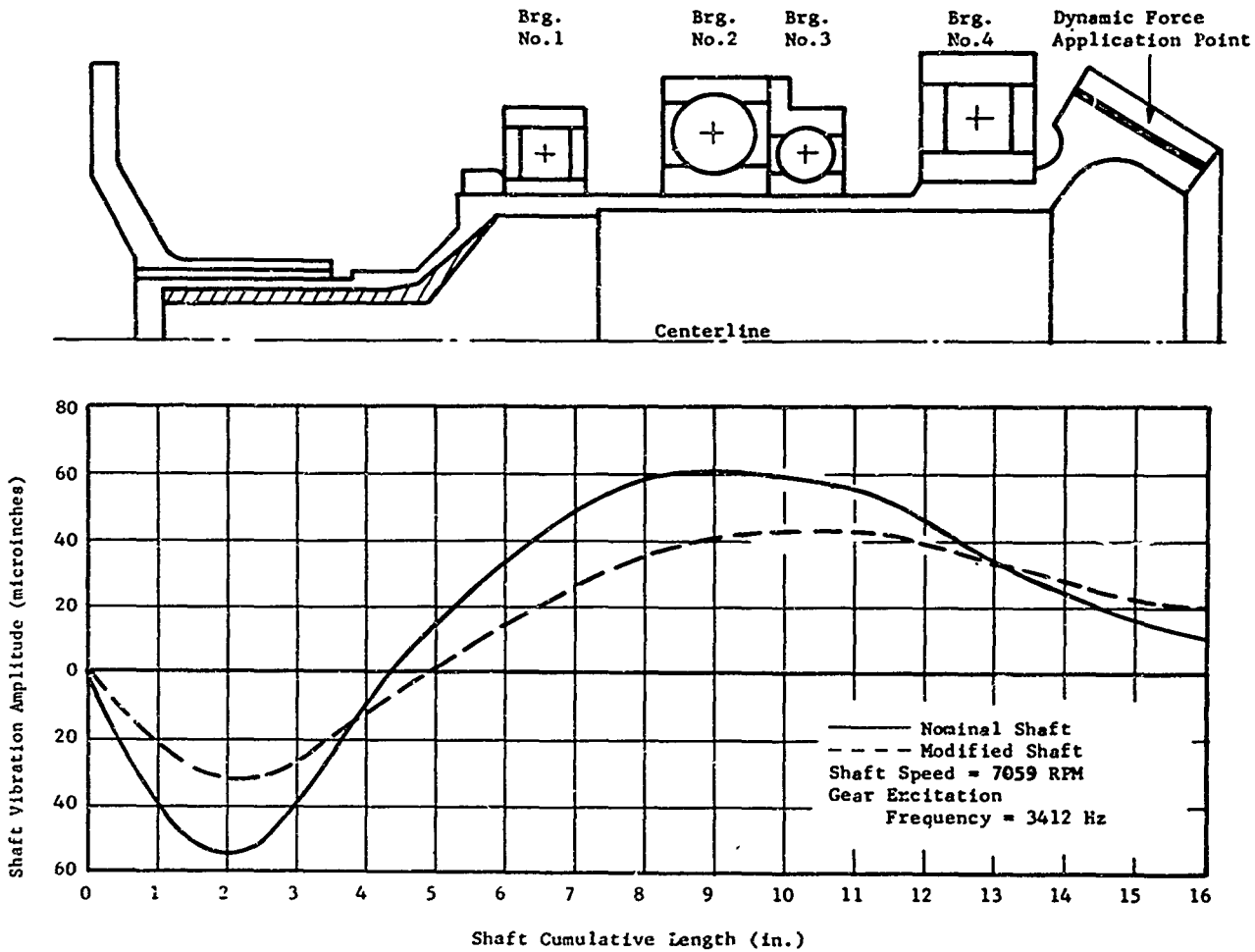

Figure 10. CH-47 Input Bevel Gear Shaft Vibration Amplitudes for Nominal and Modified Configurations.

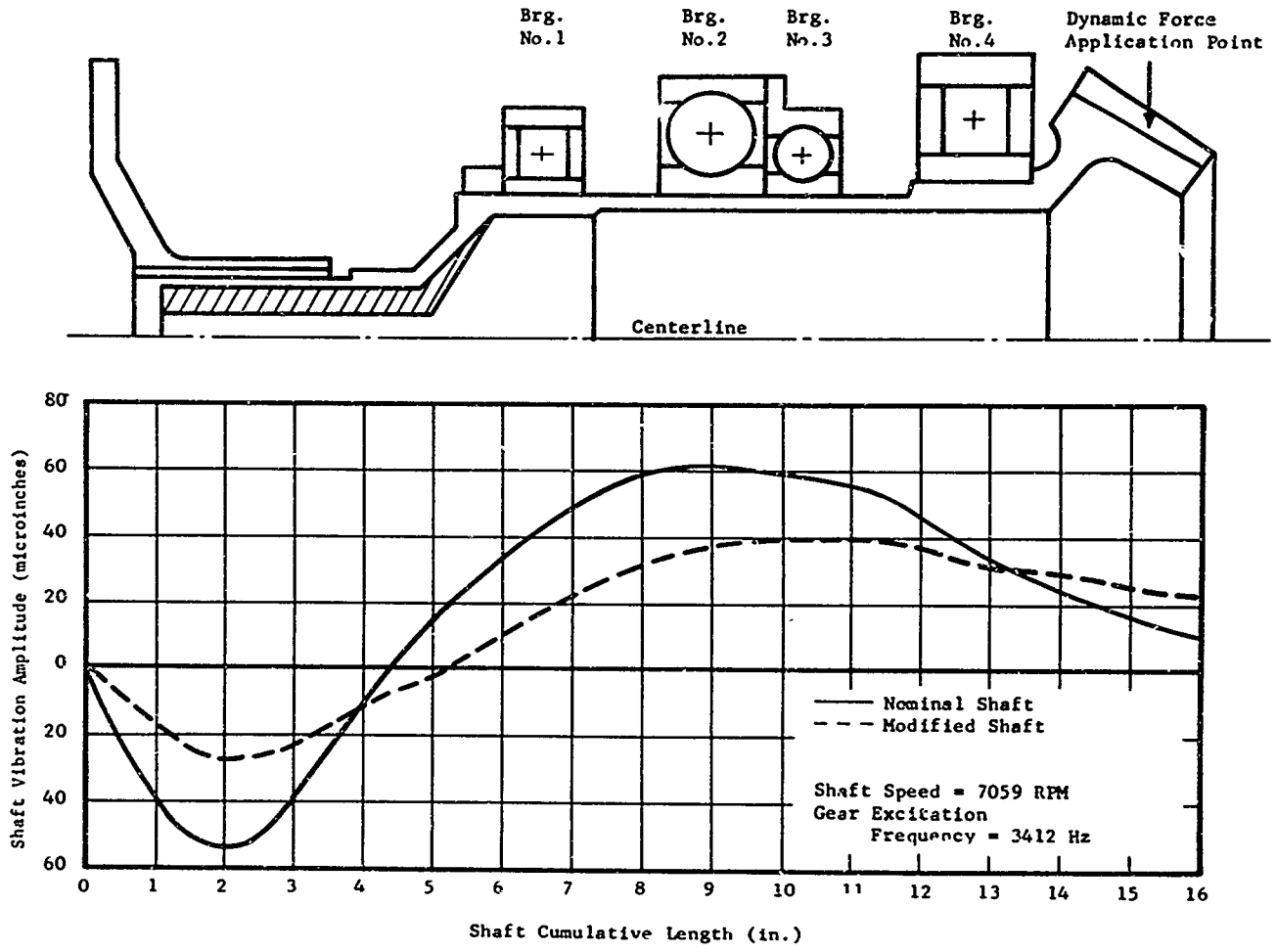

Figure 11. CH-47 Input Bevel Gear Shaft Vibration Amplitudes for Nominal and Modified Configurations.

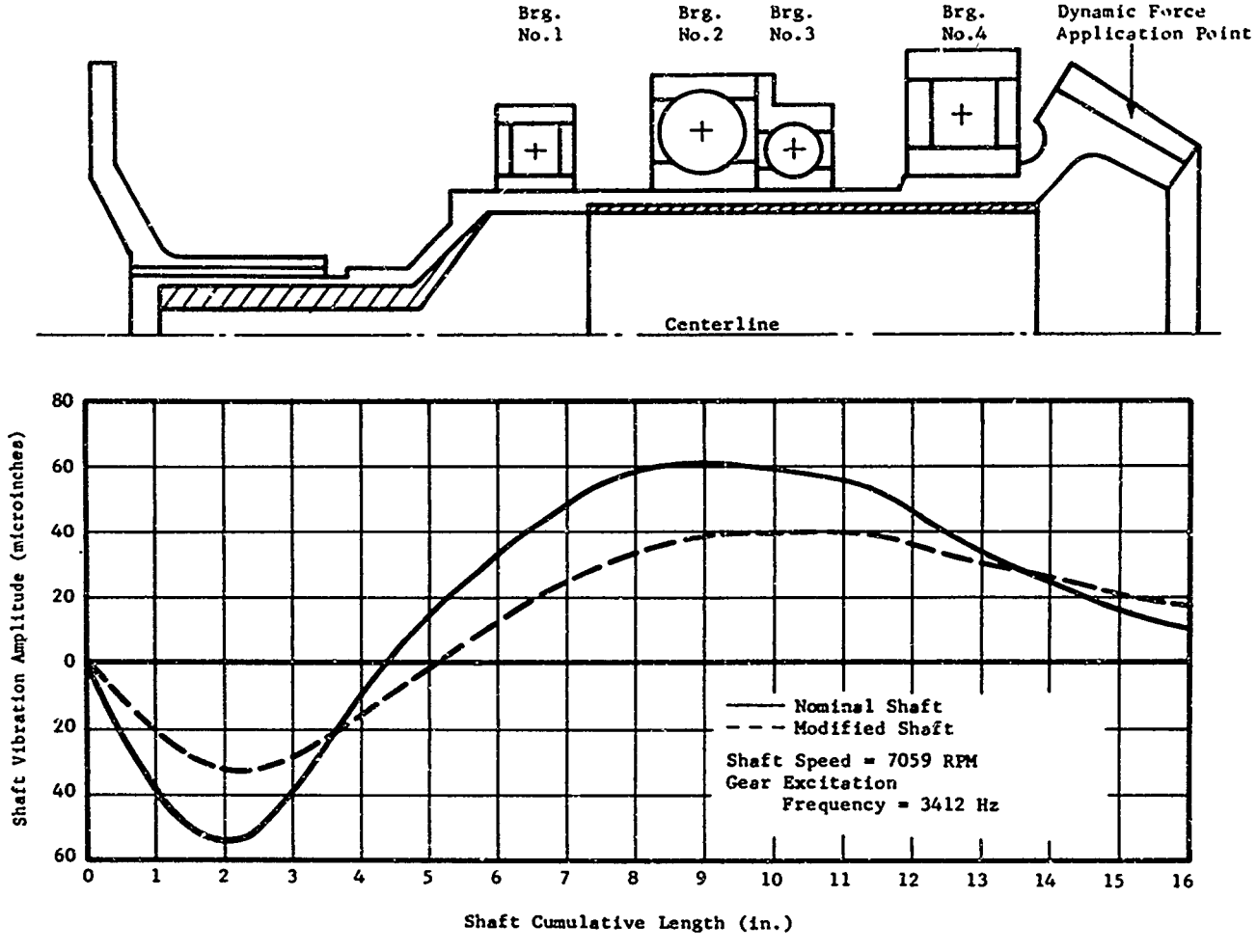

Figure 12. CH-47 Input Bevel Gear Shaft Vibration Amplitudes for Nominal and Modified Configurations.

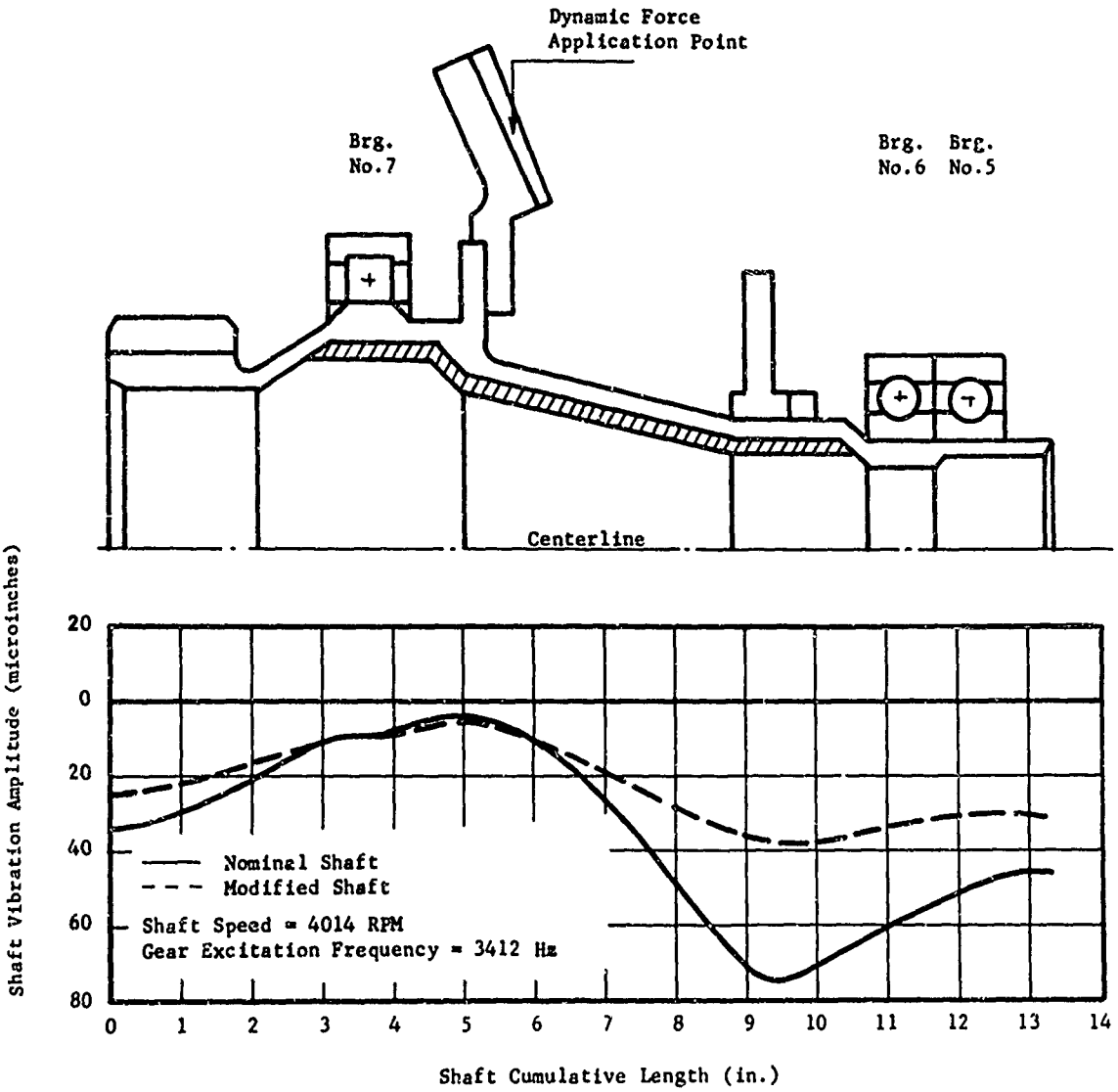

Figure 13. CH-47 Output Bevel Gear Shaft Vibration Amplitudes for Nominal and Modified Configurations.

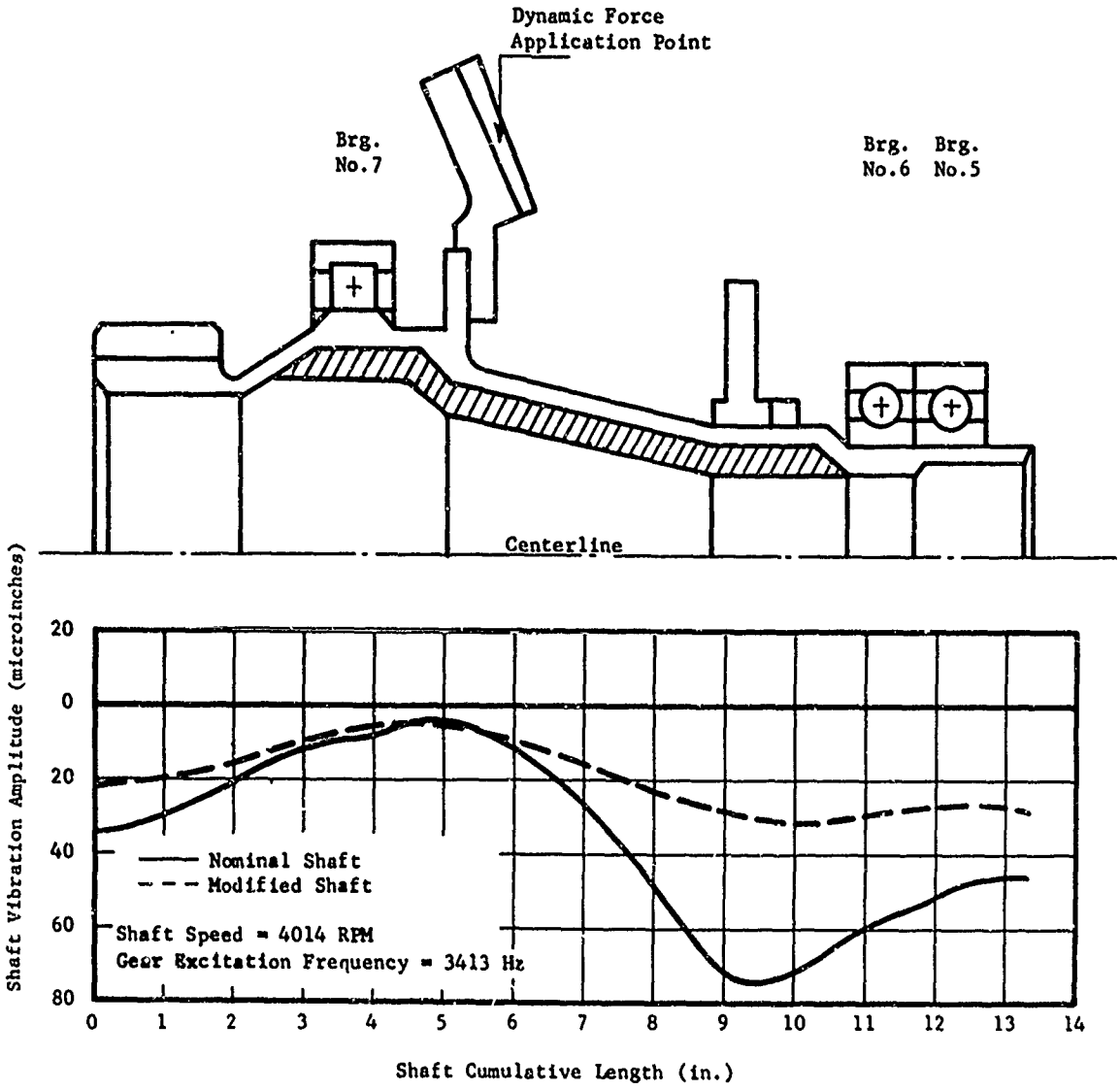

Figure 14. CH-47 Output Bevel Gear Shaft Vibration Amplitudes for Nominal and Modified Configurations.

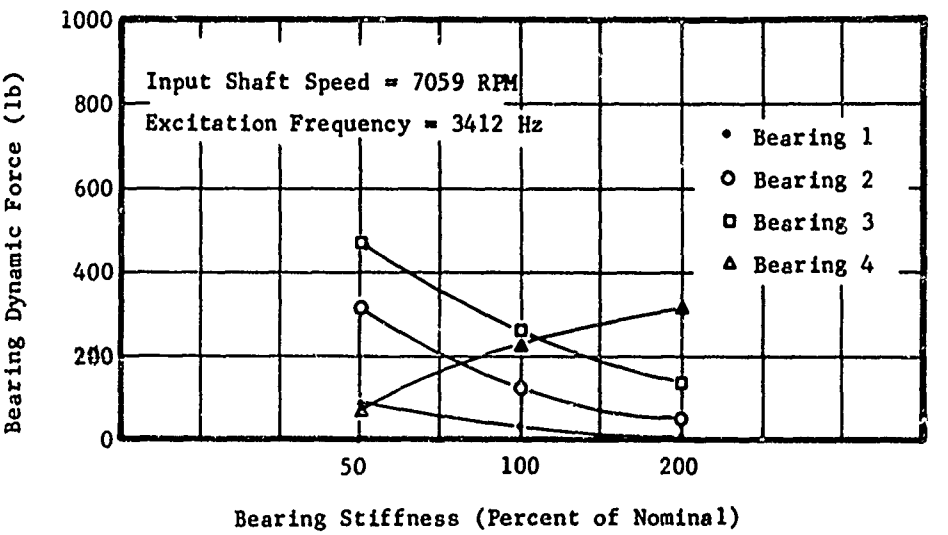

Figure 15. Effect of Bearing Stiffness Variations on Bearing Dynamic Forces for CH-47 Forward-Rotor-Drive Gearbox Input Bevel Gear Shaft - Stiffnesses Varied in Proportion to Each Other.

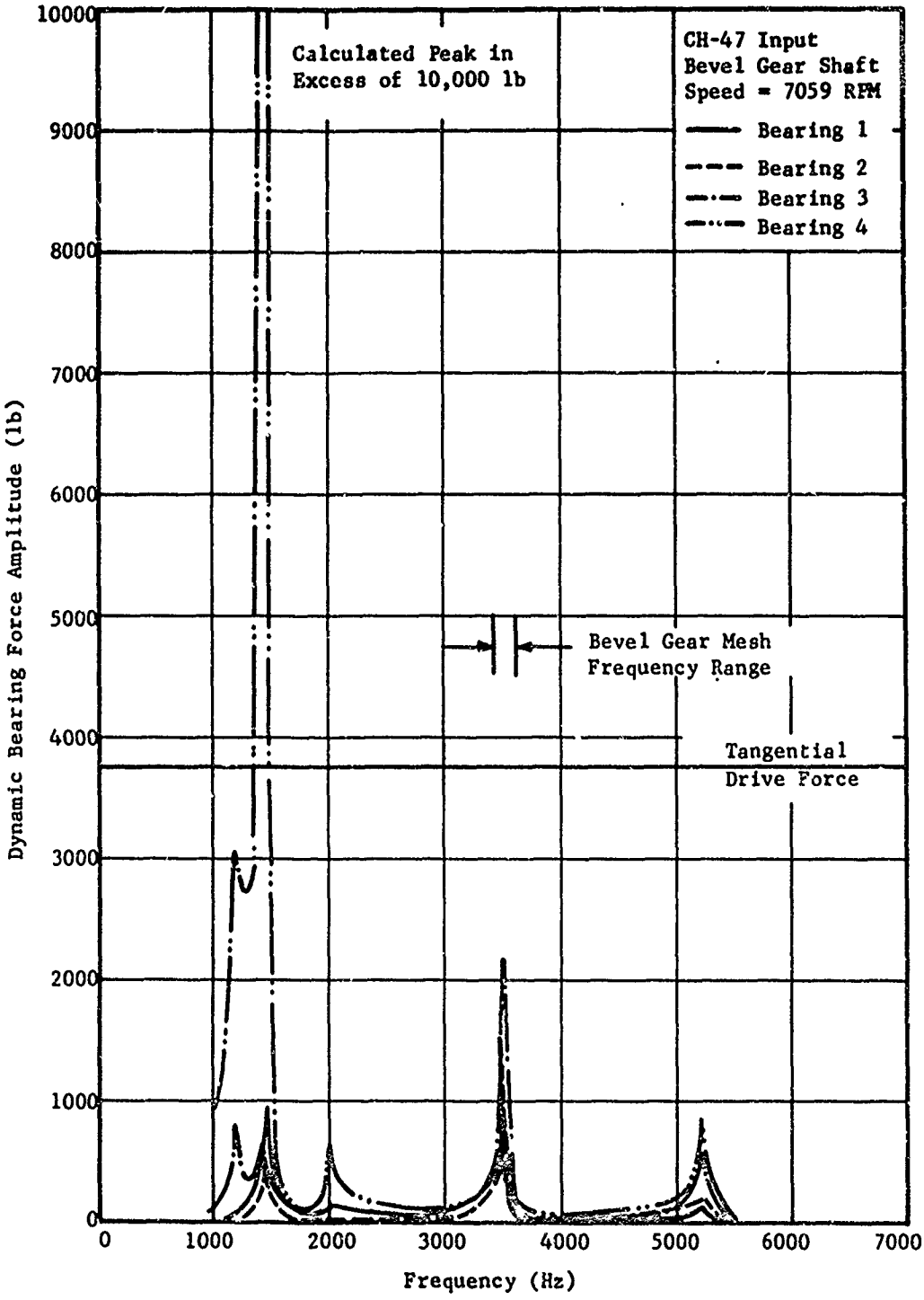

Figure 16. Calculated Dynamic Force Level With Stiffness Reduced by 50 Percent at Bearings No. 2 and 3 and Constant Value Gear-Tooth Exciting Force for CH-47 Input Bevel Gear Shaft.

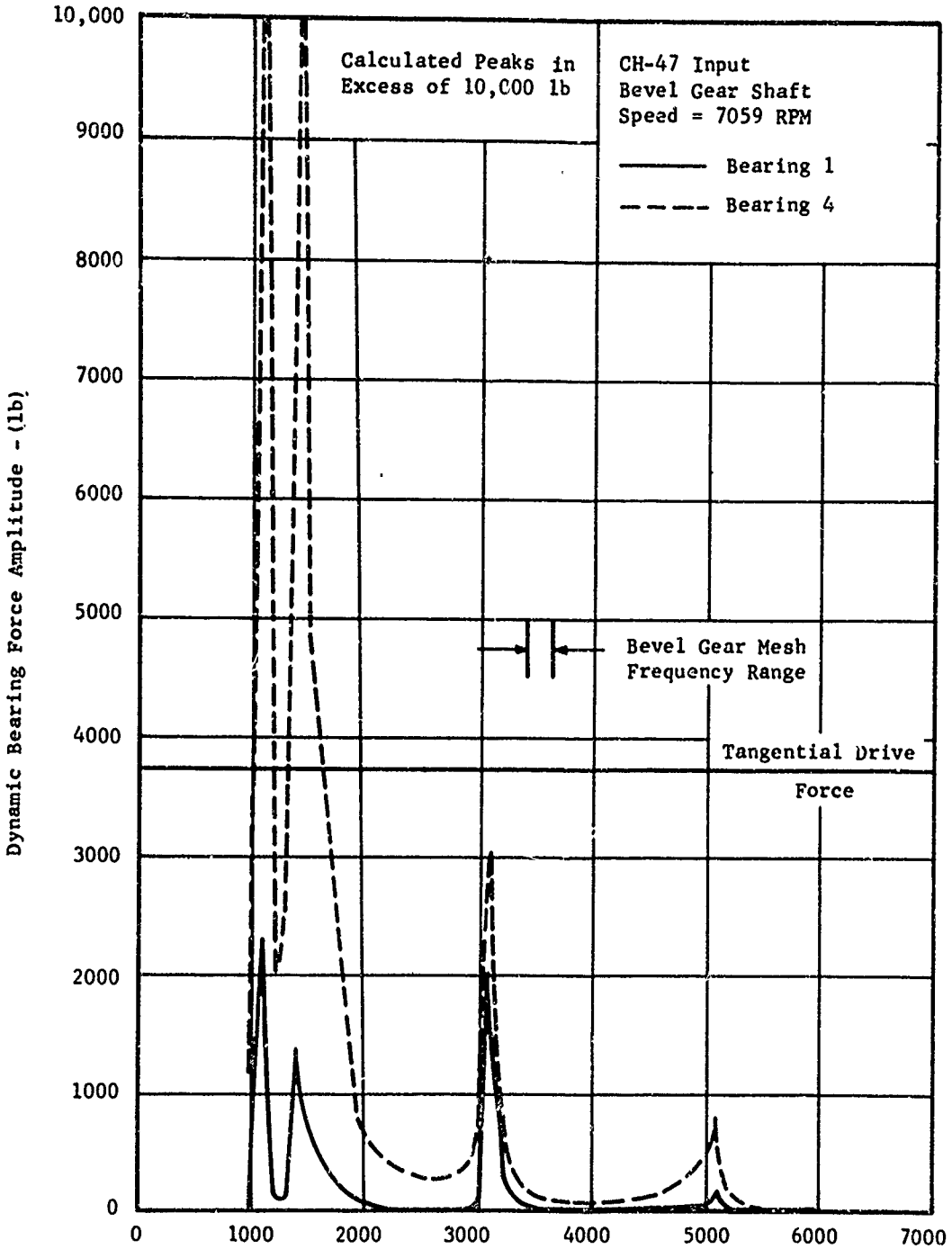

Figure 17. Calculated Dynamic Force Level at Indicated Bearings (Bearings No. 2 and 3 Removed) With Constant Value Gear-Tooth Exciting Force for CH-47 Input Bevel Gear Shaft.

DYNAMIC FORCES IN UH-1D
MAIN ROTOR-DRIVE GEARBOX BEVEL-GEAR SHAFT BEARINGS

ROLLING-ELEMENT BEARING RADIAL STIFFNESS CALCULATION

As in the CH-47 study, the first quantities required for the lateral vibrations analysis are the actual stiffnesses of the elements which support the vibrating system relative to the fixed reference plane. These calculations have been made for the bearings supporting both the input and output bevel gear shafts in the UH-1D main rotor-drive gearbox. For the purposes of the analysis, coordinate axes were assigned as follows:

	x-axis	y-axis	z-axis
Input Shaft	Horizontal (Fore-Aft, Along Shaft) Positive Forward	Vertical (Perp. to Shaft) Positive Down	Horizontal (Perp. to Shaft) Positive to Port Side
Output Shaft	Vertical (Along Shaft) Positive Upward	Horizontal (Fore-Aft, Perp. to Shaft) Positive Forward	Horizontal (Perp. to Shaft and y-axis) Positive to Port Side

Simple calculations indicated, as in the CH-47 gearbox, that the casing rolling-element support structure was reasonably rigid compared to anticipated bearing radial stiffness values. Consequently, the assumption was again made that bearing support stiffness could be neglected and that the radial stiffness of the bearings was the controlling stiffness. Such an assumption is not valid in general, however, and the gearbox designer is again cautioned to obtain guidance in this area prior to undertaking calculations of this type. (The opposite is true for turbine engines, for instance, where the bearing supports are usually quite soft compared to the bearings themselves. This situation exists because the internal forces in turbine engines are usually much lower than those in helicopter gearboxes.)

For the analyses, the following aircraft operating parameters were assumed:

Aircraft Flight Condition	Hover
Main Rotor Gearbox Horsepower	1260
Gearbox Input Shaft Speed	6600 rpm
Bevel Gear Tangential Drive Force	4320 lb

Under these operating characteristics, the steady-state forces (sign convention is with respect to the axes previously described) acting on the bevel gears are as follows:

	$F_{s,x}$ (lb)	$F_{s,y}$ (lb)	$F_{s,z}$ (lb)
Input Bevel Gear	-3540	430	4320
Output Bevel Gear	- 430	3540	-4320

Utilizing these values, the shaft dimensions and their tolerances, and the ball and roller bearing dimensions and their tolerances, the following radial stiffness values were calculated by means of a computer program developed by Mr. A.B. Jones, Newington, Connecticut, Consultant to MTI, for the bevel gear shaft bearings (bearings are numbered in the direction of power flow, and this numbering will be maintained throughout this study):

Bearing	Shaft	K_y (lb/in. x 10^{-6})	K_z (lb/in. x 10^{-6})
1	Input	3.57	2.97
2	Input	5.96	4.95
3	Input	8.93	7.66
4	Input	3.11	2.95
5	Output	5.62	2.86
6	Output	4.89	5.78
7	Output	3.96	4.70

BEVEL GEAR SHAFT LATERAL NATURAL FREQUENCIES

Bell Helicopter Company assembly drawing 205-040-001, Transmission Assembly, Mechanical, Reducer Type, Main, and subordinate drawings were used to model the input and output bevel gear shafts. Figures 18 and 19 show details of the analytical modeling which was performed for the vibration analysis. Tables IV and V present details of the dimensions and other shaft properties used in the analysis.

Following discussions with technical personnel at the Bell Helicopter Company, the model shown in Figure 18 was revised to include the mass and moment of inertia associated with that portion of the engine-to-gearbox coupling hardware in contact with the input shaft. The net effect of this mass and moment of inertia is to restrict the motion of the coupling end of the shaft, both laterally and about a diameter. The improved shaft model was used for all subsequent calculations.

The first step in a shaft lateral vibrations analysis should be the construction of a natural frequency map [5] on which are plotted the natural frequencies of the shaft-bearing system. Such a map shows the regime in which a particular shaft-bearing arrangement is operating, through comparison of the natural frequencies to each other and to the exciting frequency (in this case the mesh frequency). It also shows the behavior of the natural frequencies with respect to bearing stiffness, a characteristic which will become important during later stages in the analysis.

Natural frequency calculations were performed for the UH-1D gearbox input and output bevel gear shafts in the same manner as for the CH-47. Varying assumed bearing stiffness from 10^5 to 10^7 (all bearings assumed equal) yields the natural frequency maps shown in Figures 20 and 21 for the input and output bevel shafts, respectively. The vertical lines (bearing stiffness is typically insensitive to vibration frequency changes at constant

TABLE IV. UH-1D MAIN ROTOR-DRIVE GEARBOX INPUT BEVEL GEAR SHAFT DIMENSIONS AND PROPERTIES USED IN DYNAMICS CALCULATIONS

Shaft Station Number	Concentrated Weight (lb)	Conc. Polar Mom. of Inertia (lb-in.^{2})	Conc. Transverse Mom. of Inertia (lb-in.^{2})	Shaft Section Length to Next Station (in.)	Stiffness Outer Diameter (in.)	Mass Outer Diameter (in.)	Stiffness and Mass Inner Diameter (in.)
1	0.0	0.0	0.0	0.43	2.01	2.01	1.30
2	0.0	0.0	0.0	0.65	2.01	2.01	1.00
3	0.0	0.0	0.0	0.37	2.08	2.08	1.00
4	0.0	0.0	0.0	0.62	4.00	4.00	1.20
5	0.0	0.0	0.0	0.65	4.64	4.64	1.40
6	0.0	0.0	0.0	0.25	4.64	4.64	1.60
7	0.0	0.0	0.0	0.43	3.46	3.46	1.80
8	0.0	0.0	0.0	0.51	5.18	5.88	2.00
9	0.0	0.0	0.0	0.51	5.18	5.70	2.00
10	0.0	0.0	0.0	0.51	5.18	5.88	2.00
11	0.0	0.0	0.0	0.51	5.18	5.70	2.00
12	0.0	0.0	0.0	0.51	5.18	5.88	2.00
13	0.0	0.0	0.0	0.51	5.18	5.70	2.00
14	0.0	0.0	0.0	0.10	3.12	3.66	2.00
15	0.0	0.0	0.0	0.14	3.12	3.66	2.00
16	0.0	0.0	0.0	0.14	3.06	3.66	2.30
17	0.0	0.0	0.0	0.24	3.06	4.11	2.54
18	0.7	0.0	0.0	0.24	3.06	4.01	2.54
19	0.0	0.0	0.0	0.07	3.06	4.11	2.54
20	0.0	0.0	0.0	0.13	3.06	3.99	2.54
21	1.3	0.0	0.0	0.10	3.06	3.99	2.60
22	0.0	0.0	0.0	0.16	3.06	3.99	2.62
23	0.8	0.0	0.0	0.20	3.06	3.99	2.62
24	1.7	0.0	0.0	0.12	3.06	3.99	2.62
25	0.0	0.0	0.0	0.08	3.06	3.99	2.62
26	0.0	0.0	0.0	0.11	3.06	4.11	2.62
27	0.2	0.0	0.0	0.11	3.06	4.01	2.62
28	11.5	800000.	0.0	0.0	3.06	4.01	2.62

Young's Modulus: 29×10^6 lb/in.^{2}

Density: 0.281 lb/in.^{3}

Poisson's Ratio: 0.333

TABLE V. UH-1D MAIN ROTOR-DRIVE GEARBOX OUTPUT BEVEL GEAR SHAFT DIMENSIONS AND PROPERTIES USED IN DYNAMICS CALCULATIONS

Shaft Station Number	Concentrated Weight (lb)	Conc. Polar Mom. of Inertia (lb-in.^{2})	Conc. Transverse Mom. of Inertia (lb-in.^{2})	Shaft Section Length to Next Station (in.)	Stiffness Outer Diameter (in.)	Mass Outer Diameter (in.)	Stiffness and Mass Inner Diameter (in.)
1	0.0	0.0	0.0	1.36	4.60	4.60	3.95
2	0.0	0.0	0.0	0.35	4.29	4.29	3.95
3	0.0	0.0	0.0	0.42	4.60	4.60	3.95
4	0.0	0.0	0.0	0.20	4.73	4.73	3.95
5	0.0	0.0	0.0	0.43	4.73	5.71	3.95
6	0.0	0.0	0.0	0.43	4.73	5.71	3.95
7	0.0	0.0	0.0	0.43	4.73	5.71	3.95
8	0.0	0.0	0.0	0.43	4.73	5.71	3.95
9	0.0	0.0	0.0	0.17	5.07	5.07	3.95
10	0.0	0.0	0.0	0.57	4.72	4.72	3.95
11	0.0	0.0	0.0	0.29	4.72	4.72	3.95
12	0.0	0.0	0.0	0.29	4.72	4.72	3.95
13	0.0	0.0	0.0	0.16	4.72	7.60	3.95
14	21.0	444.0	224.4	0.16	4.72	7.60	3.95
15	0.0	0.0	0.0	0.45	4.70	4.70	3.95
16	0.0	0.0	0.0	0.45	4.70	4.70	3.95
17	0.0	0.0	0.0	0.45	4.70	4.70	3.95
18	0.0	0.0	0.0	0.45	4.70	4.70	3.95
19	0.0	0.0	0.0	0.45	4.70	4.70	3.95
20	0.0	0.0	0.0	0.45	4.70	4.70	3.95
21	0.0	0.0	0.0	0.90	4.38	4.38	3.95
22	0.0	0.0	0.0	0.90	4.38	4.38	3.95
23	0.0	0.0	0.0	0.90	4.38	4.38	3.95
24	0.0	0.0	0.0	0.57	5.15	5.15	3.95
25	0.0	0.0	0.0	0.57	5.15	5.15	3.95
26	0.0	0.0	0.0	0.12	4.38	4.38	3.95
27	0.0	0.0	0.0	.62	4.70	4.70	3.95
28	0.0	0.0	0.0	0.0	1.00	0.0	0.0

Young's Modulus: 29×10^6 lb/in.^{2}

Density: 0.281 lb/in.^{3}

Poisson's Ratio: 0.333

speed) represent the calculated bearing stiffnesses discussed earlier.

Figure 20 gives the following general information:

1. The input bevel gear shaft is being forced at the bevel mesh frequency very nearly at its second natural frequency. As the speed of the shaft increases, during run up, the input bevel gear shaft will probably pass through one natural frequency which will be of the rigid-body vibration type. (The first two critical frequencies are very nearly straight lines between stiffnesses of 10^5 and 10^7 lb/in., and thus are almost directly dependent on bearing stiffness, a characteristic of a rigid-body critical.) It should be noted that the map's vertical axis is vibration frequency, rather than shaft speed. The bearing radial stiffnesses would not, in general, be straight vertical lines on a speed versus stiffness map.

2. Bearing radial stiffnesses lower than those calculated and shown in Figure 20 will result in a lower value for the second critical frequency (decreases to the left with lower stiffness), and thus a separation between it and the mesh frequency.

When the above calculations are repeated with the radial bearing stiffness values as calculated (rather than assumed equal) in the vertical and horizontal directions separately, the following natural frequencies are obtained:

Radial Stiffnesses	First Critical (cpm (Hz))	Second Critical (cpm (Hz))
Vertical (y-axis)	88,000 (1470)	176,000 (2940)
Horizontal (z-axis)	83,000 (1380)	167,000 (2780)

Figure 21 gives the following information:

1. The output bevel gear shaft is being forced at the bevel mesh frequency at or only slightly below its second natural frequency. As the speed of the shaft increases, it will thus pass through one natural frequency, which will probably be a rigid-body vibration type. The discussion for the input shaft applies here as well.

2. Bearing radial stiffnesses lower than those calculated and shown in Figure 21 will result in a lower value for the second critical frequency, and thus increased separation between it and the mesh frequency.

When the above calculations are repeated with the radial bearing stiffnesses as calculated (rather than assumed equal) in the fore-aft and horizontal directions separately, the following natural frequencies are obtained:

Radial Stiffnesses	First Critical (cpm (Hz))	Second Critical (cpm (Hz))
Fore-Aft (y-axis)	98,200 (1635)	230,000 (3830)
Horizontal (z-axis)	95,000 (1580)	187,000 (3120)

The fact that the bearing radial stiffnesses are closer together in Figure 21 for the output shaft than in Figure 20 for the input shaft means that the results shown in Figure 21 are again somewhat easier to interpret than those in Figure 20. Both clearly indicate that the two shafts are operating in close proximity to their second critical frequencies, with the input shaft undergoing rigid-body-type vibrations and the output shaft possibly experiencing some bending.

LATERAL RESPONSE OF SHAFTS TO GEAR-MESH-INDUCED TOOTH FORCES

The results presented in Figures 20 and 21 show that both bevel gear shafts are operating with the bevel gear mesh frequency in close proximity to their second critical frequency. This portion of the analysis, which includes bearing radial stiffnesses along both the y and z axes, as well as the dynamic forces calculated in [2], is again designed to indicate more exactly the relationship between system critical frequencies and the mesh frequency. Vibration amplitudes, together with the levels of the dynamic forces transmitted across the rolling element bearings (and which are primary indicators of the levels of certain noise components), will also be obtained.

From [1], the dynamic forces (peak values) acting at the bevel gear mesh point at the mesh frequency are as follows:

	$F_{d,y}$ (lb)	$F_{d,z}$ (lb)
Input Bevel Gear	91	910
Output Bevel Gear	746	910

When these dynamic forces are applied at the bevel gear mesh frequency of 3190 Hz (equivalent to 330 rpm rotor speed), the input and output shafts vibrate (at 3190 Hz) in the mode shapes shown in Figures 22 and 23, respectively.

With respect to the input bevel gear shaft, Figure 22 shows several very important items:

1. The little bending that the shaft experiences occurs in the region between the roller bearing and the bevel gear.

2. In general, the levels of vibration are low to medium, being on the order of 0.4×10^{-3} inch or less. With calculated bearing radial stiffnesses on the order of 3×10^{6} to 9×10^{6} lb/in., therefore, dynamic forces on the order of 1000 pounds for bearing 4 (the roller bearing) to 350 pounds for the ball bearings are indicated. If forces of these magnitudes are transmitted directly to the gear-

box casing, measurable casing vibrations at the bevel mesh frequency are likely to occur, resulting in the production of noise at this frequency.

3. The roller bearing experiences about twice the vibration amplitudes of the ball bearings. The inner ball bearing experiences about twice the amplitude of the outer ball bearing.

4. Approximately the same amount of lateral vibration motion is predicted for the bevel teeth as for the roller bearing. A node is predicted, on the other hand, near the axial location of the inboard ball bearing of the overrunning clutch.

With respect to the output bevel gear shaft, Figure 23 shows several important items:

1. The shaft is experiencing bending, and since the vibrations are not at the rotational speed, it is flexing.

2. In general, the vibration levels are reasonably low, on the order of 0.2×10^{-3} inch. With bearing radial stiffnesses on the order of 3×10^6 to 6×10^6 lb/in., however, dynamic forces on the order of 900 lb are indicated for the roller bearing, and on the order of 250 lb for the ball bearings. Again, transmission of forces of this magnitude to the gearbox casing would appear likely to result in measurable casing vibration levels at this frequency.

3. The duplex ball bearings (numbers 6 and 7) experience somewhat lower vibration levels than the roller bearing (number 5).

4. The sun gear (upper end of the output bevel gear shaft) experiences considerably more lateral vibration than that part of the shaft supported by the roller bearings. It may be anticipated, therefore, that vibration side bands might be found at frequencies equal to the bevel mesh frequency plus and minus the lower planetary sun planet mesh frequency, that is, at $3190 \pm 1982 = 1208, 5172$ Hz.

In the effort to demonstrate the relationship of the shaft lateral natural frequencies to the bevel gear mesh frequency, the response calculations described above were repeated at other frequencies, while keeping the shaft rotational speed constant. Bearing stiffnesses and exciting forces were kept constant. This latter assumption is adequate with regard to the bearing properties. There is, of course, a strong likelihood that the dynamic forces would be different at any other frequency if there was a source of excitation at each frequency considered. The vibration amplitudes and forces are therefore strictly correct (analytically) at

the bevel mesh frequency of 3190 Hz. The utility of such a frequency sweep is that it immediately identifies the location of system critical frequencies (through locations of force and amplitude peaks) and it gives an indication of the relative severity of each critical frequency should a source of vibration be present at that frequency. Figures 24 and 25 present the results of frequency sweeps for the UH-1D input and output bevel gear shafts, respectively.

With respect to the input shaft, Figure 24 shows several important results:

1. There is a significant peak in the bearing transmitted forces for all four bearings very close to the normal operating range of the bevel gear mesh frequency. This peak probably corresponds to the second critical frequency identified in Figure 20.

2. There is a smaller but still significant transmitted force peak near 1300 Hz, which also happens to be approximately the second harmonic of the upper planetary mesh frequency. Thus, excitations from that source must be considered as a potential means for exciting what appears to be the shaft's first critical frequency.

3. There is apparently a third critical frequency at about 5800 Hz, which is considerably above the second critical frequency identified in Figure 20.

4. The calculated bearing dynamic force levels at the bevel gear mesh frequency (3190 Hz) are on the order of 400 to 1800 lb peak.

While very high dynamic forces are shown in Figures 24 and 25, this is calculated data which assumes both rigid supports and no damping. Both flexible supports and the presence of damping would obviously act to reduce these force levels. Of prime concern is the location of the second critical frequency peak relative to the mesh frequency. Figure 20 indicates that this peak is very nearly at the mesh frequency, while Figure 24 indicates that the peak is slightly below the mesh frequency.

It is felt to be very likely that the actual supporting structure will exhibit lower stiffness than those levels assumed for these calculations, and that the mesh frequency will therefore very likely be above the second critical frequency in actual operation. The effects of changes to various bearing stiffness properties will be explored in the next section. With the anticipated location of the force peak below the mesh frequency, it is likely that the bevel gear noise component will intensify at slightly lower gearbox shaft speeds.

Figure 25 also exhibits several interesting results:

1. A force peak is found at or slightly above the bevel mesh frequency. This peak apparently corresponds to the second system critical frequency shown in Figure 21.

2. There are distinct critical frequencies at about 1400 to 1500 Hz (84,000 to 90,000 cpm) and 1800 Hz (108,000 cpm), which appear to correspond to the first critical frequency, as shown in Figure 21. The appearance of several force peaks is apparently due to different bearing stiffnesses in the horizontal and vertical directions.

3. The bearing dynamic forces at the bevel gear mesh frequency (3190 Hz) are on the order of 250 to 1000 lb peak.

The comments made earlier relative to the calculated peak values and the likelihood of their attenuation by increased support flexibility and damping apply here as well.

SHAFT-BEARING MODIFICATIONS FOR VIBRATION AND NOISE REDUCTION

While it is impossible under this investigation to consider each of the many system modifications which could be used to reduce UH-1D bevel gear shaft vibration, and therefore noise levels, it is both instructive and useful to demonstrate the types of modifications which should be considered. The ease of considering these modifications first analytically, before proceeding to the test cell, will again become apparent as the range of modifications is explored.

The relative cost savings which may be achieved by ruling out marginal changes prior to testing will also become obvious. In each modification, as in the CH-47 studies, the criteria against which the modification will be judged are the relative reductions in shaft-to-bearing vibration amplitude, and thus in bearing transmitted force, compared to the nominally calculated vibration amplitudes (recall that bearing amplitude and force are proportional).

Structural Changes to the Shafts

Several changes to noncritical (i.e, inner or nonbearing surface) diameters were made to demonstrate the reduction in shaft vibration amplitudes which can be achieved by stiffening or selectively increasing the mass of the bevel gear shafts. Figure 26 shows the results of a change to the input bevel gear shaft, while Figures 27 and 28 present results for the output bevel gear shaft.

In Figure 26, an additional wall thickness was added to the inboard end of the input shaft, as indicated by the shaded area. The calculated result of this change is to decrease the vibration levels undergone by the gear and bearings by about 15 percent, with the vibration node location remaining fixed near the axial location of the inboard clutch ball bearing. This modification should result in lower levels of noise at the bevel mesh frequency, should reduce bevel gear tooth wear (if any) and should increase bearing lifetimes.

In Figure 27, an additional wall thickness was added in order to stiffen the shaft in the neighborhood of the gear mounting disc. Less

bending and generally lower vibration levels are achieved, with ball bearing vibration levels reduced by about 15 percent, sun gear vibration levels reduced by about 30 percent, and roller bearing vibration levels reduced by about 60 percent.

In Figure 28, additional material is added to the outer diameter, in addition to the first change shown in Figure 27. Little, if any, additional benefit is gained with respect to vibration levels at the sun gear, ball bearing, and gear locations, but roller bearing vibration levels are reduced to about 32 percent of the original value.

From these results, it appears that significant reductions in shaft vibration levels may be achieved through reasonable and carefully calculated shaft configuration changes.

Stiffening a shaft tends to increase its bending natural frequencies, in general, while the addition of mass has the opposite effect. The net result achieved will depend upon the relationship of the critical frequencies to the mesh frequency, and the relative importance of the stiffening compared to the effect of the added mass.

Bearing Stiffness Modifications

Several options are available to the designer with respect to modifications to the stiffness properties of the rolling element bearings. Changes may be made to all bearings together, or to individual bearings if prior knowledge exists about the effects of such changes upon the bearing dynamic forces. It is again instructive to first make equal percentage changes to all bearings in order to determine the effects of such changes upon the critical parameter (the bearing dynamic forces). This was done for the UH-1D input bevel gear shaft, with calculations performed at both 50 percent and 200 percent of the nominal values presented earlier. The bearing dynamic forces resulting from these calculations are shown, together with the nominal values, in Figure 29. The resulting vibration levels and mode shapes are shown in Figure 30 for comparison with the nominal values.

Figure 29 shows that increases in the stiffnesses of all the bearings would result in slightly lower dynamic forces. Figure 24 shows that the shaft's second critical frequency is predicted to be slightly below the bevel gear mesh frequency. The increase in bearing stiffnesses results in lower bearing dynamic forces because the second critical frequency is shifted upward, apparently slightly above the mesh frequency. Although Figure 29 shows that the largest calculated bearing dynamic forces occur at the nominal values of bearing stiffness, there is very likely a peak in the forces between the nominal and twice nominal values of stiffness. The major information gained from this stage of the analysis, however, is that there is apparently a shaft resonance at a frequency only slightly below the bevel mesh frequency.

While it is difficult to determine exact values of the radial stiffnesses which would be experienced during actual operation of the input and output

bevel gear shaft rolling-element bearings, it is very likely that they will be less than the nominal values discussed earlier. It is also likely that they will vary with operating parameters, such as the input shaft thrust load, which will vary with the level of power which is transmitted to the rotor. While perhaps time consuming, a dynamics analysis which considers the effects of changes in assembly fits or in operating parameters is feasible and should be considered as part of future design procedures. Only through such a study can the complex system vibration characteristics be understood and allowed for. Thus, some of the apparently conflicting observations on the effects of certain aircraft operating parameters such as rotor speed and power setting upon noise level may be explained.

A design which contains a shaft critical frequency so close to an important mesh frequency should be modified to place the critical frequency 25 percent to 30 percent below the lower limit of the mesh frequency range. This may be accomplished by radially softening the bearing supports, for instance. Properly designed, such a modification could result in lower vibration and noise levels, through avoidance of a resonance, rather than higher levels, which are usually associated with a softer system.

Shaft Material Modifications

While changes to basic shaft geometry and bearing stiffness characteristics are important methods which may prove usable for decreasing noise and acoustic-frequency vibration levels, modifications to the shaft material should be considered for completeness. Such changes were considered for the UH-1D output bevel gear shaft, both separately and in combination with geometry changes.

Figure 31 shows the vibration mode shapes for both the nominal output bevel gear shaft (6470 steel) and for the same shaft fabricated from titanium (designation C130AM) having a Young's modulus of 15.5×10^6 lb/in.^{2} and a density of 0.163 lb/in.^{3}. There is a considerable reduction in vibration amplitude predicted at the roller bearing and sun gear locations, little change at the ball bearing locations, and a definite increase at the bevel gear location. Figure 32 presents similar results for titanium material together with the modified geometry shown in Figure 28. It is not intended to specify a particular material for future designs, but rather to illustrate the magnitude of the benefits which may be achieved through use of a material with higher Young's modulus and lower density.

Damping Modifications

The addition of damping can sometimes be used to reduce vibration levels. This approach is certainly feasible to consider for the reduction of acoustic-frequency vibration amplitudes in the UH-1D. The background discussion of system damping presented in the section dealing with the CH-47 applies here as well.

The use of a radial viscous damper was investigated for the UH-1D input bevel gear shaft in order to illustrate the amount of acoustic-frequency vibration reduction which could be achieved by this method. A damper having a damping constant of 100 lb-sec/in. was positioned for calculation purposes at bearing 4 (the roller bearing). The resulting shaft mode shape and vibration amplitudes in Figure 33 show vibration reductions of about 28 percent.

Summary of Results of Modifications

The potential usefulness of several system modifications for the reduction of acoustic-frequency vibrations has been demonstrated in the foregoing sections by means of digital computer dynamic simulation. In each case, the dynamic behavior of the modified shaft/bearing system has been compared to the nominal behavior of that component, using as a basis for comparison the levels of both vibration amplitude and bearing dynamic force.

There are two ways in which this type of information may be used for the UH-1D:

1. It can be used, together with carefully conducted and documented test cell measurements, to confirm the regimes of operation of the gearbox interior shafts (bending versus rigid-body, for instance). Good correlation between calculated and measured mode shapes and levels of vibration provides a good indication of the relative importance of the several paths by which acoustic-frequency energy reaches the ear.

2. It can also be used to evaluate the usefulness of proposed gearbox modifications. It is far less costly to calculate the dynamic behavior of modified gearbox components than to build them and evaluate their performance in the test cell.

It is instructive to compare the modifications considered for the UH-1D with respect to the effective noise reduction, in db, which each could theoretically achieve. This comparison may be made by examining the changes in bearing dynamic forces which result from each modification. The assumption was made that the gearbox casing is relatively rigid compared to the bearing radial stiffness values, and the dynamic forces were calculated for both the nominal and modified configurations.

For the UH-1D as for the CH-47, even though the gearbox casing is relatively rigid, it will undergo some vibration, probably of very low amplitude (the vibration which produces the noise generated by the casing). The levels of this vibration will again be proportional to the bearing dynamic forces, assuming no local casing structural resonances. Hence, changes in dynamic force levels may be used to indicate changes in vibration amplitude, and thus in the level of certain noise components.

Since the bearing dynamic forces act on a relatively small part of the casing (particularly in the case of the input bevel gear shaft) at the

same frequency and in the same phase relationship to each other, it is convenient to sum their amplitudes and to take the resulting number as an equivalent dynamic force acting on the inside of the casing. The changes in this equivalent force are then representative of noise level changes, which may be expressed by Equation (1). The noise changes calculated by Equation (1) are shown in Table VI for the several shaft-bearing system modifications discussed above.

Several physical changes to the drive train may be beneficial from the standpoint of reducing the levels of certain noise components (not to mention increased bearing lifetime). However, these changes are only <u>representative</u> of many which may prove usable. There are very likely others which will yield even greater noise reductions. The optimum can only be determined through a systematic study. Such changes must ultimately be evaluated by a competent gearbox designer, who must be concerned with their implementation from the standpoints of practicality and safe operation.

TABLE VI. SUMMARY OF RESULTS OF SHAFT-BEARING SYSTEM MODIFICATIONS FOR REDUCTION OF BEVEL GEAR MESH-FREQUENCY NOISE COMPONENT FOR UH-1D MAIN ROTOR-DRIVE GEARBOX

Bevel Gear Shaft	Description of Modification	Peak Bearing Dynamic Force (lb) Bearing 1	Bearing 2	Bearing 3	Bearing 4	Equivalent Reduction in Bevel Gear Noise Component (db)
Input	Nominal Design	374.3	916.4	1851.7	1053.2	-
	Decrease of Inner Diameter (see Figure 26)	296.6	725.5	1465.4	854.9	2.0
	50% Decrease of Bearing Stiffness	77.8	182.9	355.5	200.3	14.2
	100% Increase of Bearing Stiffness	301.7	803.3	1749.2	999.1	0.7
	Damping of 100 lb-sec/in. Added to Bearings	263.0	641.9	1295.0	902.2	2.6
		Bearing 5	Bearing 6	Bearing 7		
Output	Nominal Design	531.9	228.0	282.1		-
	Increase of Outer Diameter (see Figure 27)	262.3	192.0	205.2		4.0
	Increase of Outer Diameter (see Figure 28)	218.9	191.7	214.7		4.4
	Titanium C 130 AM - Evaluation for Shaft Material Type of Modification	173.2	256.0	220.6		4.1

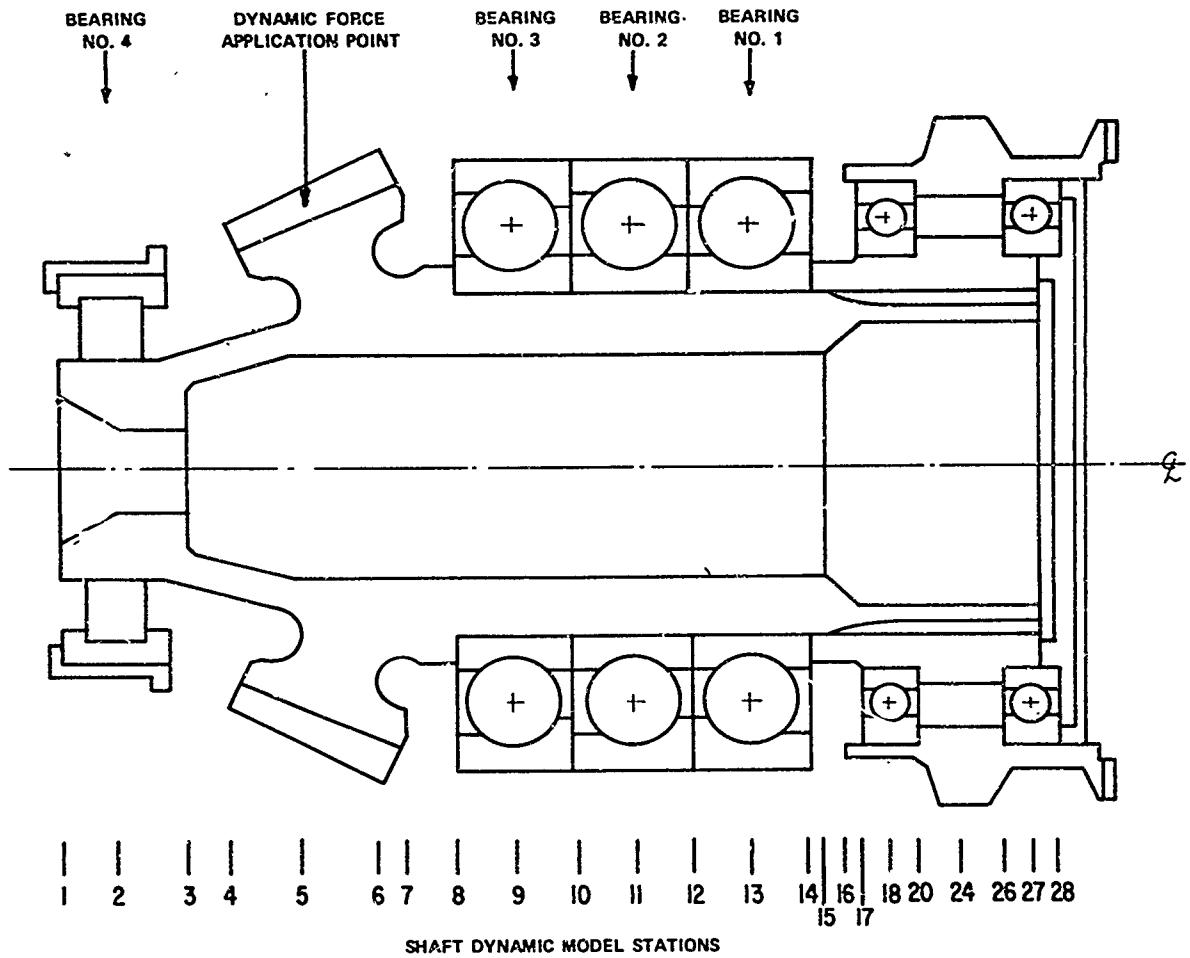

Figure 18. UH-1D Input Bevel Gear Shaft Dynamic Modeling Details.

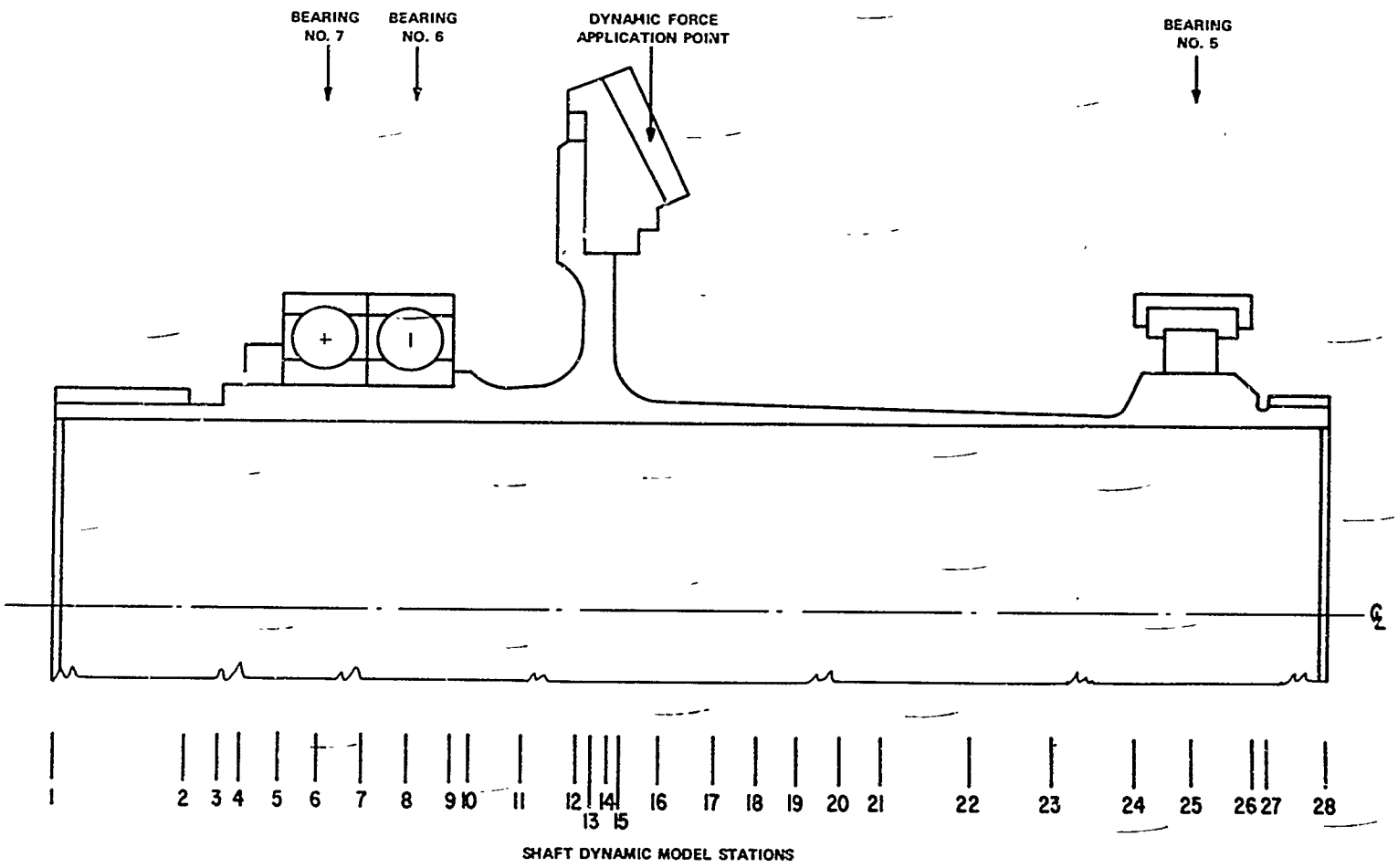

Figure 19. UH-1D Output Bevel Gear Shaft Dynamic Modeling Details.

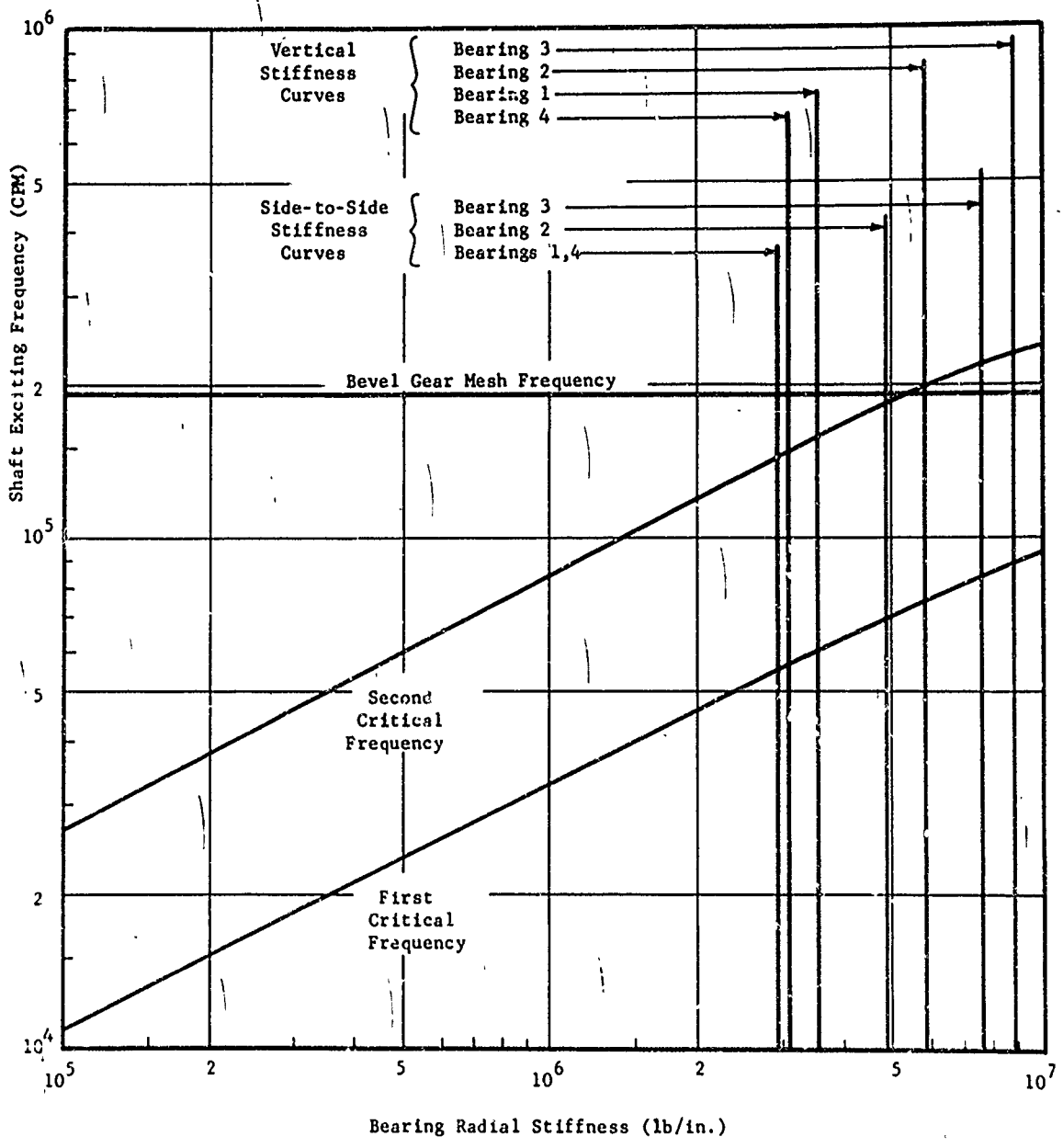

Figure 20. Critical Frequency Map for UH-1D Main Rotor Gearbox Input Bevel Gear Shaft.

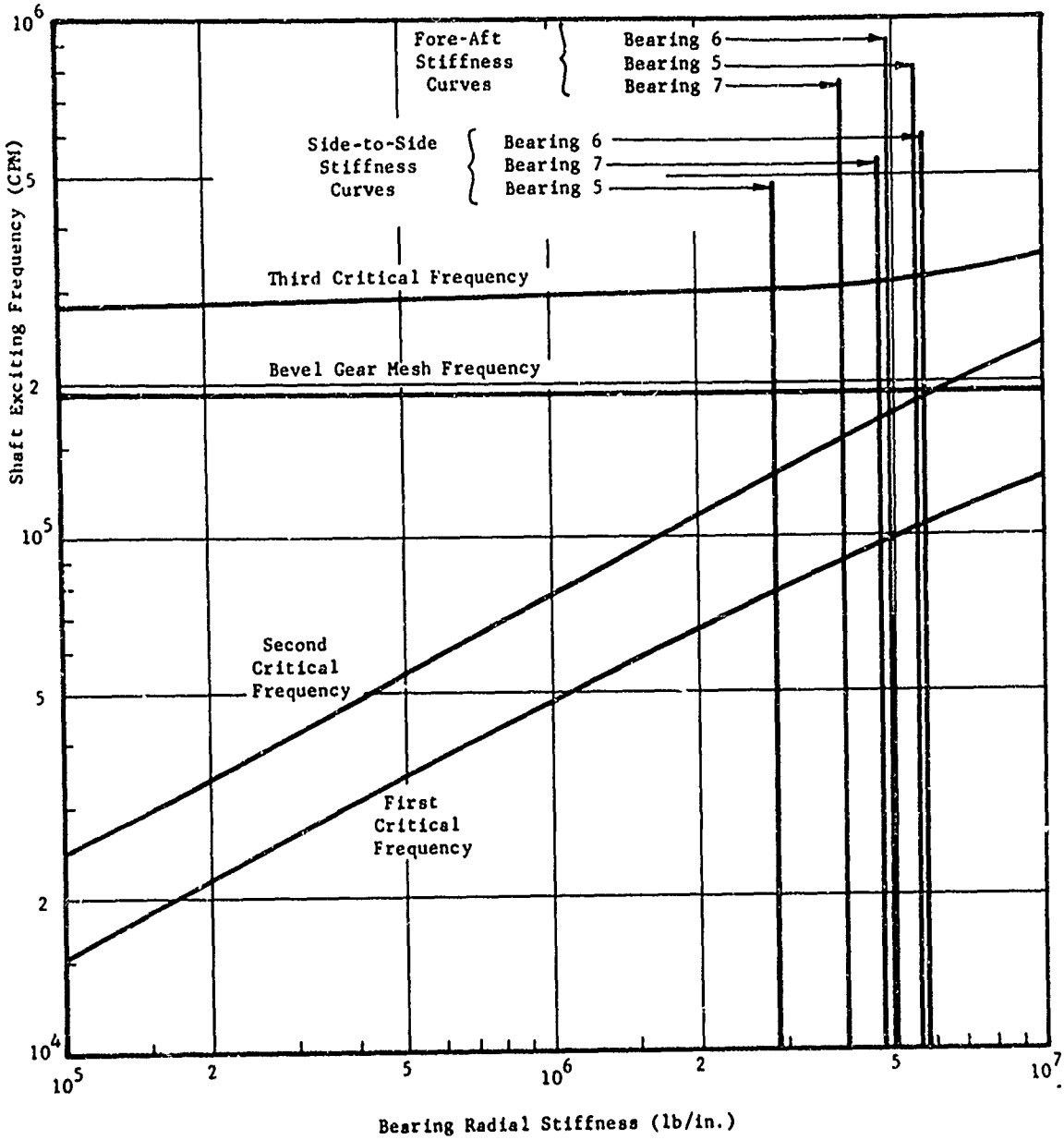

Figure 21. Critical Frequency Map for UH-1D Main Rotor Gearbox Output Bevel Gear Shaft.

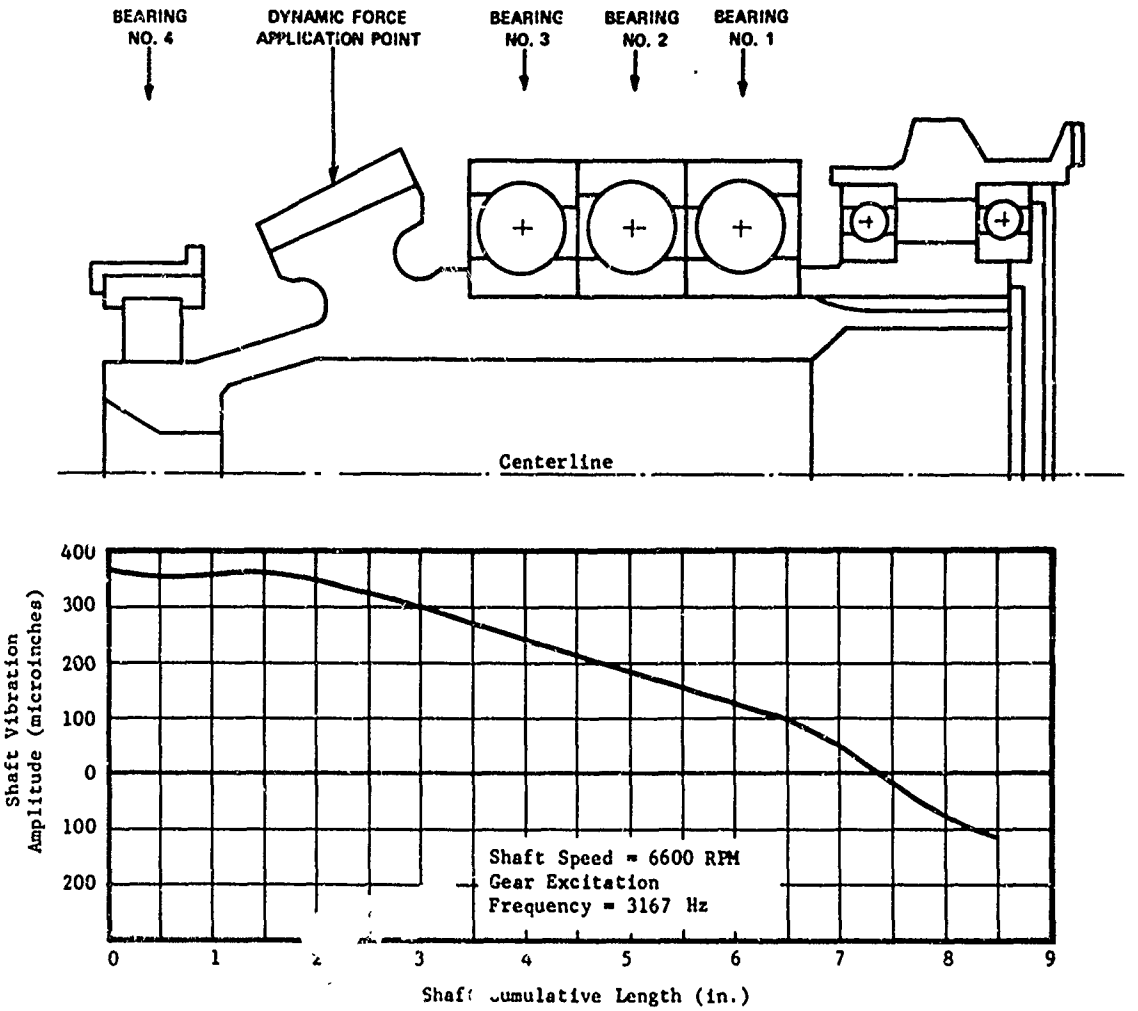

Fi .. 22. Calculated Vibration Amplitudes for UH-1D Input Bevel Gear Shaft - Nominal Configuration.

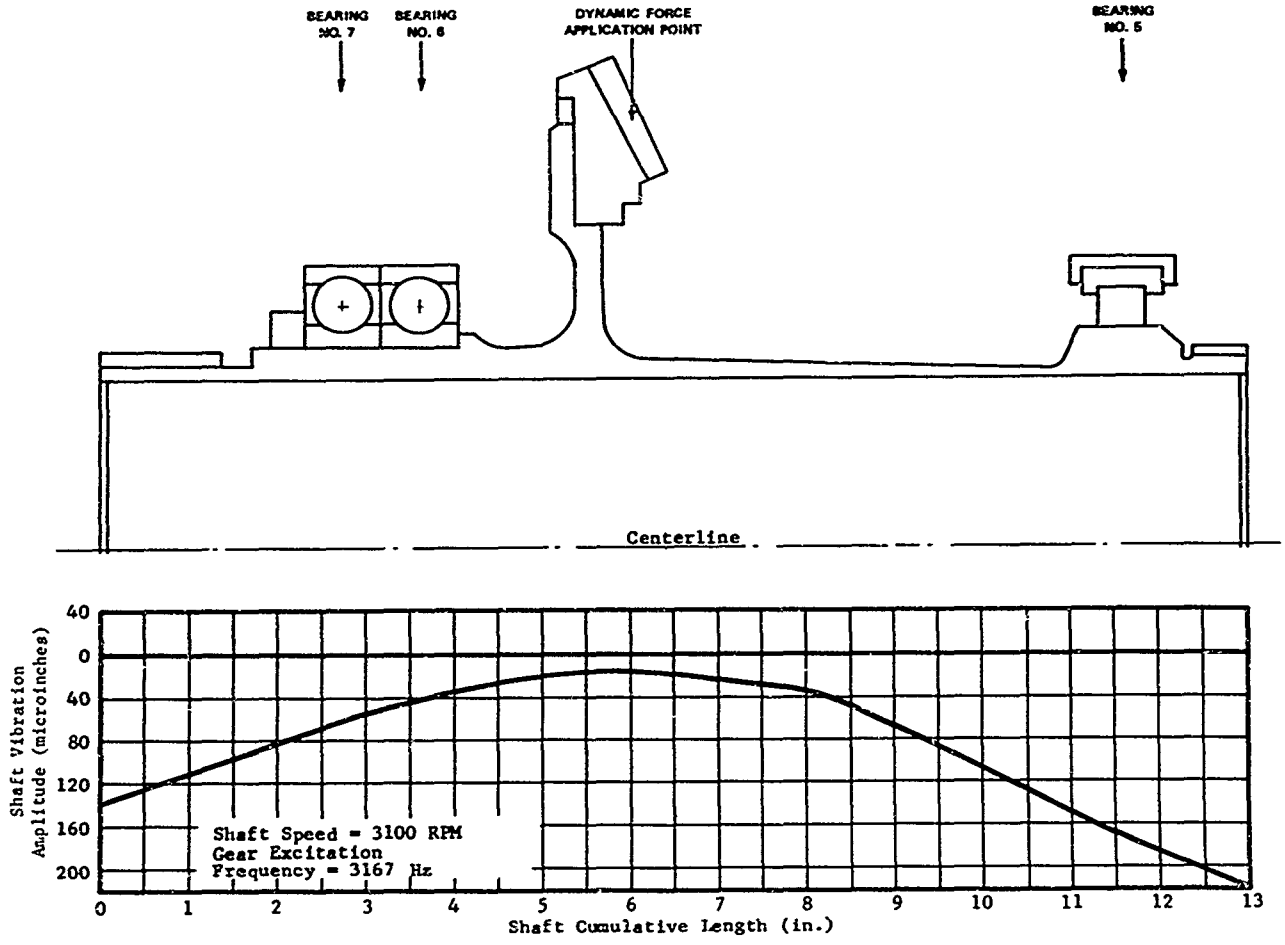

Figure 23. Calculated Vibration Amplitudes for UH-1D Output Bevel Gear Shaft — Nominal Configuration.

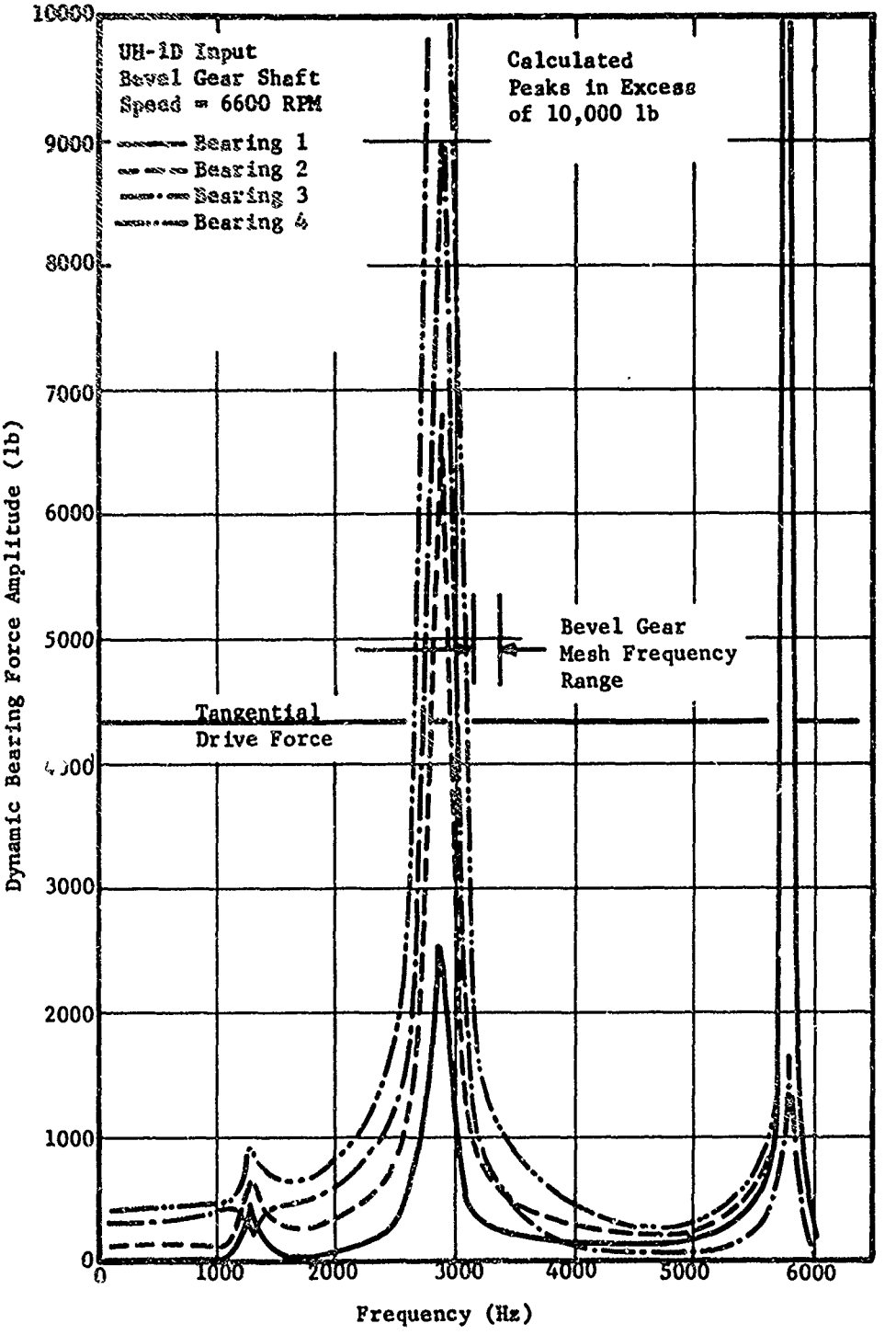

Figure 24. Calculated Dynamic Force Levels at Indicated Bearings With Constant Value Gear-Tooth Exciting Force for UH-1D Input Bevel Gear Shaft.

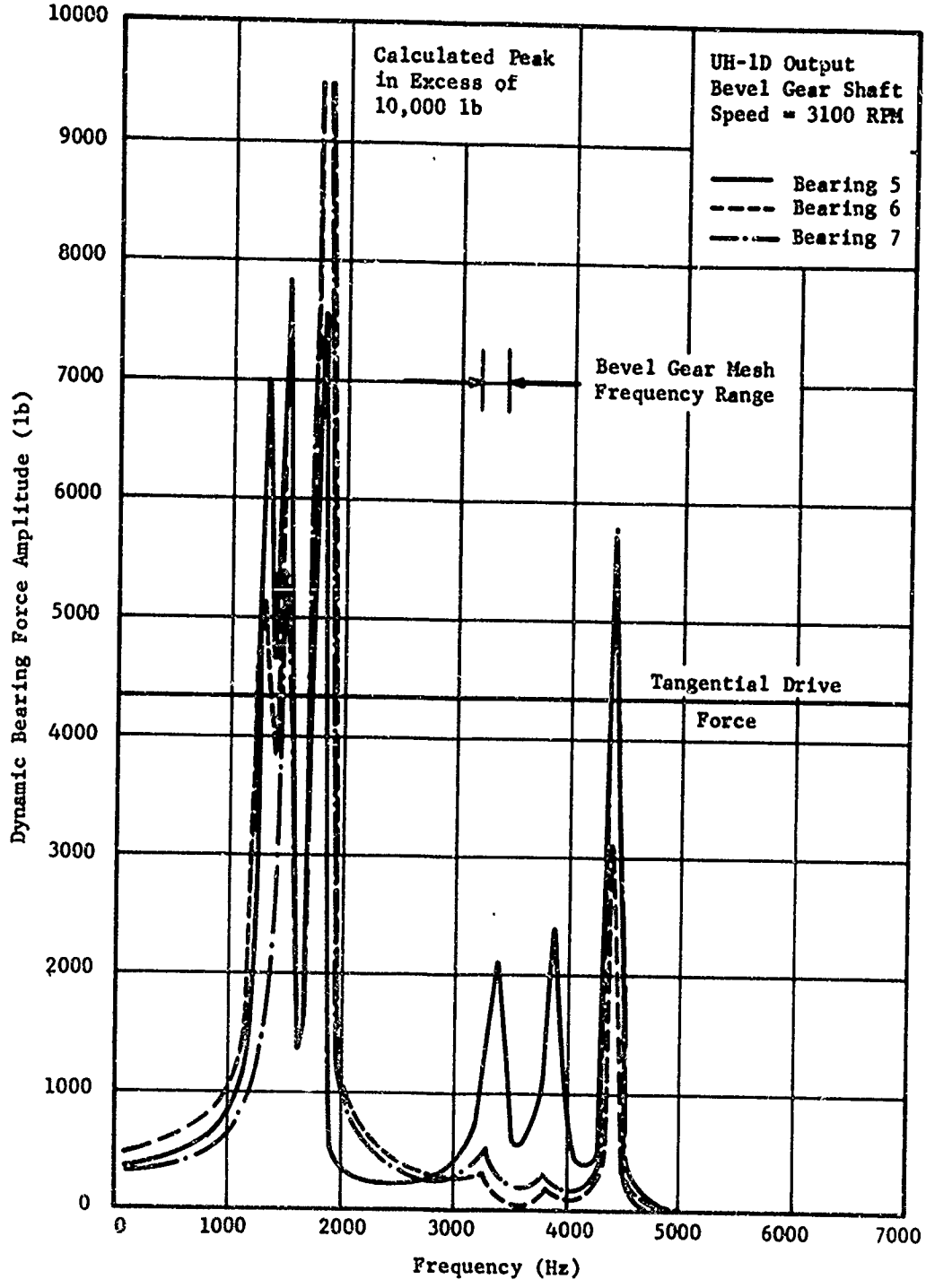

Figure 25. Calculated Dynamic Force Levels at Indicated Bearings With Constant Value Gear-Tooth Exciting Force for UH-1D Output Bevel Gear Shaft.

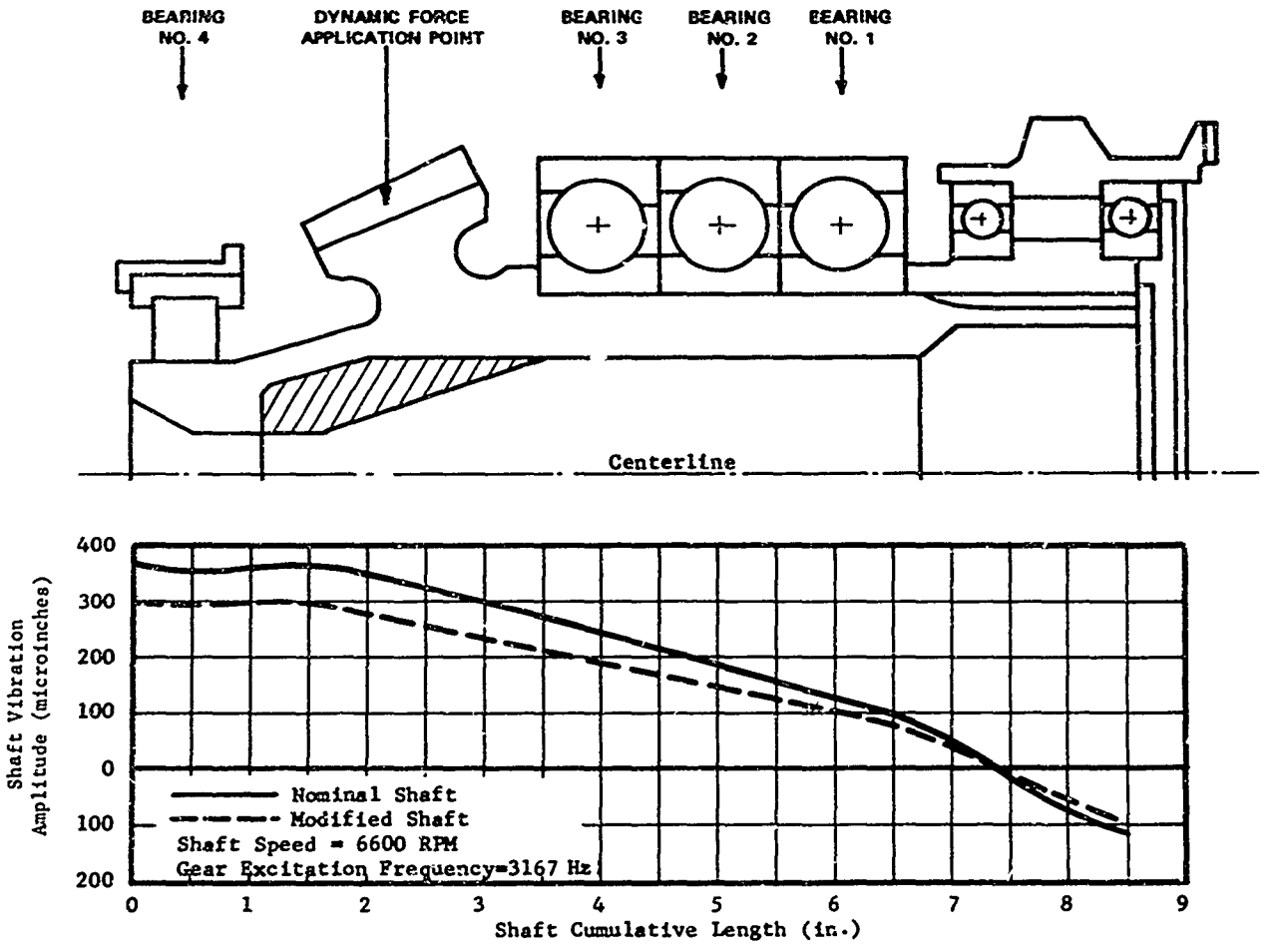

Figure 26. Calculated Vibration Amplitudes for UH-1D Input Bevel Gear Shaft for Nominal and Modified Configurations.

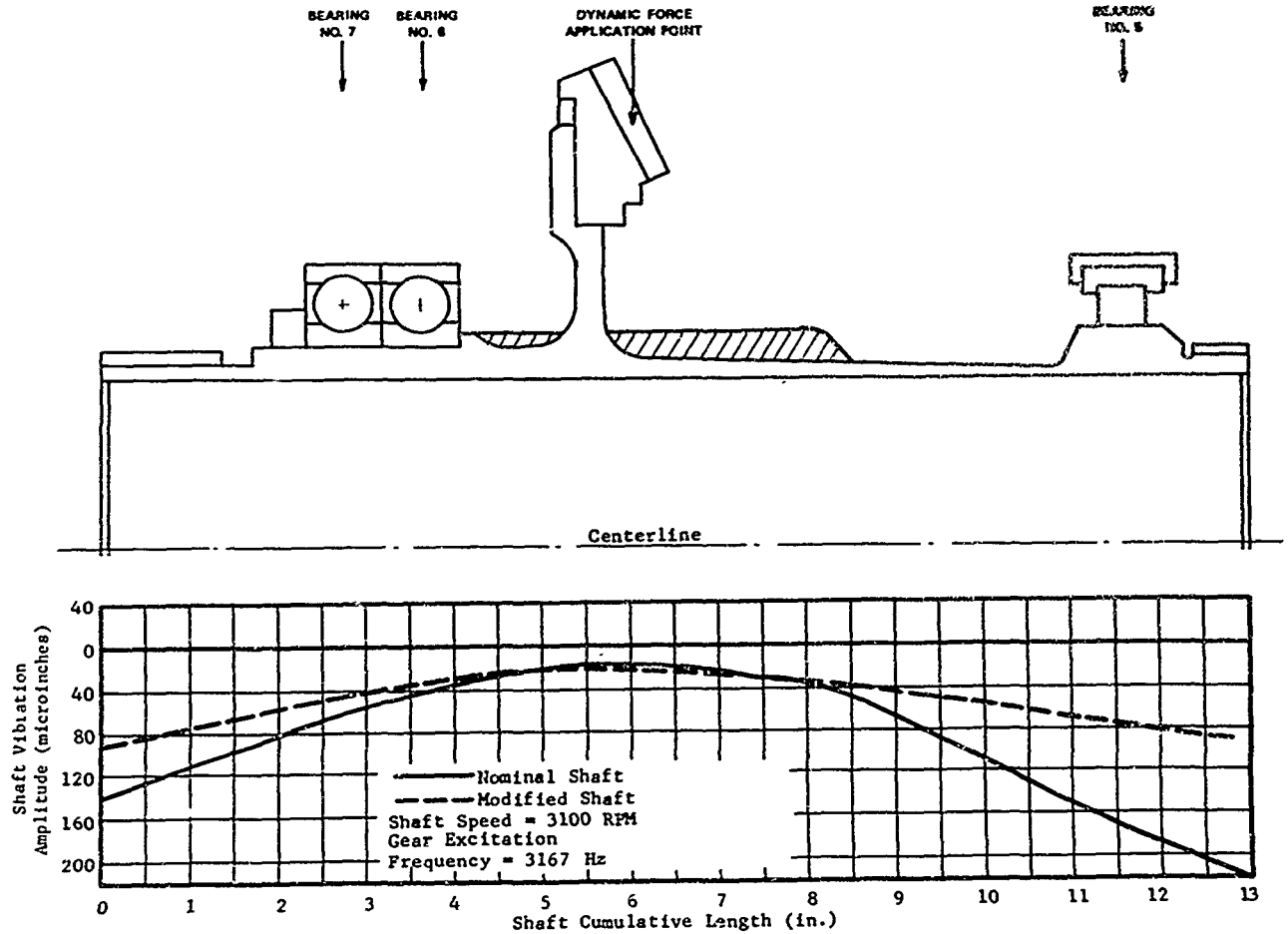

Figure 27. Calculated Vibration Amplitudes for UH-1D Output Bevel Gear Shaft for Nominal and Modified Configurations.

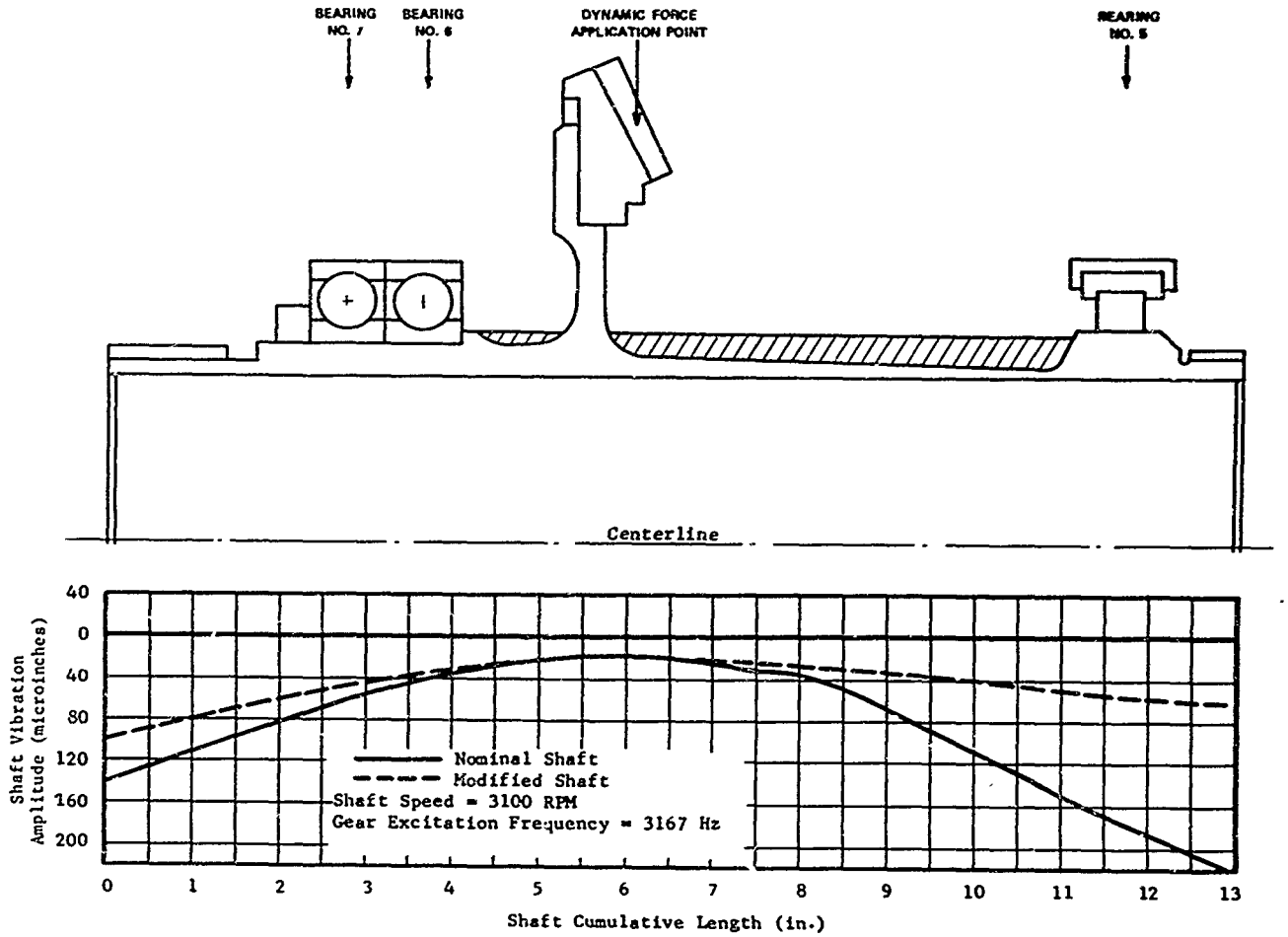

Figure 28. Calculated Vibration Amplitudes for UH-1D Output Bevel Gear Shaft for Nominal and Modified Configurations.

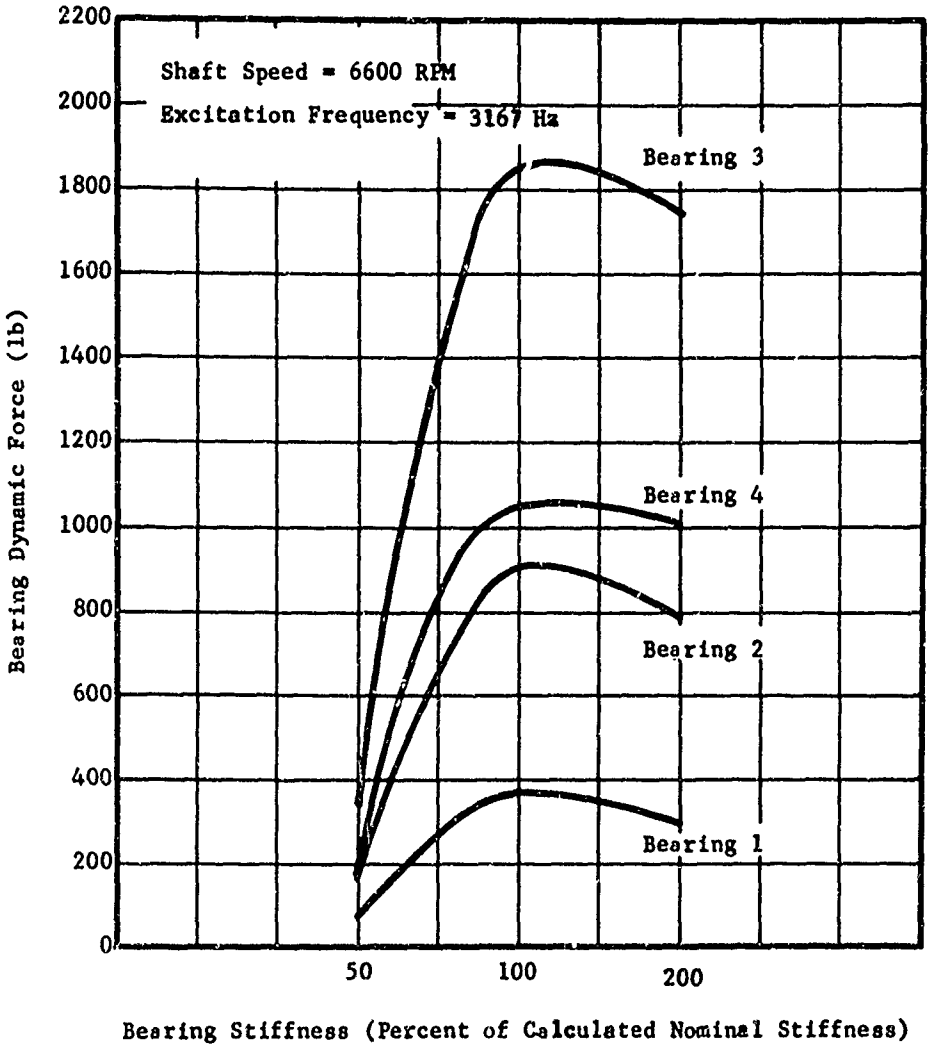

Figure 29. Effect of Bearing Stiffness Variations on Bearing Dynamic Forces for UH-1D Rotor-Drive Gearbox Input Bevel Gear Shaft - Stiffnesses Varied in Proportion to Each Other.

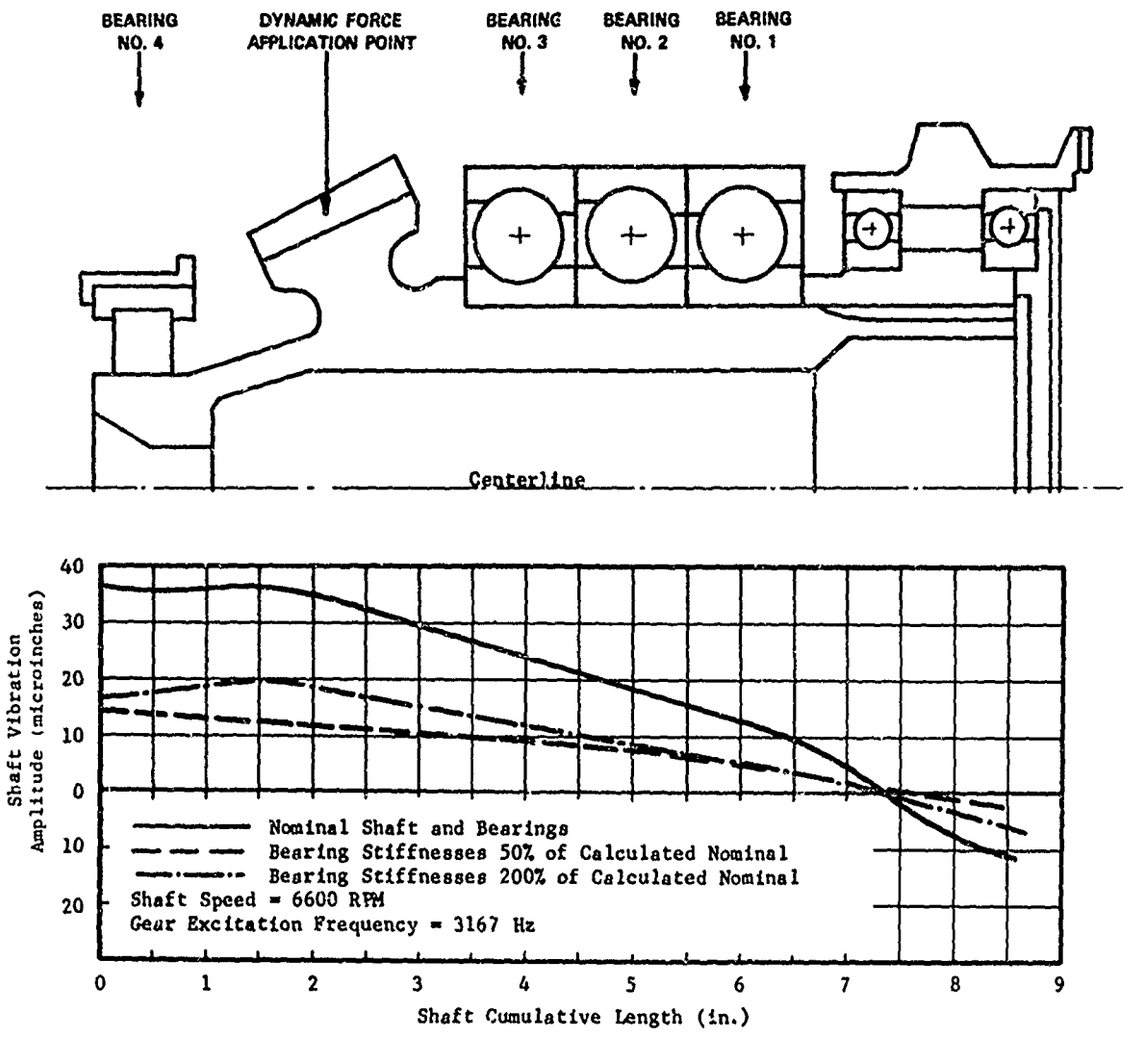

Figure 30. Calculated Vibration Amplitudes for UH-1D Input Bevel Gear Shaft for Nominal and Modified Bearing Stiffnesses.

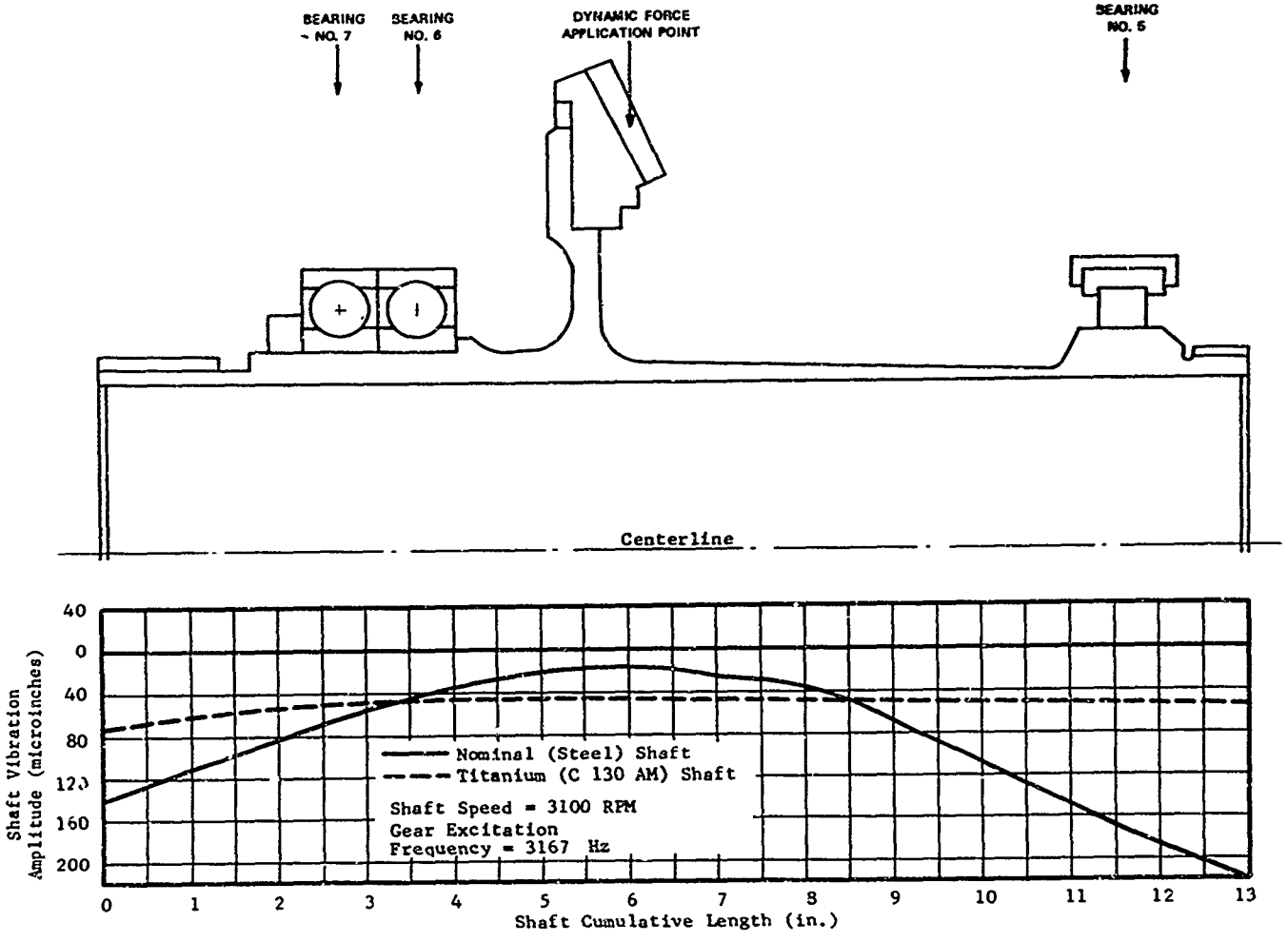

Figure 31. Calculated Vibration Amplitudes for UH-1D Output Bevel Gear Shaft for Nominal (Steel) and Titanium (C 130 AM) Configurations.

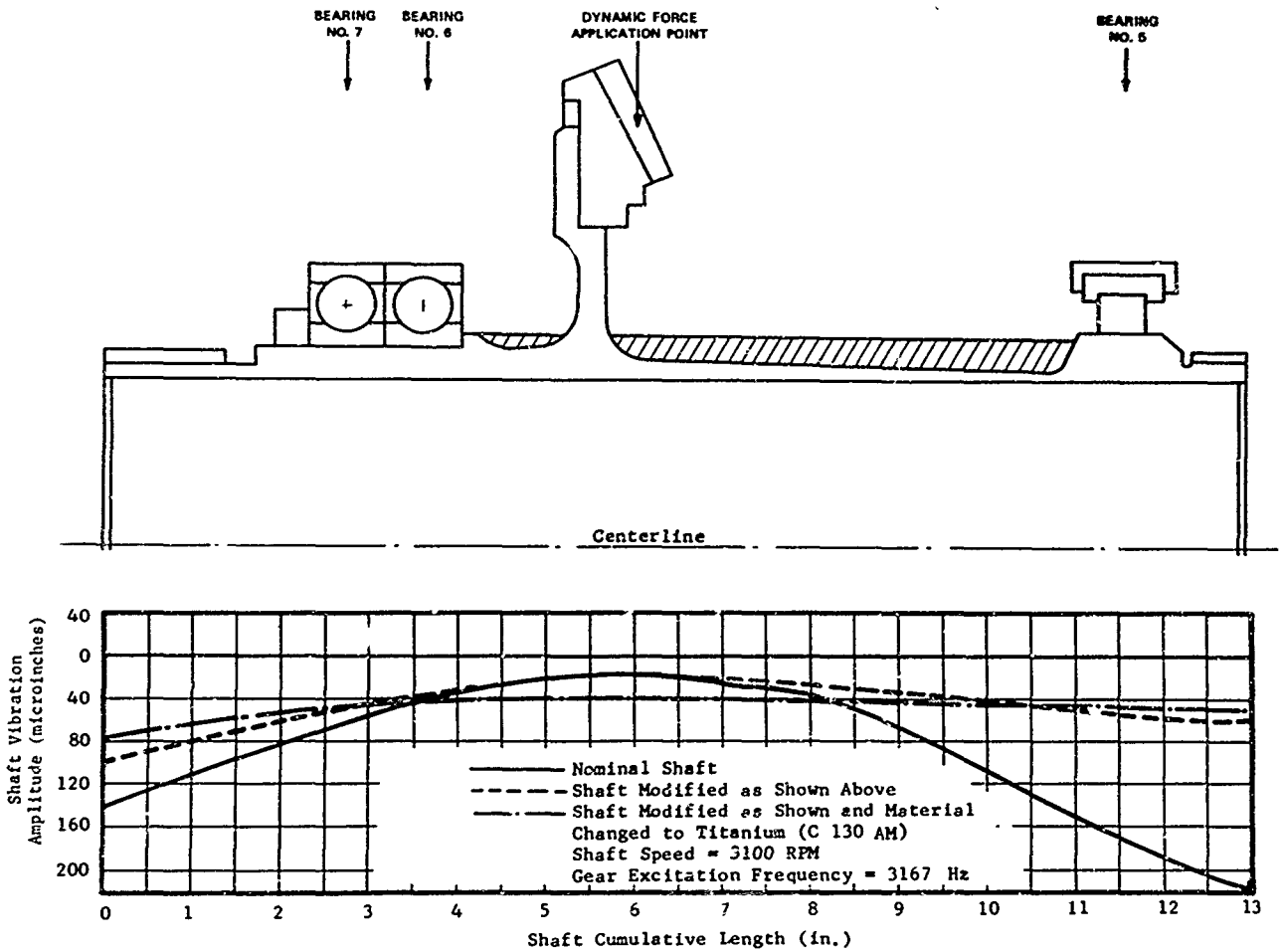

Figure 32. Calculated Vibration Amplitudes for UH-1D Output Bevel Gear Shaft for Nominal and Modified Configurations.

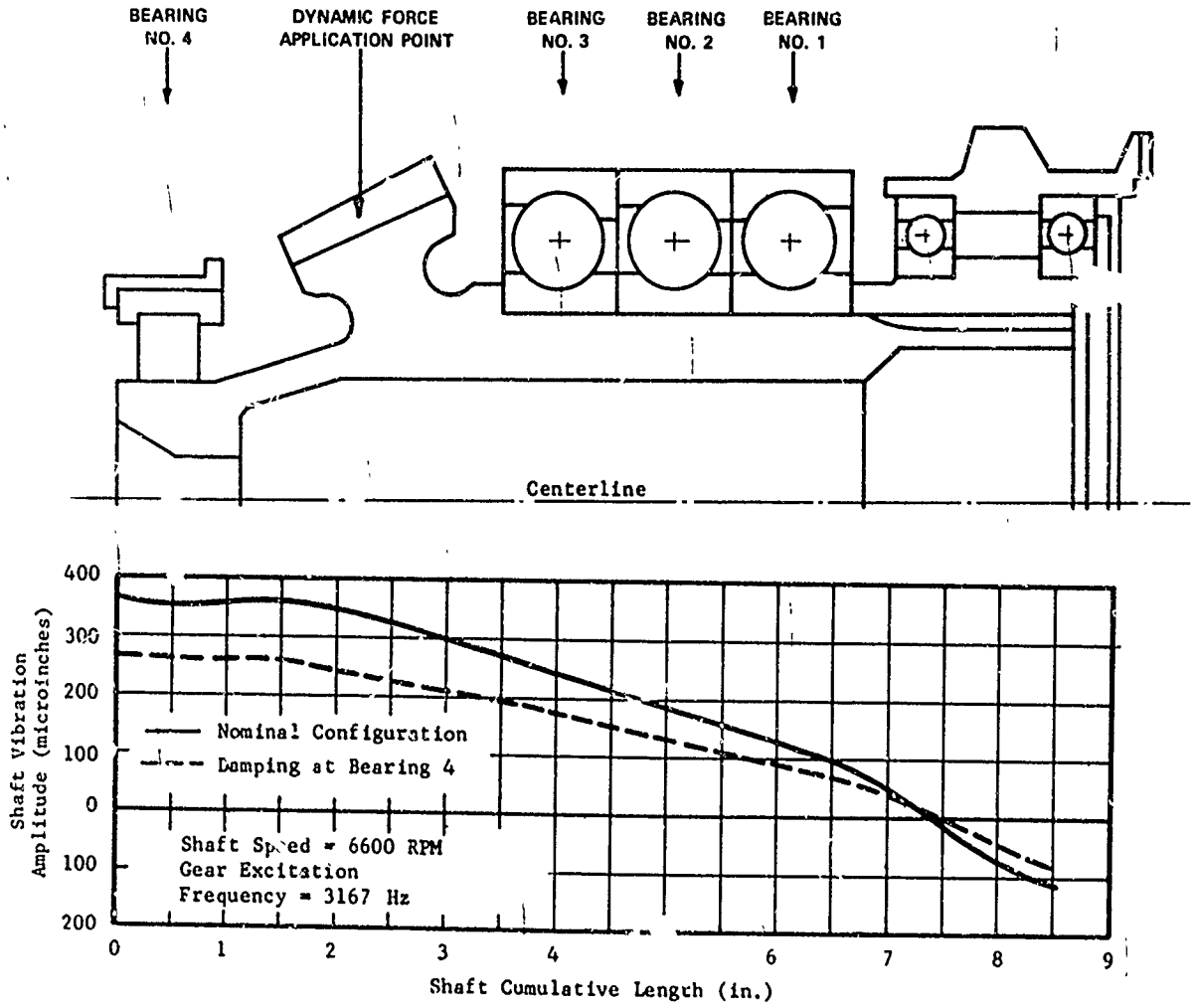

Figure 33. Calculated Vibration Amplitudes for UH-1D Input Bevel Gear Shaft for Nominal Configuration and With Damping.

DYNAMIC BEHAVIOR OF CH-47 FORWARD ROTOR-DRIVE GEARBOX RING-GEAR STRUCTURAL COMPONENTS

INTRODUCTION

In an investigation of helicopter transmission noise, special attention should always be given to elements with large surface areas and on which dynamic excitations such as gear forces may be acting. These elements, vibrating at the frequencies of the dynamic excitations, can become very effective noise generators.

The ring-gear casings of both the UH-1D and the CH-47 helicopter rotor-drive gearboxes satisfy the above criteria as potential noise generators: they have relatively large areas, and are acted upon by the dynamic tooth forces of the upper and lower planetary gears. The ring-gear casings are therefore important items for study in a noise-reduction investigation.

The results of these studies are presented in two parts. The first considers the CH-47 helicopter ring-gear casing, and the second the UH-1D helicopter ring-gear casing. Each part considers the following:

1. The natural frequencies of various ring-gear casing vibration modes are obtained and tabulated. They are compared with the fundamental frequencies of the upper and lower planetary gear meshing and their higher harmonics.

2. The dynamic tooth forces reported in [1] and [2] are taken as inputs in the present program. These dynamic forces, decomposed into Fourier components in the circumferential direction, may be used in a shell vibration response computer program to compute the dynamic response of the ring-gear casing to each separate Fourier component at each planet-to-ring-gear mesh point. The total dynamic response of the casing is then obtained by superimposing the individual responses with appropriate spatial and temporal phase relationships. From the results of the dynamic response analysis, the acoustic power generated by the vibrating ring-gear casing is calculated. This acoustic power is a direct indication of the noise emitted from a vibrating body.

3. The ring-gear casing is then modified in an effort to reduce the emitted noise. The acoustic power of the modified casing is calculated and compared with the existing casing to demonstrate the effectiveness of the modifications.

NATURAL FREQUENCIES OF CH-47 RING-GEAR CASING

The ring-gear casing of the CH-47 helicopter was modeled as shown in Figure 34 for the dynamic analysis. The casing was considered as a composite cylindrical shell with variable thickness. The following assumptions have been made:

1. The two edges of the casing are "simply supported", i.e., they are restrained from linear translation in all directions but are free to rotate about their circumferences.

2. The gear teeth do not contribute any significant bending strength in the circumferential direction, and they are neglected for the dynamic analysis.

Although the casing is axially symmetric with respect to its centerline, the natural modes of vibration may or may not be axisymmetric. For example, one possible circumferential mode, depicted in Figure 35, is that mode shape in which the amplitude repeats itself twice for each complete revolution. It is therefore convenient to define a circumferential wave number "n" to denote the number of waves in the circumferential direction. For the mode shown in Figure 35, n=2.

For the case in which n=0, the mode shape is uniform in the circumferential direction. This mode is commonly known as "hoop mode" because it resembles the situation of the hoop stress in a circular ring.

At a particular circumferential wave number, the casing may vibrate in different axial modes. Two axial mode shapes are schematically shown in Figure 36. In both modes, the two edges have zero displacements, which is consistent with the imposed boundary condition that they are "simply supported".

The natural frequencies of the CH-47 ring-gear casing were obtained by using an MTI computer program capable of solving axisymmetrical, composite, thin shells. Only the shell structure has to be axisymmetrical; the mode shapes can be axially nonsymmetrical (the n=2 mode, for example). The CH-47 ring-gear casing, consisting of cylindrical shells of variable thickness, is particularly suitable for solution by this computer program.

The natural frequencies of the CH-47 ring-gear casing are tabulated in Table VII for different circumferential wave numbers and axial mode shapes. They are also shown diagrammatically in Figure 37, together with the gear mesh frequencies. The natural frequency of the first axial mode with n=0 is very close to the third harmonic of the lower planetary mesh frequency. This could cause the casing to have a relatively large dynamic response at the lower planetary third harmonic frequency. A modified configuration with increased wall thickness near the center section will be investigated in a later section. The third axial mode was not surveyed because the frequencies were too high (above 15,000 Hz range) to be of interest in the present gearbox study.

The natural frequencies obtained so far were calculated with the assumption that the casing edges are simply supported. In an effort to understand the dynamic behavior of the CH-47 ring-gear casing, two more sets of end conditions were used to obtain the natural frequencies:

TABLE VII. NATURAL FREQUENCIES OF CH-47 RING-GEAR CASING (Hz)

Circumferential Wave Number n	First Axial Mode	Second Axial Mode
0	4350	13,500
4	5220	14,300
6	6350	15,450
8	7650	16,500
12	10,950	19,800
16	14,800	Not Calculated

1. Both edges built in (i.e., clamped)
2. Both edges free (i.e., ring gear separated from rest of gearbox)

The results of this natural frequency survey with different end conditions are summarized in Figure 38, which illustrates the effects of the shell end conditions on shell natural frequencies. The three locations on the abscissa indicate, in the order of increasing end structural constraint, free-free, both ends simply supported, and both ends built in. For the first axial mode with the circumferential mode number n=0, the casing natural frequency has a value of 2550 Hz when both ends are free, which increases to 4300 Hz when both ends are simply supported and to 12,400 Hz when both ends are built in. Therefore, the end conditions of the ring-gear casing are significant in calculating the natural frequencies. The simply supported end conditions appear to be a reasonably good compromise for the present analysis. The edges of the ring-gear casing will be assumed simply supported for dynamic analysis.

DYNAMIC RESPONSE OF CH-47 RING-GEAR CASING

The CH-47 ring-gear casing model shown in Figure 34 was also used as the model for the dynamic response analysis. The casing was again assumed to be "simply supported" at both ends. Dynamic forces of the upper and lower planetary gears were considered to be acting on the casing at their respective fundamental frequencies and their harmonics. Since these dynamic forces are at different frequencies (for example, the lower planetary fundamental is at 1482 Hz and the upper planetary fundamental is at 406 Hz), they are treated separately in the dynamic response calculation. Only the lower planetary dynamic forces at the fundamental frequency were considered in this study, which is directed at understanding the relatively large measured noise peaks near 1500 Hz.

The input data taken from Reference 2 and the CH-47 drawings referred to earlier are summarized in Appendix II. These data were further processed to a form suitable for the dynamic response calculation.

Corresponding to the dynamic forces applied to the ring-gear casing by the lower planetary gears, the normal displacement perpendicular to the casing cylindrical surface is expressed as

$$w(\theta,z,t) = W(\vartheta,z) \cos [\omega t + \varphi(\theta,z)] \qquad (2)$$

where

- W = amplitude of normal displacement
- θ = circumferential coordinate starting from planetary gear "A" (see Figure 57)
- z = axial coordinate starting from the lower casing end (see Figure 34)
- ω = frequency
- φ = temporal phase angle (advance) relative to planetary gear "A"
- t = time

Tables VIII and IX give the calculated amplitude W (θ,z) and the temporal phase angle $\varphi(\theta,z)$ of the normal displacement respectively.

Although the planetary gears are not equally spaced, this effect was neglected when the dynamic responses of the individual gears were superimposed. This is a good approximation because the deviation from uniform spacing is only 1.343 degrees (see Figure 57). This 1.343 degrees is important in determining the temporal phase angle among the planetary gear meshings. This 1.343-degree nonuniformity in spacing results in a temporal phase difference of 37.6 degrees between gear "A" and gear "C", as shown in Appendix II.

Table VIII shows that the amplitude W repeats every 90 degrees in the θ-direction, but the temporal phase angle repeats every 180 degrees in the θ-direction. This is because gears "A" and "B" are in phase, as explained in Appendix II. The values of the temporal phase angle at θ=0 degree and θ=180 degrees are very close to zero because these are the locations of gears "A" and "B." At θ=90 degrees, where the gear "C" is, the temporal phase angle is very close to 37.6 degrees, as can be anticipated.

From Equation (2) and Tables VIII and IX, a plot of the normal displacement versus θ at z = 0.9 inch and t = 0 can be generated (see Figure 39). A similar plot at z = 1.5 inches is also shown. The peaks at θ=90 degrees and 270 degrees are smaller than those at θ=0 degree and 180 degrees because of the temporal phase angle; the situation can be reversed at a later time. Thus, Equation (2) and Tables VIII and IX reveal the time history and the spatial distribution of the normal displacement dynamic response due to the dynamic forces of lower planetary gear mesh at the fundamental frequency.

An expression for the acoustic power generated by the vibrating ring-gear casing was derived in Appendix III, and is repeated here:

$$P = 1.62 \times 10^{-4} \omega^2 \overline{W}^2 A \text{ (watts)}$$

In the case of interest here,

$$\omega = 1482 \text{ Hz}$$

$$\overline{W} = 2.04 \times 10^{-6} \text{ in.} = 5.18 \times 10^{-6} \text{ cm}$$

$$A = 2\pi \times 11.2 \times 3 = 211 \text{ in.}^2 = 1360 \text{ cm}^2$$

$$P = 1.62 \times 10^{-4} (1482 \times 5.18 \times 10^{-6})^2 \times 1360$$

$$= 1.3 \times 10^{-5} \text{ watts}$$

The sound pressure level corresponding to this acoustic power level may be calculated by Equation (67) for various distances. At a distance of 1 foot, the sound pressure level is 71 db.

Thus, the acoustic power is a direct indication of the noise generated by the ring-gear casing. The acoustic power calculated above is that induced by the lower planetary gear meshing at the fundamental frequency. In the next section, the acoustic power of a modified casing is calculated. Changes in acoustic power levels indicate the effectiveness of the modification.

From the lower planetary gear mesh, dynamic forces are also transmitted through the upper and lower edges of the ring-gear casing to the adjacent parts of the aircraft structure, causing vibrations there. Therefore, these boundary dynamic forces are also of importance from the standpoint of noise and vibration reduction. Both radial (perpendicular to the ring-gear casing) and axial (along the ring-gear casing) dynamic forces per unit circumferential length due to lower planetary gear mesh were calculated by the dynamic response program. They are tabulated as follows:

Radial Dynamic Force Per Unit Circumferential Length (lb/in.)		Axial Dynamic Force Per Unit Circumferential Length (lb/in.)	
Lower Edge	Upper Edge	Lower Edge	Upper Edge
11.8	0.57	2.19	2.65

These forces are due to the meshing of one individual lower planet-to-ring tooth pair, and are those values which exist at the circumferential location where the gear mesh occurs.

MODIFICATION OF CH-47 RING-GEAR CASING FOR VIBRATION AND NOISE REDUCTION

The cross sections of the CH-47 ring-gear casing and the modified casing are shown in Figures 40 and 41. The center section of the modified casing has been reinforced as shown in Figure 41. Its wall thickness is increased to be the same as that of the sections supporting the ring-gear teeth.

The dynamic forces acting on the ring-gear casing as a result of the meshing action of the lower planetary gears at the fundamental frequency are calculated in Appendix II, and are used here as input data to calculate the dynamic response. To compare the dynamic response of the nominal and modified configurations, the dynamic response due to one single planetary gear action is calculated at the circumferential location where the meshing occurs. Although this is not the total dynamic response (in the sense that it does not include the action of all four planetary gears), it is directly related to the total dynamic response.

TABLE VIII. AMPLITUDE OF NORMAL DISPLACEMENT, W (10^{-6} INCHES) DUE TO LOWER PLANE DYNAMIC FORCES AT FUNDAMENTAL FREQUENCY, CH-47 RING-GEAR CASING

z(in.) \ θ(deg)	0.	22.5	45.0	67.5	90.0	112.5	135.0	157.5	180.0	205.5	225.0	2
0.0	0.	0.	0.	0.	0.	0.	0.	0.	0.	0.	0.	0
0.3	4.439	0.462	0.010	0.462	4.439	0.462	0.010	0.462	4.439	0.462	0.010	0
0.6	8.452	0.918	0.002	0.918	8.452	0.918	0.002	0.918	8.452	0.918	0.002	0
0.9	10.560	1.339	0.076	1.339	10.560	1.339	0.076	1.339	10.560	1.339	0.076	1
1.2	10.240	1.643	0.209	1.643	10.240	1.643	0.209	1.643	10.240	1.643	0.209	1
1.5	8.678	1.752	0.314	1.752	8.678	1.752	0.314	1.752	8.678	1.752	0.314	1
1.8	6.872	1.596	0.328	1.596	6.872	1.596	0.328	1.596	6.872	1.596	0.328	1
2.1	5.218	1.255	0.265	1.255	5.218	1.255	0.265	1.255	5.218	1.255	0.265	1
2.4	3.522	0.870	0.187	0.870	3.522	0.870	0.187	0.870	3.522	0.870	0.187	0
2.7	1.786	0.449	0.098	0.449	1.786	0.449	0.098	0.449	1.786	0.449	0.098	0
3.0	0.	0.	0.	0.	0.	0.	0.	0.	0.	0.	0.	0

DISPLACEMENT, W (10^{-6} INCHES) DUE TO LOWER PLANETARY
NDAMENTAL FREQUENCY, CH-47 RING-GEAR CASING

135.0	157.5	180.0	205.5	225.0	247.5	270.0	292.5	315.0	337.5	360.0
0.	0.	0.	0.	0.	0.	0.	0.	0.	0.	0.
0.010	0.462	4.439	0.462	0.010	0.462	4.439	0.462	0.010	0.462	4.439
0.002	0.918	8.452	0.918	0.002	0.918	8.452	0.918	0.002	0.918	8.452
0.076	1.339	10.560	1.339	0.076	1.339	10.560	1.339	0.076	1.339	10.560
0.209	1.643	10.240	1.643	0.209	1.643	10.240	1.643	0.209	1.643	10.240
0.314	1.752	8.678	1.752	0.314	1.752	8.678	1.752	0.314	1.752	8.678
0.328	1.596	6.872	1.596	0.328	1.596	6.872	1.596	0.328	1.596	6.872
0.265	1.255	5.218	1.255	0.265	1.255	5.218	1.255	0.265	1.255	5.218
0.187	0.870	3.522	0.870	0.187	0.870	3.522	0.870	0.187	0.870	3.522
0.098	0.449	1.786	0.449	0.098	0.449	1.786	0.449	0.098	0.449	1.786
0.	0.	0.	0.	0.	0.	0.	0.	0.	0.	0.

B

TABLE IX. TEMPORAL PHASE ANGLE OF NORMAL DISPLACEMENT, φ (DEGREES) DUE TO LOWE
DYNAMIC FORCES AT FUNDAMENTAL FREQUENCY, CH-47 RING-GEAR CASING

z(in.) \ θ(deg)	0	22.5	45.0	67.5	90.0	112.5	135.0	157.5	180.0	205.5	225.
0.3	-0.847	-4.557	161.200	-33.040	-36.750	-33.040	161.200	-4.557	-0.847	-4.557	161.2
0.6	-0.825	-4.298	161.200	-33.300	-36.780	-33.300	161.200	-4.298	-0.825	-4.298	161.2
0.9	-0.750	-3.480	-18.800	-34.120	-36.850	-34.120	-18.800	-3.480	-0.750	-3.480	-18.8
1.2	-0.623	-2.488	-18.800	-35.110	-36.980	-35.110	-18.800	-2.488	-0.623	-2.488	-18.8
1.5	-0.474	-1.737	-18.800	-35.860	-37.130	-35.860	-18.800	-1.737	-0.474	-1.737	-18.8
1.8	-0.367	-1.361	-18.800	-36.240	-37.230	-36.240	-18.800	-1.361	-0.367	-1.361	-18.8
2.1	-0.343	-1.283	-18.800	-36.320	-37.260	-36.320	-18.800	-1.283	-0.343	-1.283	-18.8
2.4	-0.325	-1.230	-18.800	-36.370	-37.280	-36.370	-18.800	-1.230	-0.325	-1.230	-18.8
2.7	-0.314	-1.198	-18.800	-36.400	-37.290	-36.400	-18.800	-1.198	-0.314	-1.198	-18.8

A

NORMAL DISPLACEMENT, φ (DEGREES) DUE TO LOWER PLANETARY
AMENTAL FREQUENCY, CH-47 RING-GEAR CASING

.5	135.0	157.5	180.0	205.5	225.0	247.5	270.0	292.5	315.0	337.5	360.0
40	161.200	-4.557	-0.847	-4.557	161.200	-33.040	-36.750	-33.040	161.200	-4.557	-0.847
00	161.200	-4.298	-0.825	-4.298	161.200	-33.300	-36.780	-33.300	161.200	-4.298	-0.825
20	-18.800	-3.480	-0.750	-3.480	-18.800	-34.120	-36.850	-34.120	-18.800	-3.480	-0.750
10	-18.800	-2.488	-0.623	-2.488	-18.800	-35.110	-36.980	-35.110	-18.800	-2.488	-0.623
60	-18.800	-1.737	-0.474	-1.737	-18.800	-35.860	-37.130	-35.860	-18.800	-1.737	-0.474
40	-18.800	-1.361	-0.367	-1.361	-18.800	-36.240	-37.230	-36.240	-18.800	-1.361	-0.367
20	-18.800	-1.283	-0.343	-1.283	-18.800	-36.320	-37.260	-36.320	-18.800	-1.283	-0.343
70	-18.800	-1.230	-0.325	-1.230	-18.800	-36.370	-37.280	-36.370	-18.800	-1.230	-0.325
00	-18.800	-1.198	-0.314	-1.198	-18.800	-36.400	-37.290	-36.400	-18.800	-1.198	-0.314

B

In Figure 42, the normal displacement dynamic responses, due to one lower planetary gear at the circumferential location where the meshing occurs, are plotted against z, the axial coordinate. The normal displacement vibration amplitudes of the modified casing are approximately three times smaller than those of the nominal CH-47 casing.

The normal displacement amplitude $W(\theta,z)$ and the phase angle $\varphi(\theta,z)$, as defined in Equation (2), are tabulated in Tables X and XI for the modified CH-47 casing. These are the total dynamic responses due to all four lower planetary gears. They may be compared with Tables VIII and IX which show results for the existing CH-47 casing.

Two plots of the normal displacement versus θ at $t = 0$ are shown in Figure 43. One plot at $z = 1.2$ inches is the maximum along the axial direction. The other plot is at $z = 2.1$ inches.

The acoustic power can be computed by Equation (63) with

$$\omega = 1482 \text{ Hz}$$

$$\bar{W} = 0.554 \times 10^{-6} \text{ in.} = 1.41 \times 10^{-6} \text{ cm}$$

$$A = 2\pi \times 11.2 \times 3 = 211 \text{ in.}^2 = 1360 \text{ cm}^2$$

$$P = 1.62 \times 10^{-4} (1482 \times 1.41 \times 10^{-6})^2 \times 1360$$

$$= 9.6 \times 10^{-7} \text{ watts}$$

This is equivalent to a sound pressure level of about 60 db at a distance of 1 foot as computed by Equation (67). The existing CH-47 casing has an acoustic power of 1.3×10^{-5} watts. The acoustic power of the modified CH-47 casing is approximately 13.5 times smaller than the existing CH-47 casing, which corresponds to a reduction of about 11 db in sound pressure level at a distance of 1 foot.

Dynamic forces are induced at both the upper and lower edges of the casing due to the planetary gear meshes. These dynamic forces acting at the mesh frequencies are transmitted to the adjacent parts of the aircraft structure. These edge dynamic forces calculated by the dynamic response program are tabulated as follows:

	Radial Dynamic Force Per Unit Circumferential Length (lb/in.)		Axial Dynamic Force Per Unit Circumferential Length (lb/in.)	
	Lower Edge	Upper Edge	Lower Edge	Upper Edge
Existing CH-47 Casing	11.8	0.57	2.19	2.65
Modified Casing	12.1	0.98	1.92	1.32

The dynamic forces of the existing CH-47 casing are also tabulated for comparison. The edge dynamic forces of the modified casing are not significantly higher than those of the existing CH-47 casing.

In summary, the modified casing would have an acoustic power output at the lower planetary mesh frequency 13.5 times smaller than the existing CH-47 casing without significant change in edge dynamic forces. This decrease in acoustic power is approximately equivalent, at a distance of 1 foot, to a reduction of 11 db at this particular frequency in sound pressure level, considering the acoustic energy emitted from the ring-gear casing at the lower planetary mesh frequency.

TABLE X. AMPLITUDE OF NORMAL DISPLACEMENT, W (10^{-6} INCHES) DUE TO LOWER
DYNAMIC FORCES AT FUNDAMENTAL FREQUENCY, CH-47 MODIFIED RING-GE

z(in.) \ θ (deg)	0.	22.5	45.0	67.5	90.0	112.5	135.0	157.5	180.0	205.5	225.0
0.	0.	0.	0.	0.	0.	0.	0.	0.	0.	0.	0.
0.3	1.529	0.051	0.088	0.051	1.529	0.051	0.088	0.051	1.529	0.051	0.088
0.6	2.591	0.062	0.136	0.062	2.591	0.062	0.136	0.062	2.591	0.062	0.136
0.9	3.142	0.038	0.143	0.038	3.142	0.038	0.143	0.038	3.142	0.038	0.143
1.2	3.254	0.029	0.129	0.029	3.254	0.029	0.129	0.029	3.254	0.029	0.129
1.5	3.056	0.055	0.106	0.055	3.056	0.055	0.106	0.055	3.056	0.055	0.106
1.8	2.635	0.073	0.081	0.073	2.635	0.073	0.081	0.073	2.635	0.073	0.081
2.1	2.066	0.075	0.057	0.075	2.066	0.075	0.057	0.075	2.066	0.075	0.057
2.4	1.410	0.062	0.035	0.062	1.410	0.062	0.035	0.062	1.410	0.062	0.035
2.7	0.708	0.035	0.016	0.035	0.708	0.035	0.016	0.035	0.708	0.035	0.016
3.0	0.	0.	0.	0.	0.	0.	0.	0.	0.	0.	0.

OF NORMAL DISPLACEMENT, W (10^{-6} INCHES) DUE TO LOWER PLANETARY
ORCES AT FUNDAMENTAL FREQUENCY, CH-47 MODIFIED RING-GEAR CASING

112.5	135.0	157.5	180.0	205.5	225.0	247.5	270.0	292.5	315.0	337.5	360.0
0.	0.	0.	0.	0.	0.	0.	0.	0.	0.	0.	0.
0.051	0.088	0.051	1.529	0.051	0.088	0.051	1.529	0.051	0.088	0.051	1.529
0.062	0.136	0.062	2.591	0.062	0.136	0.062	2.591	0.062	0.136	0.062	2.591
0.038	0.143	0.038	3.142	0.038	0.143	0.038	3.142	0.038	0.143	0.038	3.142
0.029	0.129	0.029	3.254	0.029	0.129	0.029	3.254	0.029	0.129	0.029	3.254
0.055	0.106	0.055	3.056	0.055	0.106	0.055	3.056	0.055	0.106	0.055	3.056
0.073	0.081	0.073	2.635	0.073	0.081	0.073	2.635	0.073	0.081	0.073	2.635
0.075	0.057	0.075	2.066	0.075	0.057	0.075	2.066	0.075	0.057	0.075	2.066
0.062	0.035	0.062	1.410	0.062	0.035	0.062	1.410	0.062	0.035	0.062	1.410
0.035	0.016	0.035	0.708	0.035	0.016	0.035	0.708	0.035	0.016	0.035	0.708
0.	0.	0.	0.	0.	0.	0.	0.	0.	0.	0.	0.

B

TABLE XI. TEMPORAL PHASE ANGLE OF NORMAL DISPLACEMENT, φ (
DYNAMIC FORCES AT FUNDAMENTAL FREQUENCY, CH-47 H

z(in.) \ θ(deg)	0.	22.5	45.0	67.5	90.0	112.5	135.0	157.5	180.0
0.3	-1.224	-162.900	161.2	125.30	-36.38	125.30	161.2	-162.900	-1.224
0.6	-0.870	-157.000	161.2	119.40	-36.73	119.40	161.2	-157,000	-0.870
0.9	-1.022	-135.600	161.2	97.95	-36.58	97.95	161.2	-135.600	-1.022
1.2	-0.918	-59.800	161.2	22.20	-36.68	22.20	161.2	-59.800	-0.918
1.5	-0.831	-23.230	161.2	-14.37	-36.77	-14.37	161.2	-23.230	-0.831
1.8	-0.760	-13.680	161.2	-23.92	-36.84	-23.92	161.2	-13.680	-0.760
2.1	-0.705	-9.766	161.2	-27.83	-36.89	-27.83	161.2	-9.766	-0.705
2.4	-0.663	-7.706	161.2	-29.89	-36.94	-29.89	161.2	-7.706	-0.663
2.7	-0.632	-6.477	161.2	-31.12	-36.97	-31.12	161.2	-6.477	-0.632

Preceding page blank

ORAL PHASE ANGLE OF NORMAL DISPLACEMENT, φ (DEGREES) DUE TO LOWER PLANETARY
MIC FORCES AT FUNDAMENTAL FREQUENCY, CH-47 MODIFIED RING-GEAR CASING

90.0	112.5	135.0	157.5	180.0	205.5	225.0	247.5	270.0	292.5	315.0	337.5	360.0
6.38	125.30	161.2	-162.900	-1.224	-162.900	161.2	125.30	-36.38	125.30	161.2	-162.900	-1.224
6.73	119.40	161.2	-157.000	-0.870	-157.000	161.2	119.40	-36.73	119.40	161.2	-157.000	-0.870
6.58	97.95	161.2	-135.600	-1.022	-135.600	161.2	97.95	-36.58	97.95	161.2	-135.600	-1.022
6.68	22.20	161.2	-59.800	-0.918	-59.800	161.2	22.20	-36.68	22.20	161.2	-59.800	-0.918
6.77	-14.37	161.2	-23.230	-0.831	-23.230	161.2	-14.37	-36.77	-14.37	161.2	-23.230	-0.831
6.84	-23.92	161.2	-13.680	-0.760	-13.680	161.2	-23.92	-36.84	-23.92	161.2	-13.680	-0.760
6.89	-27.83	161.2	-9.766	-0.705	-9.766	161.2	-27.83	-36.89	-27.83	161.2	-9.766	-0.705
6.94	-29.89	161.2	-7.706	-0.663	-7.706	161.2	-29.89	-36.94	-29.89	161.2	-7.706	-0.663
6.97	-31.12	161.2	-6.477	-0.632	-6.477	161.2	-31.12	-36.97	-31.12	161.2	-6.477	-0.632

B

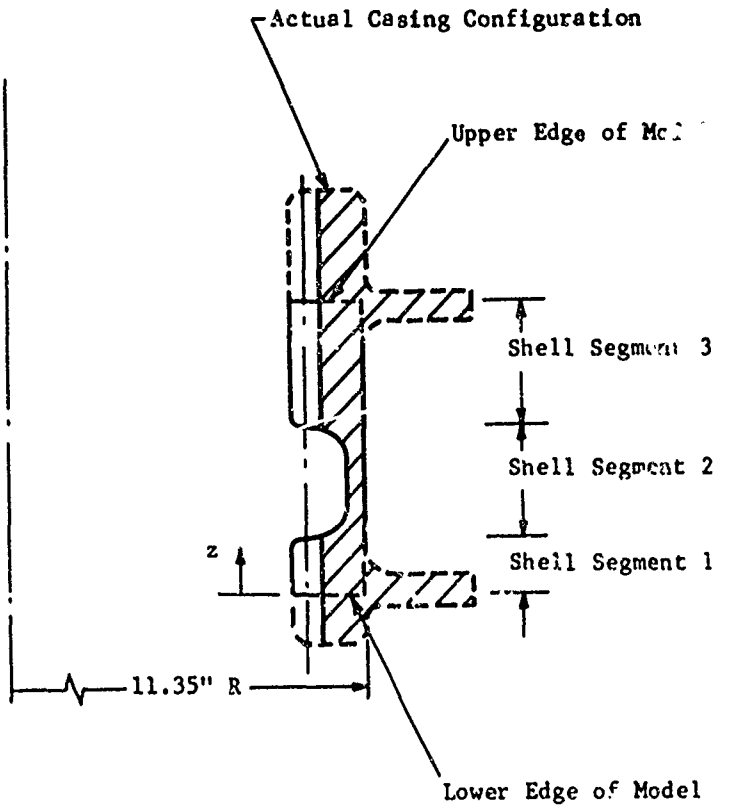

Figure 34. Model for CH-47 Ring-Gear-Casing Dynamic Analysis.

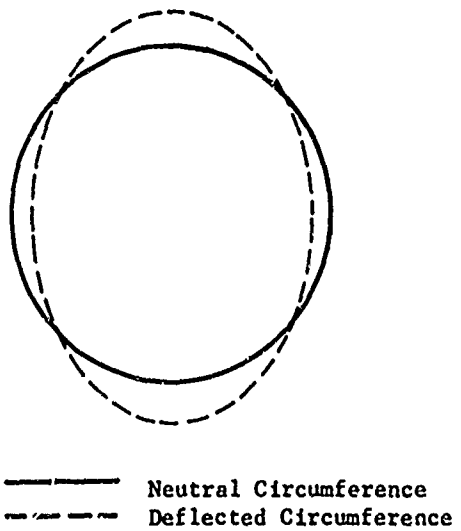

Figure 35. Illustration of n=2 Circumferential Mode Shape.

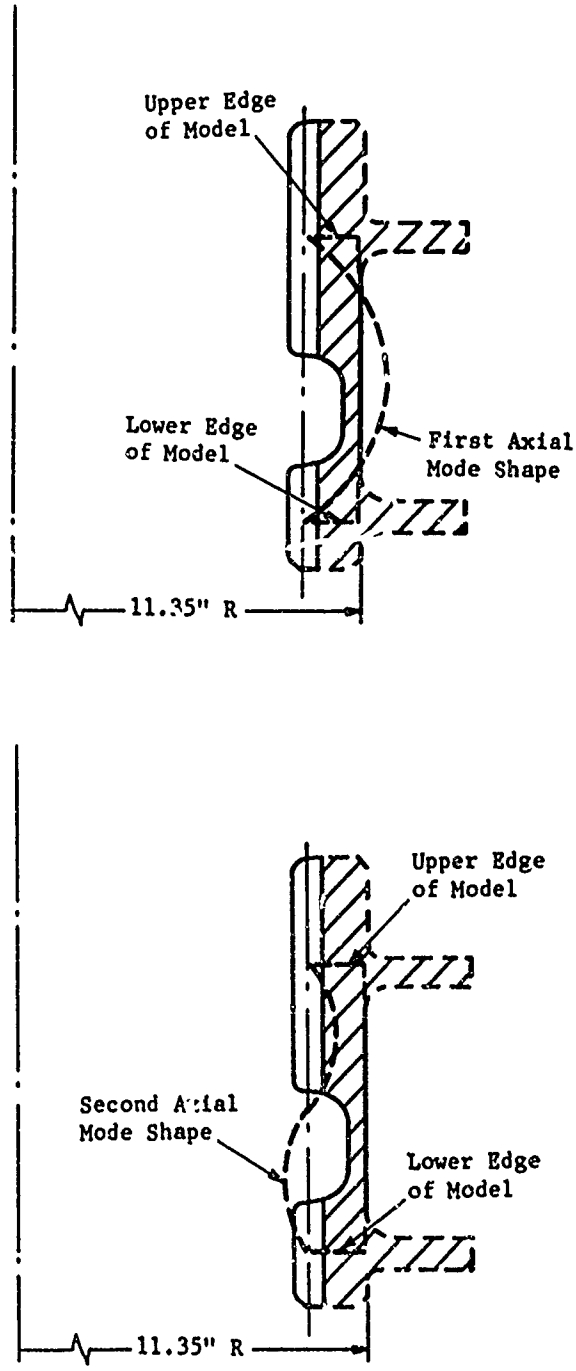

Figure 36. Illustration of CH-47 Ring-Gear-Casing Axial Mode Shapes.

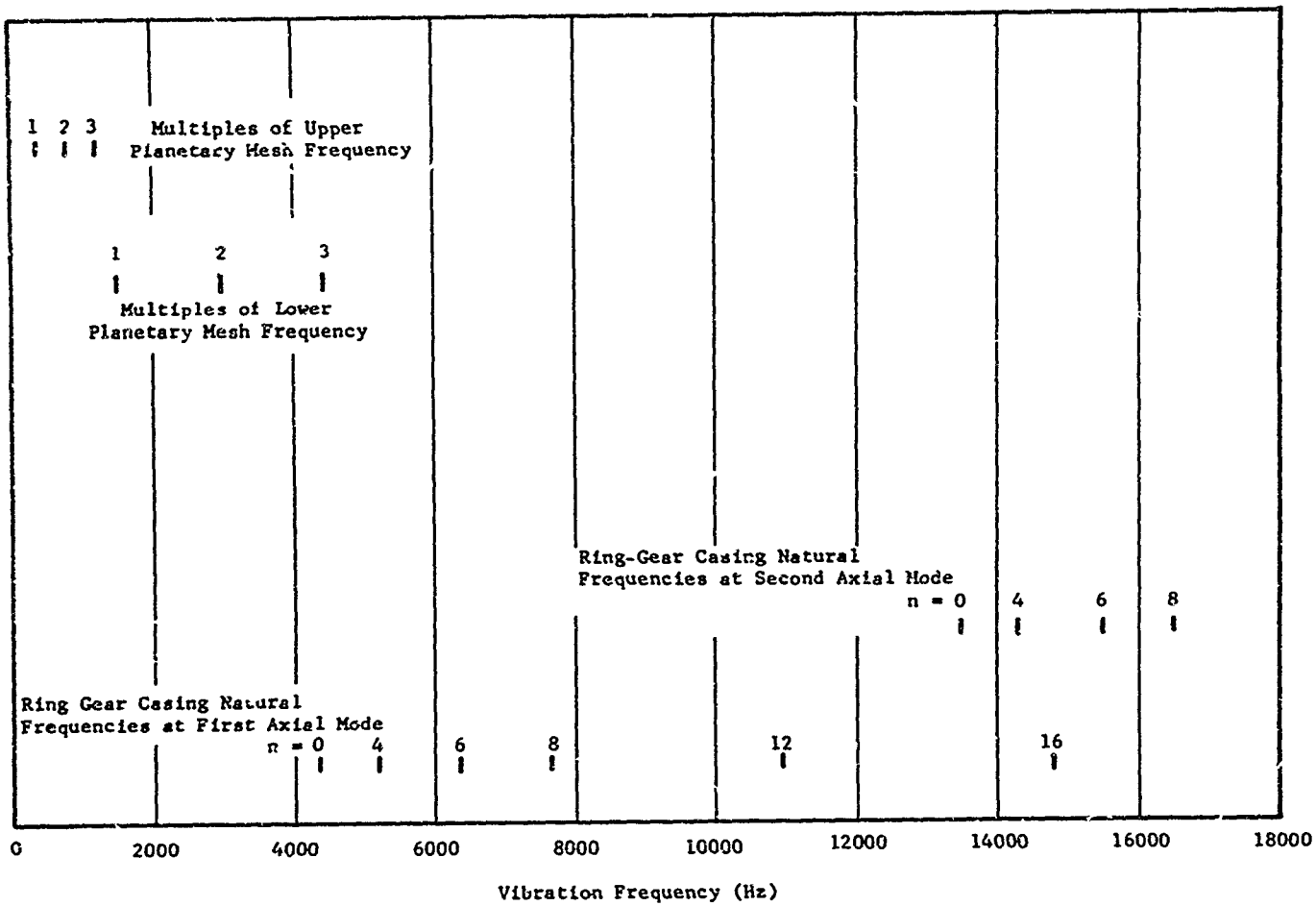

Figure 37. Frequency Diagram for CH-47 Ring-Gear Casing With Edges Simply Supported.

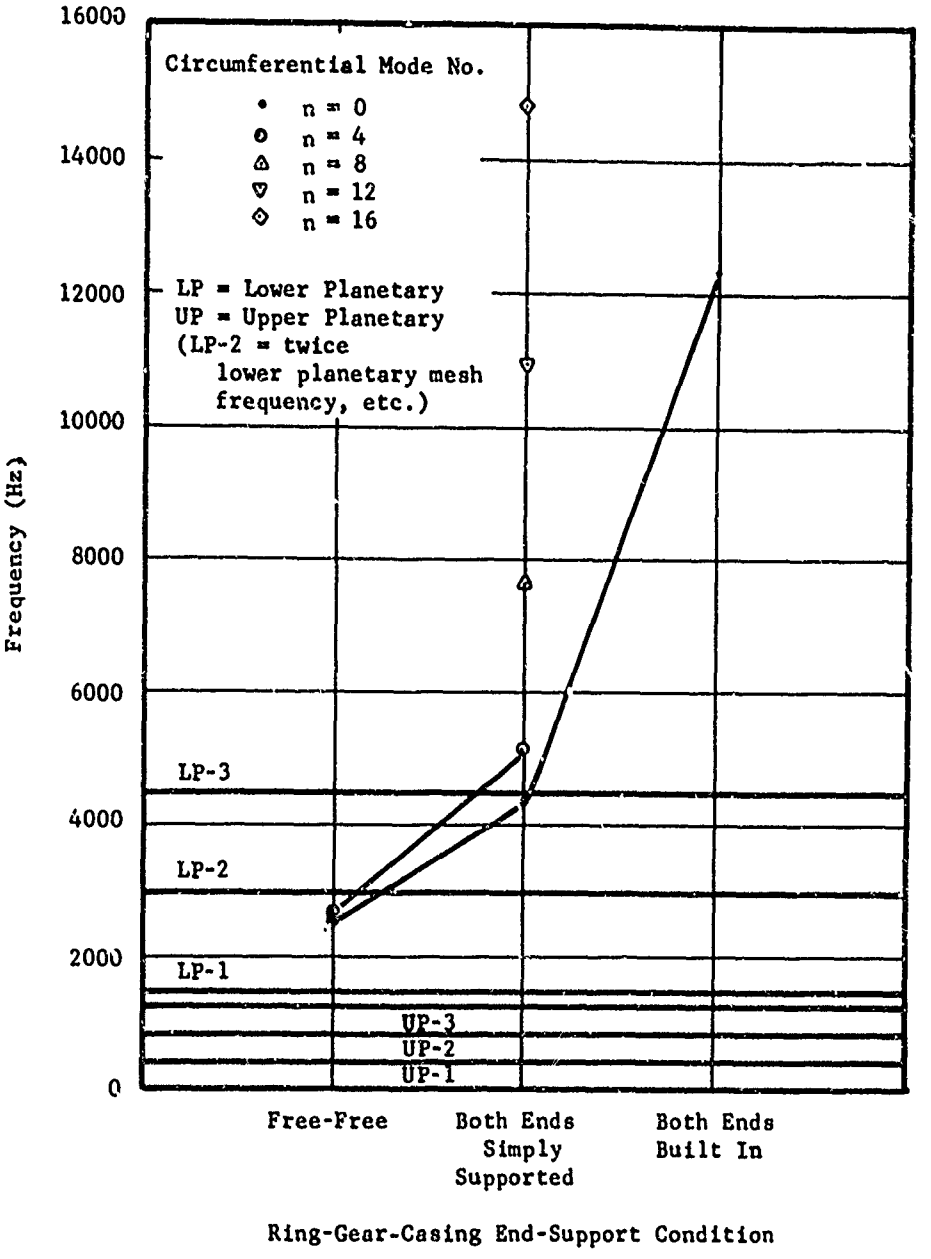

Figure 38. CH-47 Frequency Diagram Illustrating the Effects of End Conditions on Ring-Gear-Casing Natural Frequencies for First Axial Mode Vibrations.

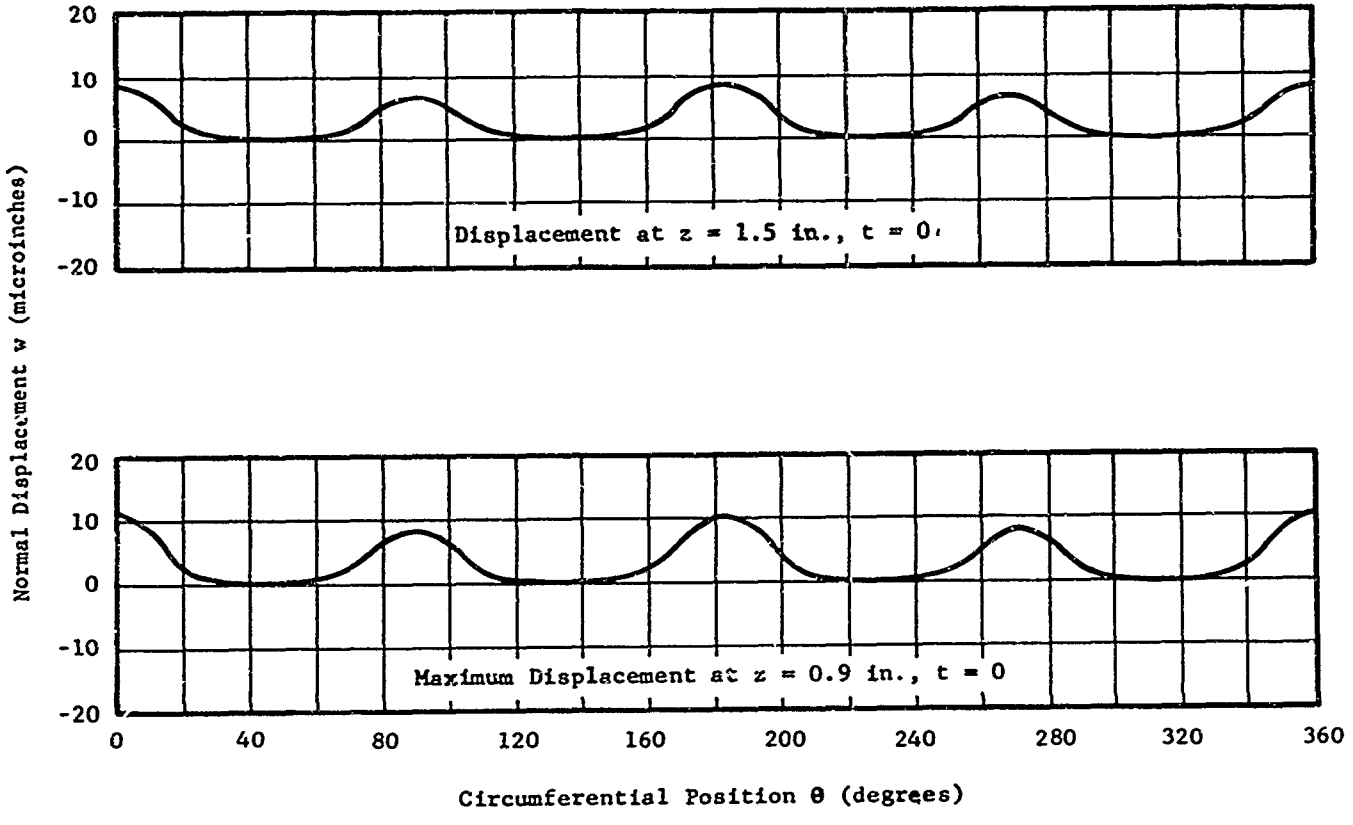

Figure 39. Normal Displacement of CH-47 Ring-Gear Casing due to Lower Planetary Gear Forces at Mesh Frequency.

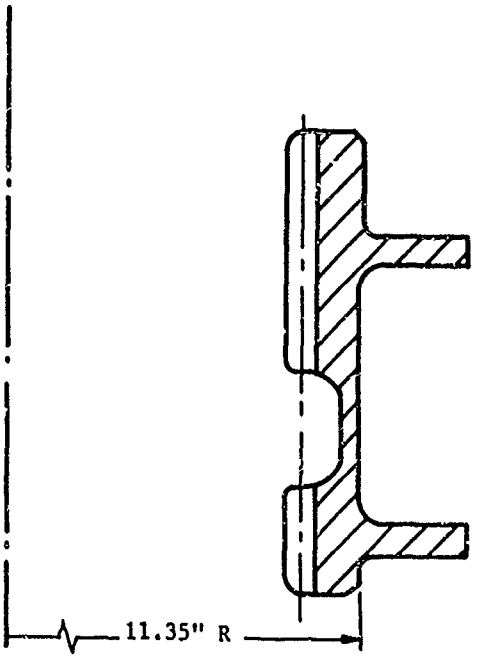

Figure 40. CH-47 Ring-Gear-Casing Nominal Configuration.

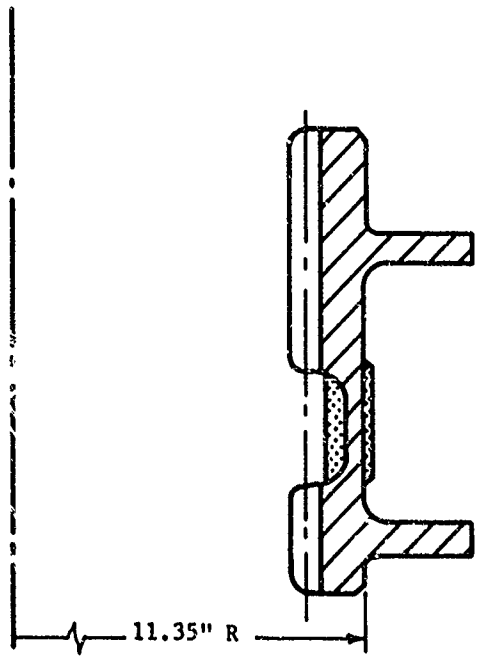

Figure 41. CH-47 Ring-Gear-Casing Modified Configuration.

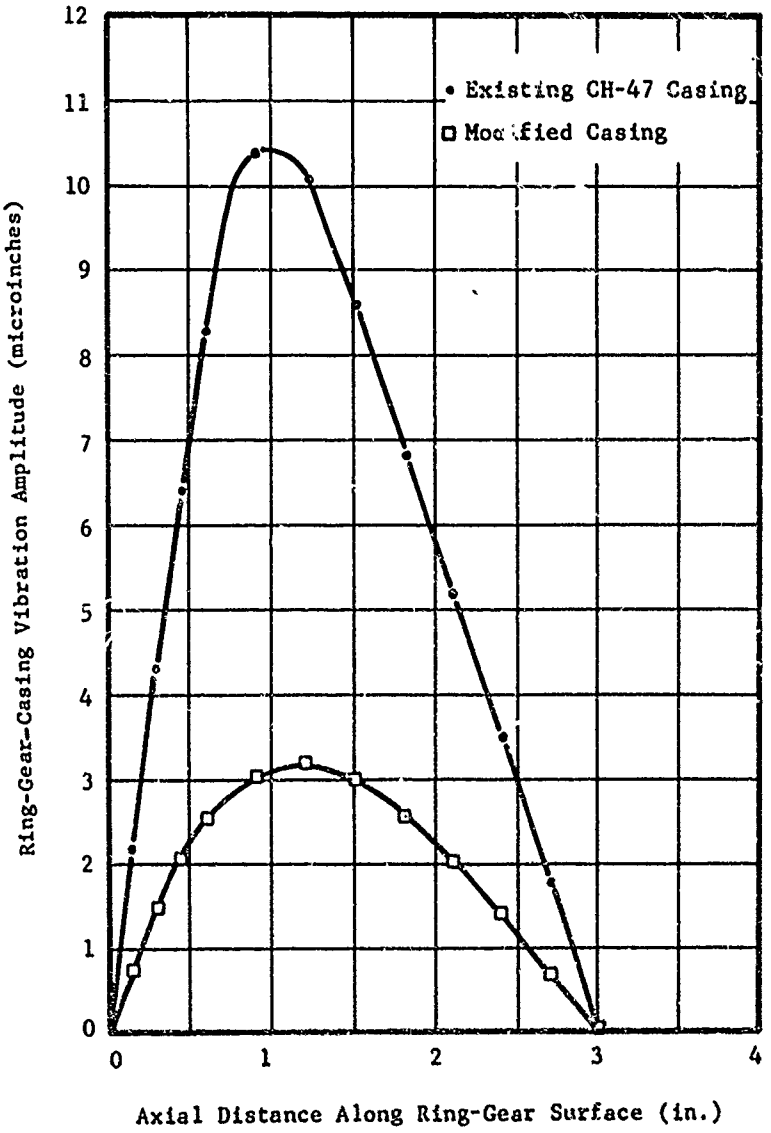

Figure 42. CH-47 Ring-Gear-Casing Vibration Amplitudes due to Forces From One Lower Planetary Gear at Mesh Frequency.

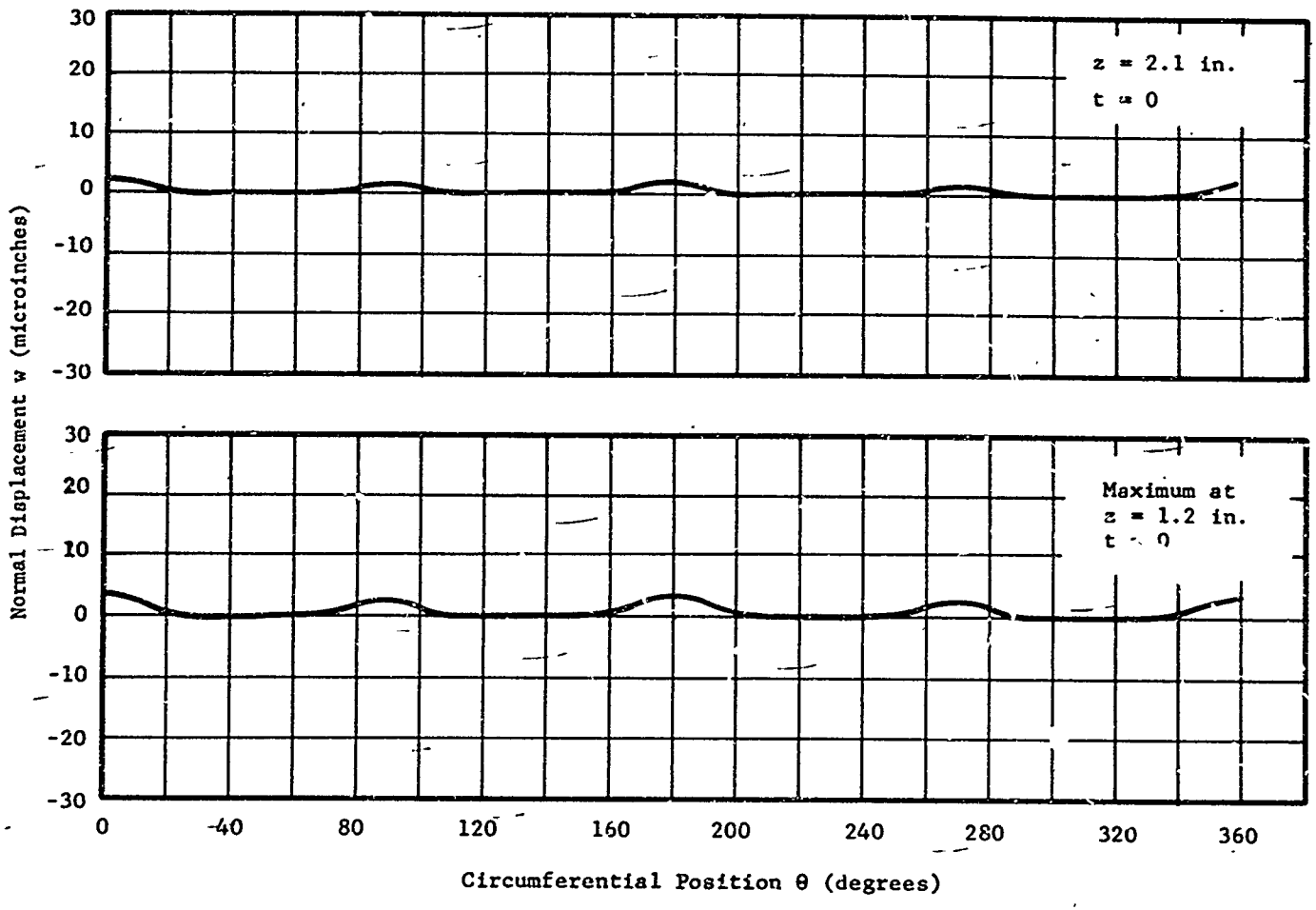

Figure 43. Normal Displacement of CH-47 Modified Ring-Gear Casing due to Lower Planetary Gear Forces at Mesh Frequency.

DYNAMIC BEHAVIOR OF UH-1D ROTOR-DRIVE GEARBOX RING-GEAR STRUCTURAL COMPONENTS

NATURAL FREQUENCIES OF UH-1D RING-GEAR CASING

The ring-gear casing of the UH-1D helicopter was modeled as shown in Figure 44 for the dynamic analysis. The casing was again considered as a composite cylindrical shell with variable thickness. The procedures used for the survey of the casing natural frequencies were similar to those used in the CH-47 study. The edges were again assumed to be simply supported. In addition to this assumption, the circumferential, strengthening ridges were evenly distributed over the gear face width on the outside of the casing to facilitate the modeling.

To describe the natural modes of casing vibration, it is again convenient to use the circumferential wave number "n" as defined earlier, and to specify an axial mode shape. Three axial mode shapes are schematically shown in Figure 45. The results in the form of natural frequencies for different circumferential wave numbers and axial mode shapes are presented in Table XII. For a given circumferential wave number, the natural frequency increases for higher axial modes. This can be explained by the fact that at a higher axial mode, the casing structure is strained more severely than at a lower axial mode. Also, in general, for a given axial mode, the natural frequency increases with increasing "n" because of the higher bending strain. However, the trend is reversed at n=0 where the natural frequency is 4380 Hz, which is higher than the natural frequencies at n=2 and n=4. This is because the hoop strain at n=0 is higher than the bending strain of the n=2 mode and the n=4 mode; this situation is not uncommon for thin shells, and is discussed in texts dealing with thin shell vibrations.

These natural frequencies and the gear mesh frequencies of the upper and lower planetaries are shown in Figure 46, which gives a general view of the frequency range and relationships involved. The second harmonic of the lower planetary is very close to the natural frequencies of the first axial mode with n=2 and 4. In a later section, the ring-gear casing will be strengthened to yield higher natural frequencies.

The natural frequencies of the UH-1D ring-gear casing at different end conditions were also obtained as in the case of the CH-47. The end conditions considered include the case of both ends built in and the case of both ends free. The results, together with the natural frequencies previously obtained for the simply supported end condition, are summarized in Figure 47. The three locations on the abscissa represent, in the order of increasing end structural constraint, free-free, both ends simply supported and both ends built in. For the first axial mode with the circumferential wave number n=0, the natural frequencies with the free-free end condition and the simply supported end condition are both approximately at 4000 Hz. This natural frequency increases to 6000 Hz when the ends are assumed to be built in. Again for the first axial mode but with n=2, the casing natural frequency has a value of about 1000 Hz when both ends are free. This natural frequency increases to 4100 Hz when both ends are simply supported

TABLE XII. NATURAL FREQUENCIES (IN Hz) OF UH-1D RING-GEAR CASING

Circumferential Wave Number n	First Axial Mode	Second Axial Mode	Third Axial Mode
0	4,380	5,470	10,750
2	4,020	5,370	10,900
4	3,960	5,440	11,420
8	5,800	7,500	12,900
12	9,450		
16	13,100	Not Calculated	Not Calculated

and to 13,000 Hz when both ends are built in. The simply supported end conditions again appear to be a reasonably good compromise for the UH-1D ring-gear dynamic analysis, and this assumption has been carried throughout this portion of the study.

DYNAMIC RESPONSE OF UH-1D RING-GEAR CASING

The UH-1D ring-gear casing model shown in Figure 44 was also used as a model for the dynamic response analysis. The casing edges were assumed to be "simply supported". Dynamic forces due to the meshing action of the upper and lower planetary gears were imposed on the casing at their respective fundamental frequencies and their harmonics. Since these dynamic forces are at different frequencies (for example, the lower planetary fundamental is at 1982 Hz and the upper planetary fundamental is at 644 Hz), they are treated separately in the dynamic response calculation. Only the lower planetary dynamic forces at the fundamental frequency were considered in this study.

The input data taken from Reference 1 and the UH-1D drawings referred to earlier are summarized in Appendix I. These input data were further processed to a form suitable for the dynamic response calculation.

Corresponding to the dynamic forces applied to the ring-gear casing by the lower planetary gears, the normal displacement perpendicular to the casing cylindrical surface is expressed as

$$w(\theta,z,t) = W(\theta,z) \cos [\omega t + \varphi(\theta,z)] \qquad (3)$$

where

W = amplitude of normal displacement

θ = circumferential coordinate starting from planetary gear A

z = axial coordinate starting from the lower casing end (see Figure 44)

t = time

ω = frequency

φ = temporal phase angle (advance) relative to planetary gear A

As in the case of the CH-47 ring-gear casing, the normal displacement is of particular interest because it may contribute directly to noise. Knowing the normal displacement distribution throughout the ring-gear casing, the radiated acoustic power can be calculated as was done for the CH-47 casing. In Tables XIII and XIV, the calculated amplitude $W(\theta,z)$ and temporal phase angle $\varphi(\theta,z)$ of the normal displacement are tabulated respectively.

These tables show that the amplitude W repeats itself every 90 degrees in the θ-direction, but the temporal phase angle φ does not. The temporal phase angle is zero degrees at θ = 0 degrees, -90 degrees at θ = 90 degrees, -180 degrees at θ = 180 degrees, and 90 degrees at θ = 270 degrees. At time t = 0, the dynamic force due to gear A (see Figure 56) is at its peak. The angle φ describes, with reference to Equation (3), the phase relationship of the dynamic normal displacement with respect to the dynamic forces of gear A as shown in Figure 56. Table XIII shows that the normal displacement is in phase with gear A at θ = 0 degrees, is lagging 90 degrees at θ = 90 and so on. A plot of the normal displacement versus θ at z = 1.3 inches and t = 0 is shown in Figure 48; the normal displacement is zero at θ = 90 degrees and 270 degrees, and it has peak and negative peak values at θ = 0 degrees and 180 degrees respectively. This normal displacement plot at z = 1.3 inches is a maximum along the z-direction. A similar plot of the normal displacement at z = 3.5 inches and t = 0 is also shown. Therefore, in summary, Equation (3) and Tables XIII and XIV reveal the time history and the spatial distribution of the normal displacement dynamic response due to the dynamic forces of lower planetary gear mesh at the fundamental frequency.

An expression for the acoustic power generated by the vibrating ring-gear casing was derived in Appendix III, and is repeated here.

$$P = 1.62 \times 10^{-4} \omega^2 \bar{W}^2 A \text{ (watts)}$$

In the case of interest here,

$$\omega = 1982 \text{ Hz}$$

$$\bar{W} = 28.6 \times 10^{-6} \text{ in.} = 72.6 \times 10^{-6} \text{ cm}$$

$$A = 2\pi \times 7.5 \times 4.3 = 202.6 \text{ in.}^2 = 1310 \text{ cm}^2$$

$$P = 1.62 \times 10^{-4} (1982 \times 72.6 \times 10^{-6})^2 \times 1310$$

$$= 4.38 \times 10^{-3} \text{ watts}$$

From the acoustic power, the sound pressure level at a distance of 1 foot as calculated by Equation (67) is 97 db. Thus, the acoustic power is a direct indication of the noise generated by the ring-gear casing. The acoustic power calculated above is that induced by the lower planetary gear meshing at the fundamental frequency. In the next section, the acoustic power of a modified casing will be calculated. A comparison of the values of the acoustic power shows the effectiveness of the modification for the reduction of this particular noise component.

From the lower planetary gear mesh, dynamic forces may also be transmitted through the upper and lower edges of the ring-gear casing to the adjacent parts of the aircraft structure, causing vibrations there. Therefore, these boundary dynamic forces are also of importance from the standpoint of noise and vibration reduction. Both radial (perpendicular to the ring-gear casing)

TABLE XIII. AMPLITUDE OF NORMAL DISPLACEMENT, W (10^{-6} INCHES) DUE TO DYNAMIC FORCES AT FUNDAMENTAL FREQUENCY, UH-1D RING GEAR

z (in.) \ θ (deg)	0.	22.5	45.0	67.5	90.0	112.5	135.0	157.5	180.0	202.5
0.	0.	0.	0.	0.	0.	0.	0.	0.	0.	0.
0.25	93.700	8.048	3.131	8.048	93.700	8.048	3.131	8.048	93.700	8.048
0.50	153.700	11.360	6.415	11.360	153.700	11.360	6.415	11.360	153.700	11.360
0.90	191.100	7.169	11.470	7.169	191.100	7.169	11.470	7.169	191.100	7.169
1.30	225.900	7.418	15.660	7.418	225.900	7.418	15.660	7.418	225.900	7.418
1.7125	212.500	7.581	18.660	7.581	212.500	7.581	18.660	7.581	212.500	7.581
2.125	149.500	5.866	18.740	5.866	149.500	5.866	18.740	5.866	149.500	5.866
2.5375	83.800	4.430	16.240	4.430	83.800	4.430	16.240	4.430	83.800	4.430
2.95	44.520	3.942	12.390	3.942	44.520	3.942	12.390	3.942	44.520	3.942
3.50	23.110	2.268	6.882	2.268	23.110	2.268	6.882	2.268	23.110	2.268
4.05	5.222	0.456	1.627	0.456	5.222	0.456	1.627	0.456	5.222	0.456
4.30	0.	0.	0.	0.	0.	0.	0.	0.	0.	0.

A

ITUDE OF NORMAL DISPLACEMENT, W (10^{-6} INCHES) DUE TO LOWER PLANETARY
IC FORCES AT FUNDAMENTAL FREQUENCY, UH-1D RING-GEAR CASING

90.0	112.5	135.0	157.5	180.0	202.5	225.0	247.5	270.0	292.5	315.0	337.5	360.0
.	0.	0.	0.	0.	0.	0.	0.	0.	0.	0.	0.	0.
.700	8.048	3.131	8.048	93.700	8.048	3.131	8.048	93.700	8.048	3.131	8.048	93.700
.700	11.360	6.415	11.360	153.700	11.360	6.415	11.360	153.700	11.360	6.415	11.360	153.700
.100	7.169	11.470	7.169	191.100	7.169	11.470	7.169	191.100	7.169	11.470	7.169	191.100
.900	7.418	15.660	7.418	225.900	7.418	15.660	7.418	225.900	7.418	15.660	7.418	225.900
.500	7.581	18.660	7.581	212.500	7.581	18.660	7.581	212.500	7.581	18.660	7.581	212.500
.500	5.866	18.740	5.866	149.500	5.866	18.740	5.866	149.500	5.866	18.740	5.866	149.500
.800	4.439	16.240	4.430	83.800	4.430	16.240	4.430	83.800	4.430	16.230	4.430	83.800
.520	3.942	12.390	3.942	44.520	3.942	12.390	3.942	44.520	3.942	12.390	3.942	44.520
.110	2.268	6.882	2.268	23.110	2.268	6.882	2.268	23.110	2.268	6.882	2.268	23.110
.222	0.456	1.627	0.456	5.222	0.456	1.627	0.456	5.222	0.456	1.627	0.456	5.222
0.	0.	0.	0.	0.	0.	0.	0.	0.	0.	0.	0.	0.

TABLE XIV. TEMPORAL PHASE ANGLE OF NORMAL DISPLACEMENT, φ (DEGREES)
DYNAMIC FORCES AT FUNDAMENTAL FREQUENCY, UH-1D RING GEA

z (in.) \ θ (deg)	0.	22.5	45.0	67.5	90.0	112.5	135.0	157.5	180.0	202.5	2
0.25	0.	158.800	135.000	111.200	-90.000	68.840	45.000	21.160	-180.000	-21.160	-45.
0.50	0.	154.900	135.000	115.100	-90.000	64.860	45.000	25.140	-180.000	-25.140	-45.
0.90	0.	122.400	135.000	147.600	-90.000	32.360	45.000	57.640	-180.000	-57.640	-45.
1.30	0.	82.940	135.000	-172.900	-90.000	-7.064	45.000	97.060	-180.000	-97.060	-45.
1.7125	0.	72.470	135.000	-162.500	-90.000	-17.530	45.000	107.500	-180.000	-107.500	-45.
2.125	0.	73.270	135.000	-163.300	-90.000	-16.730	45.000	106.700	-180.000	-106.700	-45.
2.5375	0.	60.280	135.000	-150.300	-90.000	-29.720	45.000	119.700	-180.000	-119.700	-45.
2.95	0.	40.180	135.000	-130.200	-90.000	-49.820	45.000	139.800	-180.000	-139.800	-45.
3.50	0.	38.430	135.000	-128.000	-90.000	-51.570	45.000	141.600	-180.000	-141.600	-45.
4.05	0.	49.070	135.000	-139.100	-90.000	-40.930	45.000	130.900	-180.000	-130.900	-45.

A

Preceding page blank

RAL PHASE ANGLE OF NORMAL DISPLACEMENT, φ (DEGREES) DUE TO LOWER PLANETARY
IC FORCES AT FUNDAMENTAL FREQUENCY, UH-1D RING-GEAR CASING

112.5	135.0	157.5	180.0	202.5	225.0	247.5	270.0	292.5	315.0	337.5	360.0
8.840	45.000	21.160	-180.000	-21.160	-45.000	-68.840	90.000	-111.200	-135.000	-158.800	0.
4.860	45.000	25.140	-180.000	-25.140	-45.000	-64.860	90.000	-115.100	-135.000	-154.900	0.
2.360	45.000	57.640	-180.000	-57.640	-45.000	-32.360	90.000	-147.600	-135.000	-122.400	0.
7.064	45.000	97.060	-180.000	-97.060	-45.000	7.064	90.000	172.900	-135.000	-82.940	0.
7.530	45.000	107.500	-180.000	-107.500	-45.000	17.530	90.000	162.500	-135.000	-72.470	0.
6.730	45.000	106.700	-180.000	-106.700	-45.000	16.730	90.000	163.300	-135.000	-73.270	0.
9.720	45.000	119.700	-180.000	-119.700	-45.000	29.720	90.000	150.300	135.000	-60.280	0.
9.820	45.000	139.800	-180.000	-139.800	-45.000	49.820	90.000	130.200	-135.000	-40.180	0.
1.570	45.000	141.600	-180.000	-141.600	-45.000	51.58	90.000	128.400	-135.000	-38.420	0.
0.930	45.000	130.900	-180.000	-130.900	-45.000	40.93	90.000	139.100	-135.000	-49.070	0.

B

and axial (along the ring-gear casing) dynamic forces per unit circumferential length due to lower planetary gear mesh were calculated by the dynamic response program. They are tabulated as follows:

Radial Dynamic Force Per Unit Circumferential Length (lb/in.)		Axial Dynamic Force Per Unit Circumferential Length (lb/in.)	
Lower Edge	Upper Edge	Lower Edge	Upper Edge
6.84	0.68	11.4	4.35

These forces are due to the meshing of one individual gear pair at the lower planetary and are those values which exist at the circumferential location where the gear mesh occurs. These dynamic forces are at the same frequency as the forcing frequency, namely, 1982 Hz.

MODIFICATIONS OF UH-1D RING-GEAR CASING FOR VIBRATION AND NOISE REDUCTION

The cross section of the UH-1D ring-gear casing (nominal configuration) is shown in Figure 49. The two sections where the upper and lower planetary ring-gear teeth are located are relatively strong, as can be seen from their wall thicknesses. The thinner center section and the two sections at each end of the casing are somewhat weaker.

The modifications of the ring-gear casing considered in this study are directed at the reinforcement of the ring-gear supporting structure for two reasons: (1) it is not considered practical to reduce the structural rigidity from the present casing design, and (2) from the structural natural frequency point of view, it is more desirable to have a stiffer structure. As shown in Table XII, the lowest natural frequency of the UH-1D casing is 3960 Hz which is the first axial, n=4 mode. Also shown in the same table, the first axial hoop mode (n=0) has a natural frequency of 4380 Hz. Any attempt to reduce the structural rigidity by, for example, making the wall thinner, would not significantly lower the natural frequency of the hoop mode. Since considerable axial bending appears to be taking place both in the center section and also near the ends of the casing, modifications are made to increase the wall thicknesses in these areas to approximately the same thickness as that in the gear sections in the attempt to reduce the vibration amplitude and hence the emitted noise levels. Three typical modifications to the casing configuration have been made, and their dynamic response vibration amplitudes have been calculated:

1. Reinforced center section (see Figure 50).

2. Reinforced sections near the casing ends (see Figure 51).

3. Reinforced center section and sections near the casing ends (see Figure 52).

The dynamic forces acting on the ring-gear casing as a result of the meshing action of lower planetary gears at the fundamental mesh frequency were summarized in Appendix I and are used here as input data to calculate the dynamic response. For comparison, the dynamic response due to one single planetary gear action is calculated at the circumferential location where the meshing occurs. Although this is not the total dynamic response (in the sense that it does not include the action of all four planetary gears), it is directly related to the total dynamic response. This dynamic response will be used as a basis for comparison among the modifications.

In Figure 53, the normal displacement dynamic responses due to one lower planetary gear at the circumferential location where the meshing occurs are plotted against z, the axial coordinate. The third modification considered, which is the stiffest among all the modifications, has the smallest vibration amplitudes. This modification was therefore investigated further for its total dynamic response, its emitted acoustic power, and the dynamic forces transmitted by it to the supporting structure. For this third modification, both casing center and ends were structurally stiffened.

The normal displacement amplitude $W(\theta,z)$ and the phase angle $\varphi(\theta,z)$ as defined in Equation (3) are tabulated in Tables XV and XVI for the modified UH-1D casing. They are to be compared with Tables XIII and XIV of the existing UH-1D ring-gear casing. In general, the normal displacement amplitude of the modified UH-1D casing is smaller than the existing casing, as can be anticipated from Figure 53.

Two plots of the normal displacement versus θ at t=0 are shown in Figure 54. One plot at z=0.9 inch is the maximum along the axial direction. The other plot is at z=3.5 inches.

The acoustic power can be computed from Equation (63) with

$$\omega = 1982 \text{ Hz}$$

$$\bar{W} = 10.4 \times 10^{-6} \text{ in.} = 26.4 \times 10^{-6} \text{ cm}$$

$$A = 202.6 \text{ in.}^2 = 1310 \text{ cm}^2$$

$$P = 1.62 \times 10^{-4} \omega^2 \bar{W}^2 A$$

$$= 1.62 \times 10^{-4} (1982 \times 26.4 \times 10^{-6})^2 \times 1310$$

$$= 5.83 \times 10^{-4} \text{ watts}$$

This is equivalent to a sound pressure level of 88 db at a distance of 1 foot as computed by Equation (67). Compared to the acoustic power generated by the existing casing (4.38×10^{-3} watts), there is a reduction by a factor of 7.5 with the modified casing, which corresponds to a reduction of 9 db in sound pressure level for this particular noise component at a distance of 1 foot.

TABLE XV. AMPLITUDE OF NORMAL DISPLACEMENT, W (10^{-6} INCHES) DUE TO I
DYNAMIC FORCES AT FUNDAMENTAL FREQUENCY, UH-1D MODIFIED R

z(in.) \ θ(deg)	0.	22.5	45.0	67.5	90.0	112.5	135.0	157.5	180.0	202.5	2
0.	0.	0.	0.	0.	0.	0.	0.	0.	0.	0.	0.
0.25	18.620	1.076	0.077	1.076	18.620	1.076	0.077	1.076	18.620	1.076	0.
0.50	34.940	2.200	0.251	2.200	34.940	2.200	0.251	2.200	24.940	2.200	0.
0.90	53.650	3.973	0.911	3.973	53.650	3.973	0.911	3.973	53.650	3.973	0.
1.30	62.660	5.364	2.053	5.364	62.660	5.364	2.053	5.364	62.660	5.364	2.
1.7125	62.210	6.148	3.398	6.148	62.210	6.148	3.398	6.148	62.210	6.148	3.
2.125	54.990	6.165	4.345	6.165	54.990	6.165	4.345	6.165	54.990	6.165	4.
2.5375	44.720	5.547	4.598	5.547	44.720	5.547	4.598	5.547	44.720	5.547	4.
2.95	33.560	4.526	4.147	4.526	33.560	4.526	4.147	4.526	33.560	4.526	4.
3.50	19.180	2.808	2.747	2.808	19.180	2.808	2.747	2.808	19.180	2.808	2.
4.05	5.845	0.897	0.896	0.897	5.845	0.897	0.896	0.897	5.845	0.897	0.
4.30	0.	0.	0.	0.	0.	0.	0.	0.	0.	0.	0.

A

OF NORMAL DISPLACEMENT, W (10^{-6} INCHES) DUE TO LOWER PLANETARY
ORCES AT FUNDAMENTAL FREQUENCY, UH-1D MODIFIED RING-GEAR CASING

112.5	135.0	157.5	180.0	202.5	225.0	247.5	270.0	292.5	315.0	337.5	360.0
0.	0.	0.	0.	0.	0.	0.	0.	0.	0.	0.	0.
1.076	0.077	1.076	18.620	1.076	0.077	1.076	18.620	1.076	0.077	1.076	18.620
2.200	0.251	2.200	24.940	2.200	0.251	2.200	34.940	2.200	0.251	2.200	34.940
3.973	0.911	3.973	53.650	3.973	0.911	3.973	53.650	3.973	0.911	3.973	53.650
5.364	2.053	5.364	62.660	5.364	2.053	5.364	62.660	5.364	2.053	5.364	62.660
6.148	3.398	6.148	62.210	6.148	3.398	6.148	62.210	6.148	3.398	6.148	62.210
6.165	4.345	6.165	54.990	6.165	4.345	6.165	54.990	6.165	4.345	6.165	54.990
5.547	4.598	5.547	44.720	5.547	4.598	5.547	44.720	5.547	4.598	5.547	44.720
4.526	4.147	4.526	33.560	4.526	4.147	4.526	33.560	4.526	4.147	4.526	33.560
2.808	2.747	2.808	19.180	2.808	2.747	2.808	19.180	2.808	2.747	2.808	19.180
0.897	0.896	0.897	5.845	0.897	0.896	0.897	5.845	0.897	0.896	0.897	5.845
0.	0.	0.	0.	0.	0.	0.	0.	0.	0.	0.	0.

B

TABLE XVI. TEMPORAL PHASE ANGLE OF NORMAL DISPLACEMENT, φ (DEGREES) DUE T
DYNAMIC FORCES AT FUNDAMENTAL FREQUENCY, UH-1D MODIFIED RING-G

z(in.) \ θ(deg)	0.	22.5	45.0	67.5	90.0	112.5	135.0	157.5	180.0	202.5	225
0.25	0.	44.590	135.000	-134.600	-90.000	-45.410	45.00	135.40	-180.00	-135.40	-45.
0.50	0.	39.470	135.000	-129.500	-90.000	-50.530	45.00	140.50	-180.00	-140.50	-45.
0.90	0.	32.090	135.000	-122.100	-90.000	-57.910	45.00	147.90	-180.00	-147.90	-45.
1.30	0.	26.860	135.000	-116.900	-90.000	-63.140	45.00	153.10	-180.00	-153.10	-45.
1.7125	0.	22.750	135.000	-112.800	-90.000	-67.250	45.00	157.20	-180.00	-157.20	-45.
2.125	0.	19.990	135.000	-110.000	-90.000	-70.010	45.00	160.00	-180.00	-160.00	-45.
2.5375	0.	18.340	135.000	-108.300	-90.000	-71.660	45.00	161.70	-180.00	-161.70	-45.
2.95	0.	17.310	135.000	-107.300	-90.000	-72.690	45.00	162.70	-180.00	-162.70	-45.
3.50	0.	16.500	135.000	-106.500	-90.000	-73.500	45.00	163.50	-180.00	-163.50	-45.
4.05	0.	16.060	135.000	-106.100	-90.000	-73.940	45.00	163.90	-180.00	-163.90	-45.

A

ASE ANGLE OF NORMAL DISPLACEMENT, φ (DEGREES) DUE TO LOWER PLANETARY
CES AT FUNDAMENTAL FREQUENCY, UH-1D MODIFIED RING-GEAR CASING

112.5	135.0	157.5	180.0	202.5	225.0	247.5	270.0	292.5	315.0	337.5	360.0
45.410	45.00	135.40	-180.00	-135.40	-45.00	45.41	90.00	134.60	-135.00	-44.59	0.
50.530	45.00	140.50	-180.00	-140.50	-45.00	50.53	90.00	129.50	-135.00	-39.47	0.
57.910	45.00	147.90	-180.00	-147.90	-45.00	57.91	90.00	122.10	-135.00	-32.09	0.
63.140	45.00	153.10	-180.00	-153.10	-45.00	63.14	90.00	116.90	-135.00	-26.86	0.
67.250	45.00	157.20	-180.00	-157.20	-45.00	67.25	90.00	112.80	-135.00	-22.75	0.
70.010	45.00	160.00	-180.00	-160.00	-45.00	70.01	90.00	110.00	-135.00	-19.99	0.
71.660	45.00	161.70	-180.00	-161.70	-45.00	71.66	90.00	108.30	-135.00	-18.34	0.
72.690	45.00	162.70	-180.00	-162.70	-45.00	72.69	90.00	107.30	-135.00	-17.31	0.
73.500	45.00	163.50	-180.00	-163.50	-45.00	73.50	90.00	106.50	-135.00	-16.50	0.
73.940	45.00	163.90	-180.00	-163.90	-45.00	73.94	90.00	106.10	-135.00	-16.06	0.

B

Dynamic forces are induced at both the upper and lower edges of the casing due to the planetary gear meshes. These dynamic forces, acting at the mesh frequencies, may be transmitted to the adjacent parts of the aircraft structure. These edge dynamic forces calculated by the dynamic response program are tabulated as follows:

	Radial Dynamic Force Per Unit Circumferential Length (lb/in.)		Axial Dynamic Force Per Unit Circumferential Length (lb/in.)	
	Lower Edge	Upper Edge	Lower Edge	Upper Edge
Existing UH-1D Casing (Figure 49)	6.84	0.68	11.4	4.35
Modified Casing (Figure 52)	7.80	0.76	5.83	2.79

Those of the existing UH-1D casing are also tabulated for comparison. The edge dynamic forces of the modified casing are not, in general, significantly different from the edge dynamic forces in the nominal UH-1D casing.

In summary, the modified casing would have an acoustic power 7.5 times smaller than the existing UH-1D casing without significant change in the edge dynamic forces. This decrease in acoustic power is approximately equivalent, at a distance of 1 foot, to a 9 db reduction in sound pressure level at the lower planetary mesh frequency.

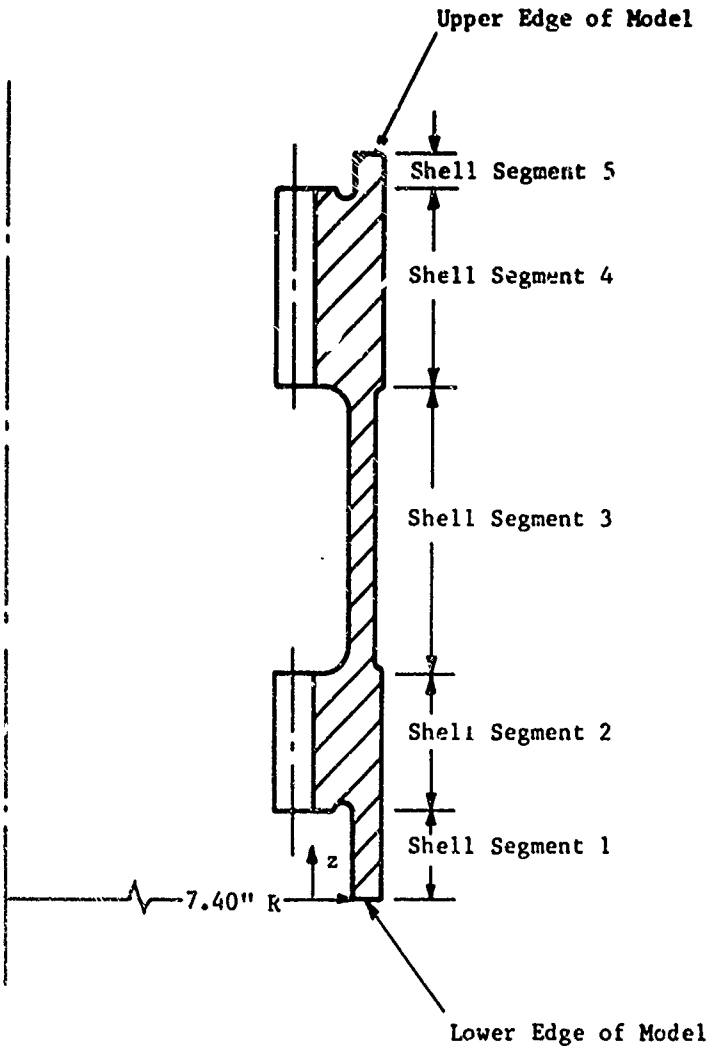

Figure 44. Model for UH-1D Ring-Gear-Casing Dynamic Analysis.

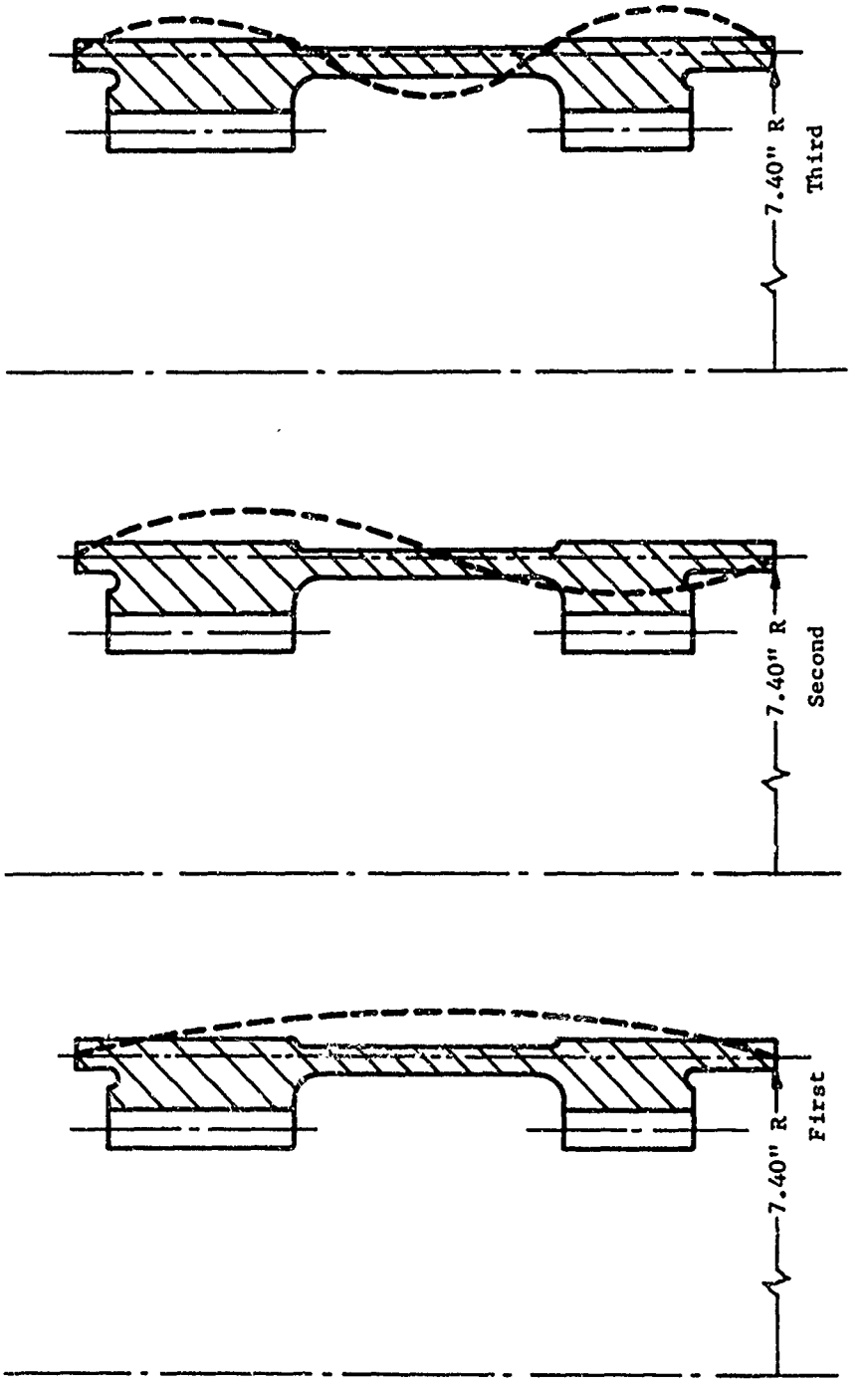

Figure 45. Illustration of UH-1D Ring-Gear-Casing Axial Mode Shapes.

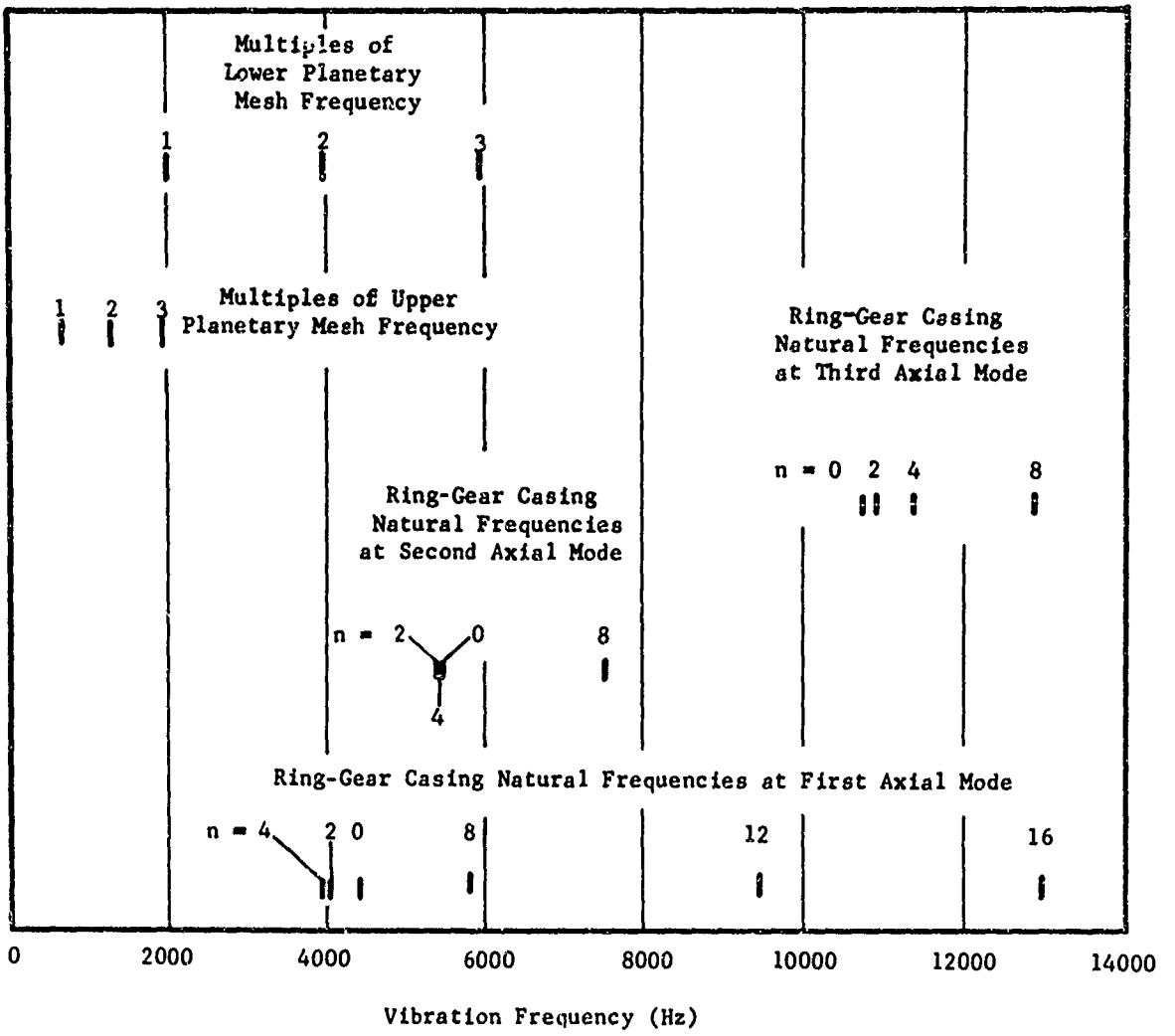

Figure 46. Frequency Diagram for UH-1D Ring-Gear Casing With Edges Simply Supported.

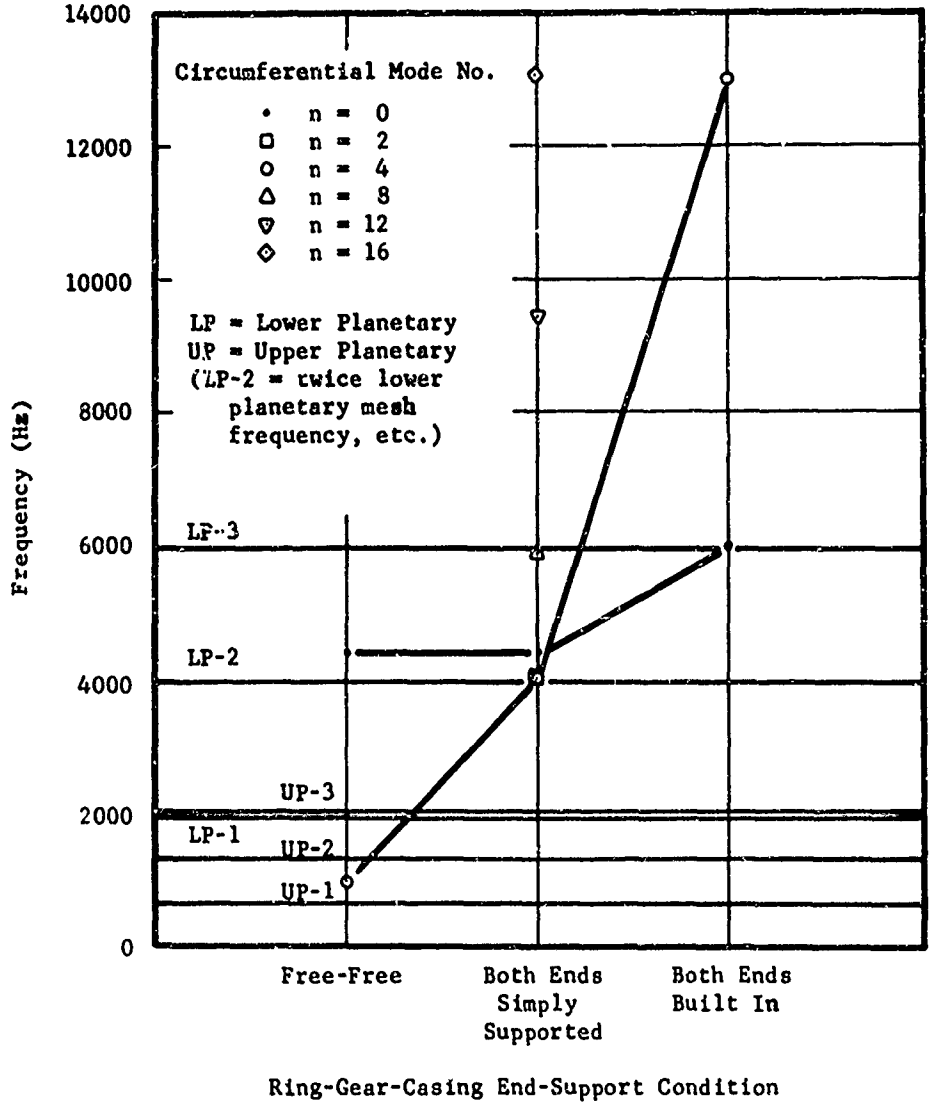

Figure 47. UH-1D Frequency Diagram Illustrating the Effects of End Conditions on Ring-Gear-Casing Natural Frequencies for First Axial Mode Vibrations.

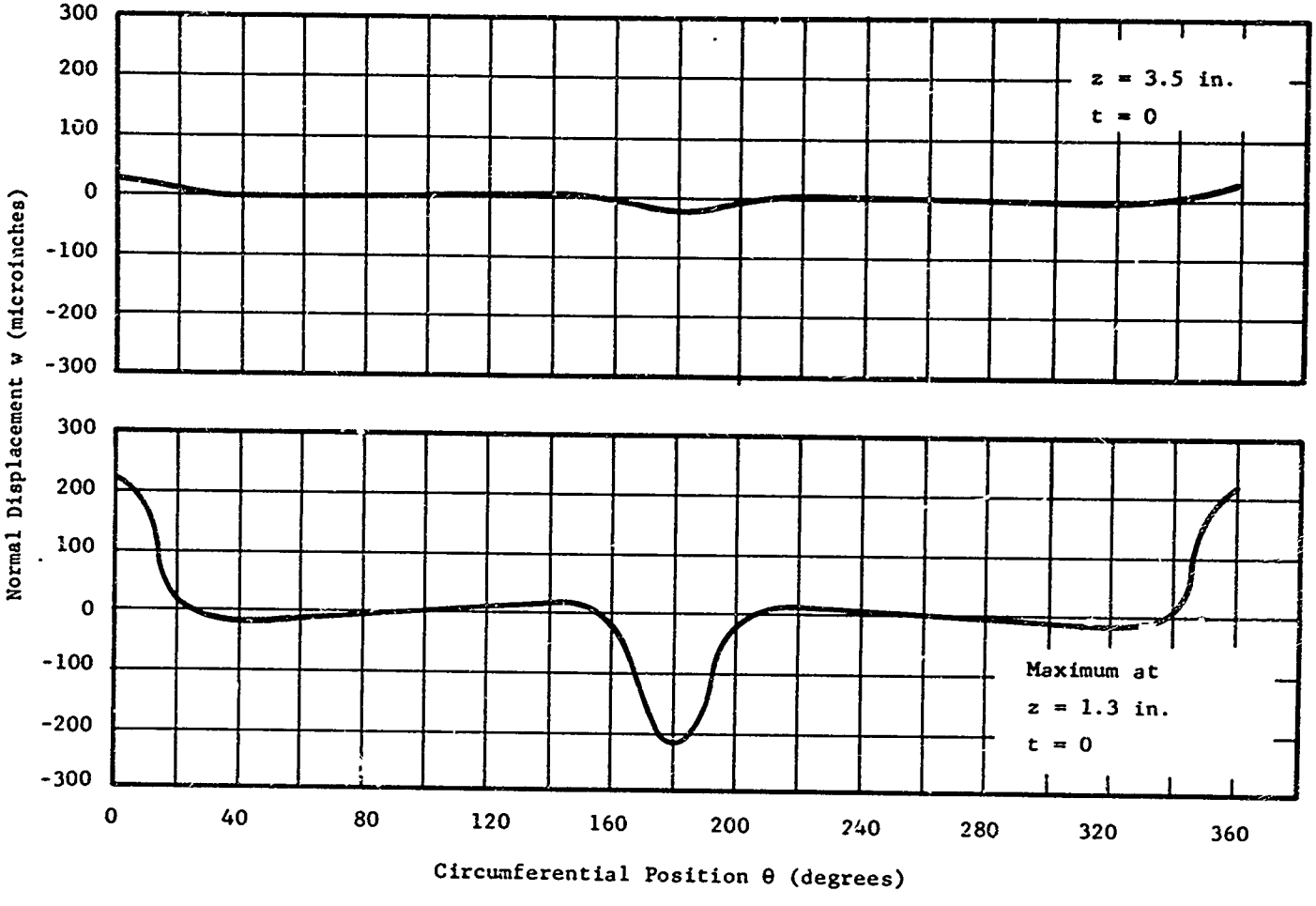

Figure 48. Normal Displacement of UH-1D Ring-Gear Casing due to Lower Planetary Gear Forces at Mesh Frequency.

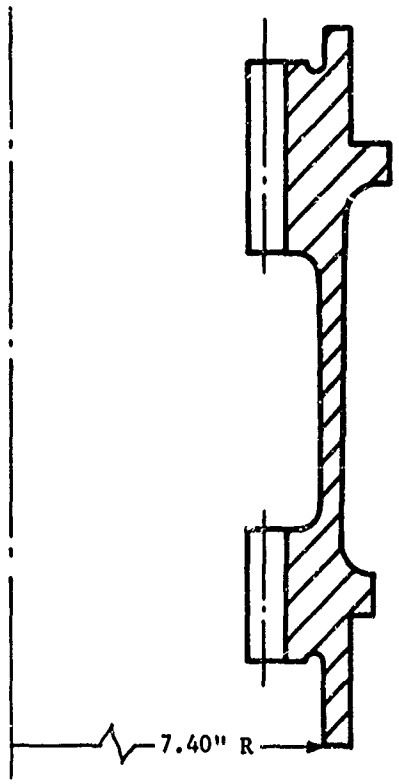

Figure 49. UH-1D Ring-Gear-Casing Nominal Configuration.

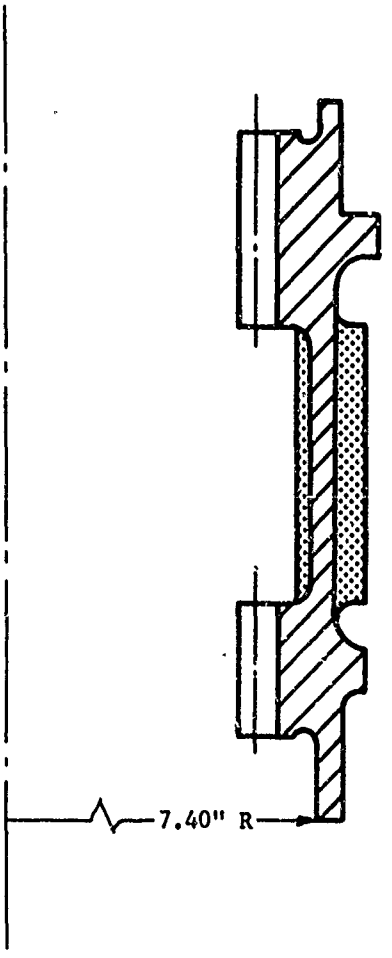

Figure 50. UH-1D Ring-Gear Casing With Center Section Modification.

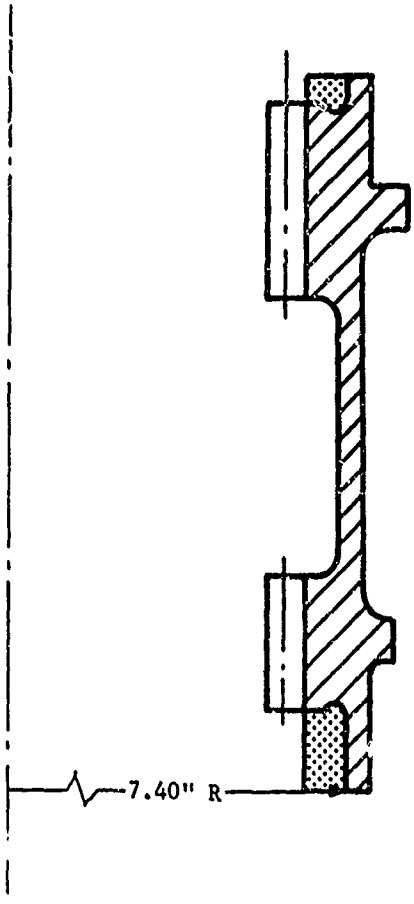

Figure 51. UH-1D Ring-Gear Casing With End Section Modifications.

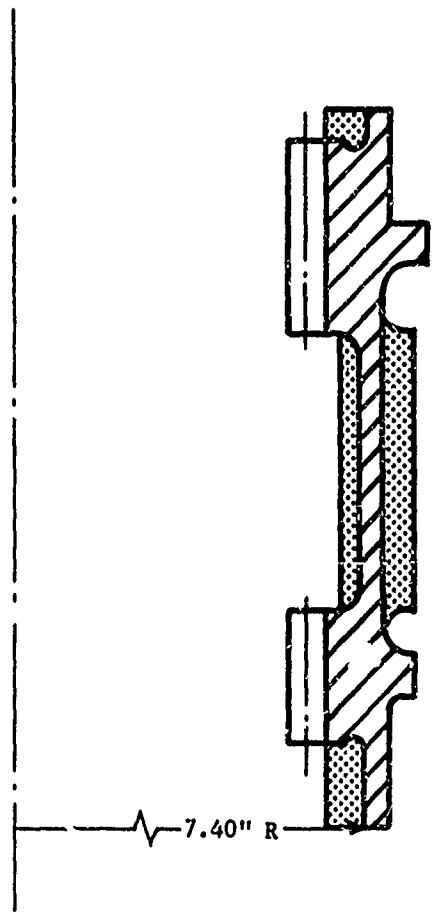

Figure 52. UH-1D Ring-Gear Casing With Center and End Section Modifications.

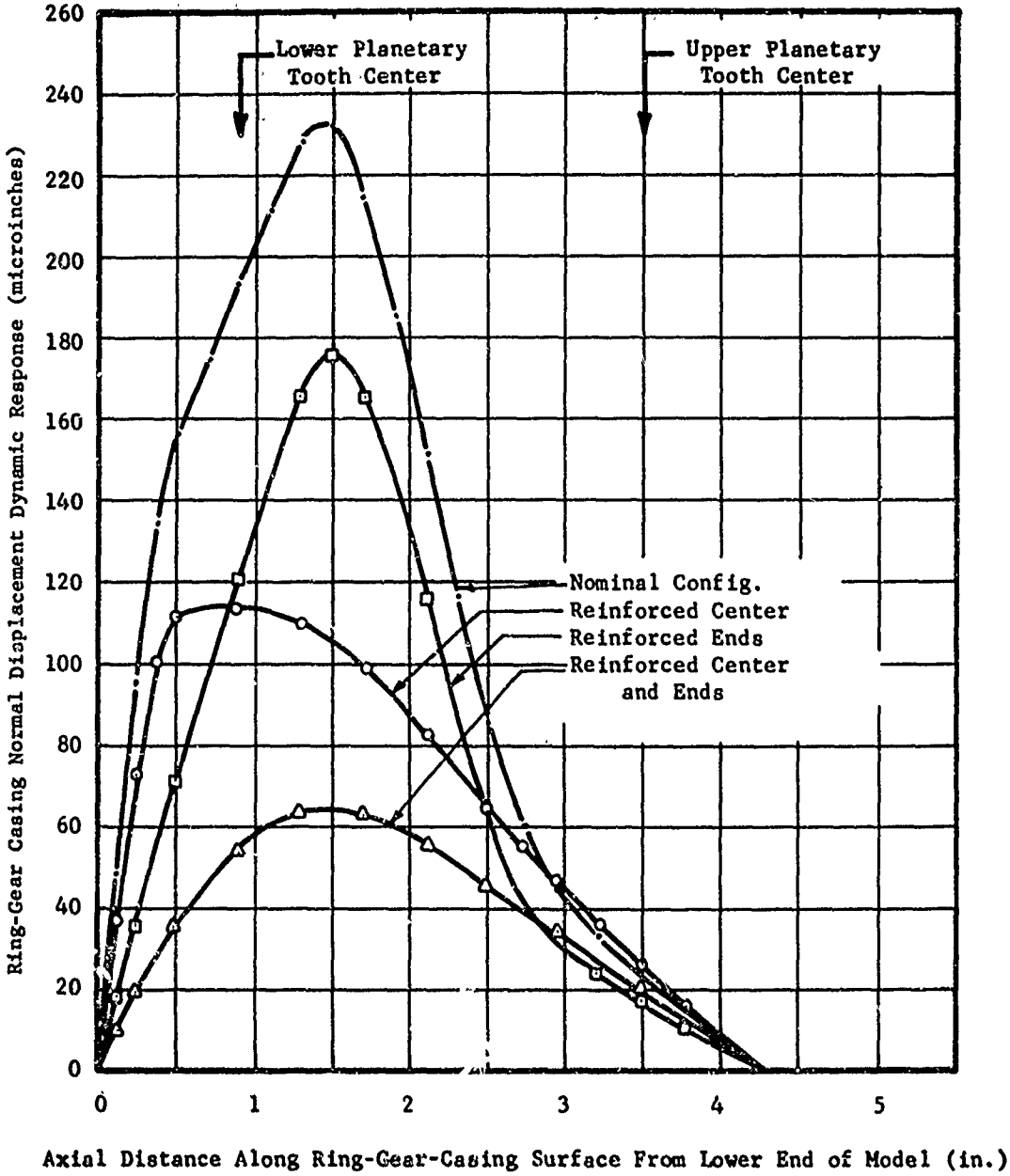

Figure 53. UH-1D Ring-Gear-Casing Vibration Amplitudes due to Forces From One Lower Planetary Gear at Mesh Frequency.

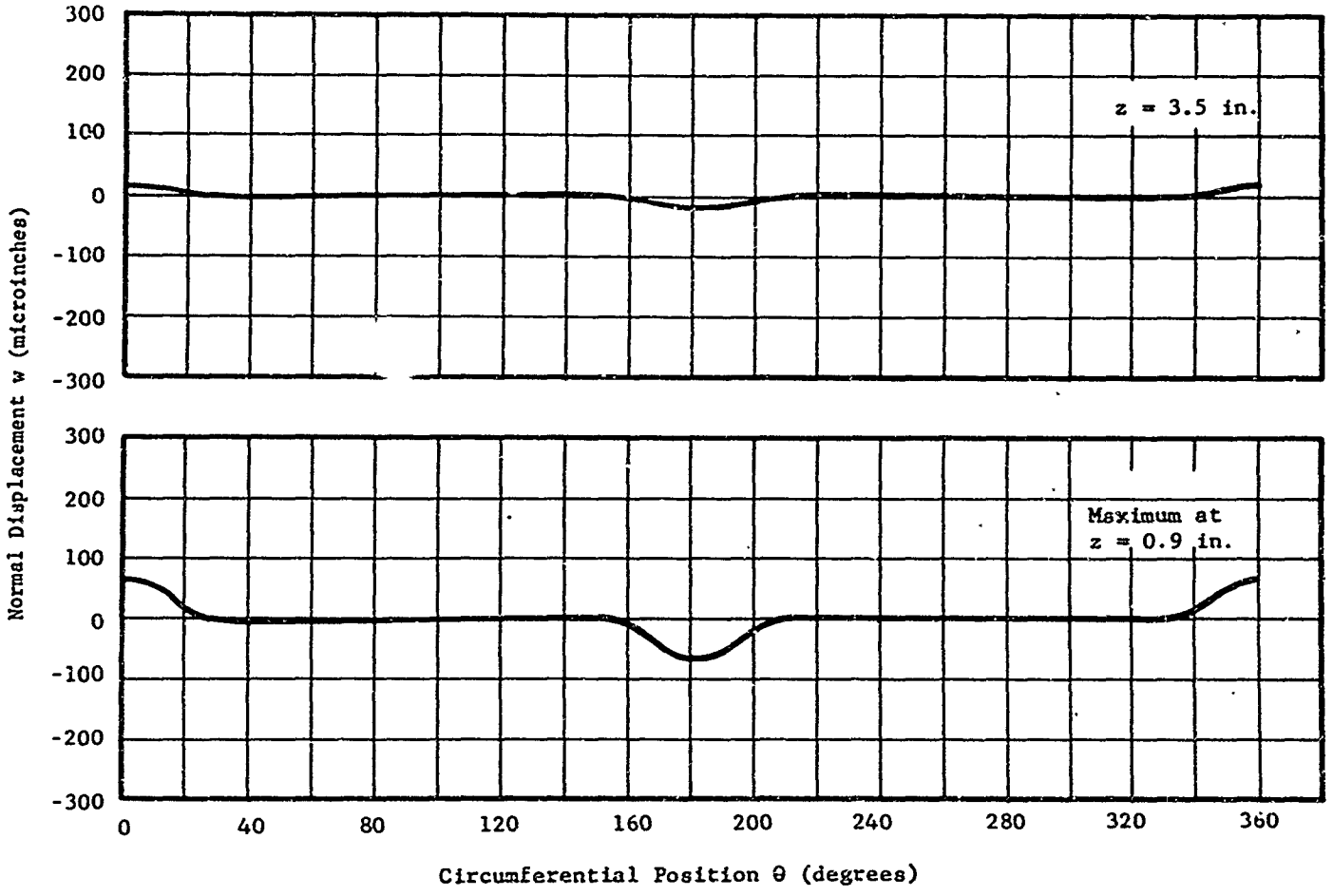

Figure 54. Normal Displacement of UH-1D Ring-Gear Casing due to Lower Planetary Gear Forces at Mesh Frequency.

VIBRATION ISOLATION ANALYSIS OF GEARBOX MOUNT COMPONENTS

Dynamic excitations, originating at the gear mesh locations, have been identified as an important, if not the major, source of gearbox component lateral vibrations at the mesh frequencies and their harmonics. These gearbox drive train component vibrations may result in the generation of acoustic power, and therefore noise, right at the gearbox casing surface when the casing walls are caused to vibrate under the action of the internal components. At the same time, since the gearbox is mounted to the aircraft structure in such a way as to support the aircraft weight, vibrations may be transmitted across the mounting surfaces to the rest of the structure. The mounts can therefore serve as either vibration isolators or vibration transmitters, depending upon their dynamic force and motion transmission properties. From the noise-reduction standpoint, it is desirable to design the mounts as vibration isolators.

The modeling of the gearbox mount structure, a mount-to-airframe connector, and the aircraft structure is shown in Figure 55. The gearbox mount structure is modeled as a mass-spring-dashpot (damping) combination, and so is the aircraft structure. The following analysis is based upon the representation of these system quantities as linear elements. Nonlinear stiffness and damping properties may sometimes exist in systems such as this, requiring somewhat different solution techniques. Such techniques are well known, however, and represent no obstacle to the development of an adequate analytical approach to the problem of acoustic-frequency vibration isolation. The mount connector (or isolator) is assumed to be massless and is also represented by a spring and dashpot. The vibration source may be considered to be applied at the gearbox mount structure as an oscillatory force $F_o \cos \omega t$ and a vibration motion x_1, as defined in Figure 55. The following analysis is devoted to the determination of mathematical relationships by which the force and motion amplitudes transmitted to the aircraft structure may be calculated.

Analytically determining values of m_1, k_1, and c_1, and m_2, k_2, and c_2 (as defined below) for a given physical configuration may not be an easy task. Elaborate computer program systems, such as STARDYNE or NASTRAN, exist by which the spring and mass quantities may be computed for various structures. Alternatively, if the structure already exists, as in the case of operational helicopter airframes, these quantities may be determined experimentally by attaching a vibrator at the desired location. The vibrator applies a harmonic force, the frequency of which can be varied gradually. By measuring the force, the velocity and the phase angle for each frequency, the mechanical impedance, as defined in Equation (12), may be determined. There are, in fact, commercially available automatic mechanical impedance measuring systems which can provide impedance data plots for an existing structure. The mechanical impedance, whether calculated or measured, is required as input for the transmissibility analysis developed below.

Returning to Figure 55, the equations of motion of masses m_1 and m_2 can be written as

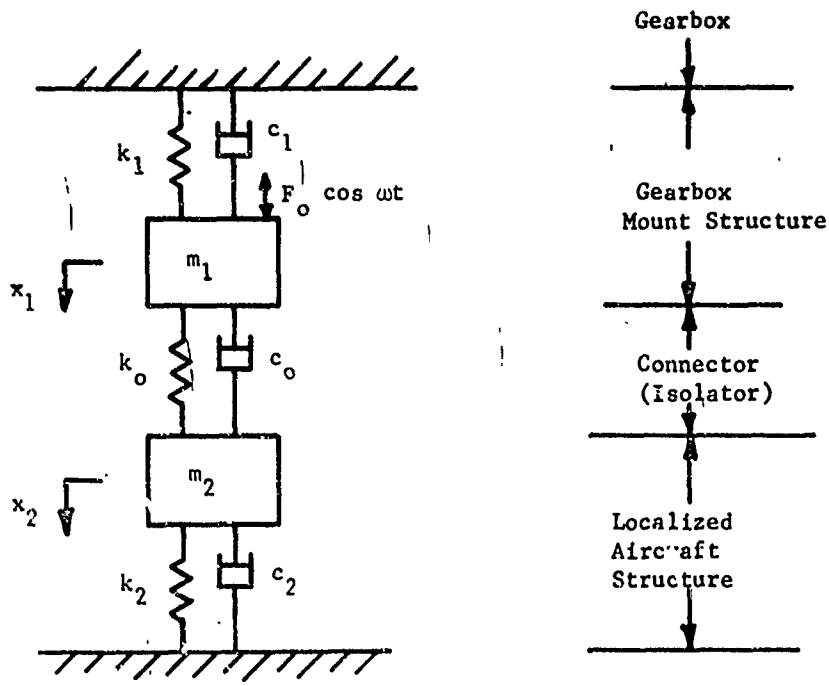

Figure 55. Analytical Model for Analysis and Design of Gearbox-to-Airframe Isolators.

$$m_1\ddot{x}_1 + c_o(\dot{x}_1 - \dot{x}_2) + c_1\dot{x}_1 + k_o(x_1 - x_2) + k_1x_1 = F_o \cos \omega t \quad (4)$$

$$m_2\ddot{x}_2 + c_o(\dot{x}_2 - \dot{x}_1) + c_2\dot{x}_2 + k_o(x_2 - x_1) + k_2x_2 = 0 \quad (5)$$

The following are defined

$$x_1 = \text{Re}\,(a_1 e^{i\omega t}) \quad (6)$$

$$x_2 = \text{Re}\,(a_2 e^{i\omega t}) \quad (7)$$

where a_1 and a_2 are the complex amplitudes and Re represents the real part of a complex quantity. The forcing function can be written in complex notation:

$$F_o \cos \omega t = \text{Re}\,(F_o e^{i\omega t})$$

Substituting x_1 and x_2 into Equations (4) and (5), we find that

$$-m_1a_1\omega^2 + i\omega c_o(a_1 - a_2) + i\omega c_1a_1 + k_o(a_1 - a_2) + k_1a_1 = F_o$$

$$-m_2a_2\omega^2 + i\omega c_o(a_2 - a_1) + i\omega c_2a_2 + k_o(a_2 - a_1) + k_2a_2 = 0$$

Note that the notation Re has been omitted. It is implied, however, that only the real parts are of physical significance.

Rearranging the above two equations, we find that

$$[-m_1\omega^2 + i\omega(c_o + c_1) + k_o + k_i]\,a_1 + [-i\omega c_o - k_o]\,a_2 = F_o \quad (8)$$

$$[-i\omega c_o - k_o]\,a_1 + [-m_2\omega^2 + i\omega(c_o + c_2) + k_o + k_2]\,a_2 = 0 \quad (9)$$

For the vibration isolation analysis, it is useful to define a motion transmissibility T_m and a force transmissibility T_f.

$$T_m = \text{motion transmissibility} = \frac{|x_2|}{|x_1|} = \frac{|a_2|}{|a_1|} \quad (10)$$

$$T_f = \text{force transmissibility} = \frac{\text{force acting on } m_2}{F_o} \quad (11)$$

The motion transmissibility may also be interpreted as the displacement transmissibility or the velocity transmissibility.

Defining a mechanical impedance Z as the ratio of force to velocity, we find that

$$Z = \text{mechanical impedance} = \frac{\text{force}}{\text{velocity}} \tag{12}$$

For a spring-mass-dashpot system,

$$Z = c + i\left(m\omega - \frac{k}{\omega}\right) \tag{13}$$

In some texts, the mechanical impedance is defined as the ratio of force to displacement. The definition chosen here, as expressed in Equation (12), is in accordance with that quantity measured by most commercially available mechanical impedance measuring systems.

The mechanical impedances of the isolator, the local gearbox mount structure and the local aircraft structure may be denoted by Z_o, Z_1 and Z_2, respectively. Then, from Equation (13), we find that

$$Z_o = \text{mechanical impedance of isolator} = c_o + i\left(-\frac{k_o}{\omega}\right) \tag{14}$$

Z_1 = mechanical impedance of local gearbox mount structure

$$= c_1 + i\left(m_1\omega - \frac{k_1}{\omega}\right) \tag{15}$$

Z_2 = mechanical impedance of local aircraft structure

$$= c_2 + i\left(m_2\,\omega - \frac{k_2}{\omega}\right) \tag{16}$$

The transmissibilities can be expressed in terms of these mechanical impedances. From Equation (9), we find that

$$\frac{a_2}{a_1} = \frac{i\,\omega\,c_o + k_o}{-m_2\omega^2 + i\,\omega\,(c_o + c_2) + k_o + k_2}$$

Multiplying both the numerator and the denominator by $(-\,i/\omega)$ yields

$$\frac{a_2}{a_1} = \frac{c_o - i\,\frac{k_o}{\omega}}{c_2 + i\left(m_2\omega - \frac{k_2}{\omega}\right) + c_o - i\,\frac{k_o}{\omega}} = \frac{Z_o}{Z_2 + Z_o} \tag{17}$$

Thus,

$$T_m = \frac{|a_2|}{|a_1|} = \frac{|Z_o|}{|Z_2 + Z_o|} \tag{18}$$

It is observed that T_m is independent of Z_1. In order for T_m to be small, Z_o must be small in magnitude. Therefore, the isolator must be relatively soft and possess low damping.

The force transmissibility as defined by Equation (11) can be expressed in terms of Z_2:

$$T_f = \frac{|i\,\omega\, a_2\, Z_2|}{F_o} \tag{19}$$

To simplify this further, multiply both sides of Equation (8) by $-i/\omega$. Thus,

$$(Z_o + Z_1)\, a_1 - Z_o a_2 = i\, F_o/\omega$$

Using Equation (17) to eliminate a_1, the above equation becomes

$$(Z_o + Z_1)\, \frac{Z_2 + Z_o}{Z_o}\, a_2 - Z_o a_2 = -\, i\, F_o/\omega$$

Rearranging this equation, we find that

$$\frac{F_o}{i\,\omega\, a_2} = \frac{(Z_o + Z_1)\,(Z_o + Z_2) - Z_o^2}{Z_o} = \frac{Z_1 Z_2 + Z_o(Z_1 + Z_2)}{Z_o}$$

Thus,

$$T_f = \frac{|i\,\omega\, a_2 Z_2|}{F_o} = \frac{|Z_o\, Z_2|}{|Z_1\, Z_2 + Z_o\, Z_1 + Z_o\, Z_2|} \tag{20}$$

From Equation (20), the force transmissibility ratio T_f will be small if

a. Z_1 is large

b. Z_o is small

Small values of impedance Z_2 would also make T_f small. But in the meantime, it would make T_m large, which is undesirable. Therefore, the conditions under which both T_m and T_f will be small are

a. large Z_1 and Z_2

b. small Z_o (21)

In other words, the mechanical impedances of the gearbox mount structure and the aircraft structure must be large and the mechanical impedance of the isolator must be small. Since the isolator impedance consists of spring and damping coefficients, the isolator should be designed to be as soft as possible. Furthermore, adding damping characteristics to an isolator design would yield adverse effects on both the motion and the force transmissibilities from the viewpoint of vibration and noise reduction.

The above equations may be used to size acoustic-frequency isolators once the gearbox mount and aircraft structural impedances have been determined.

DISCUSSION OF RESULTS

BEVEL GEAR MESH FREQUENCY SHAFT-BEARING DYNAMICS STUDIES

Radial stiffness calculations have been performed for the rolling-element bearings which support the bevel gear shafts in the UH-1D main and CH-47 forward rotor-drive gearboxes. These shaft-bearing systems have been analytically modeled for acoustic-frequency vibrations analyses. These analyses have yielded both shaft lateral natural frequencies, in the form of critical frequency maps, and also vibration amplitude and dynamic force responses to the gear-mesh-induced tooth dynamic forces calculated in References 1 and 2. Various shaft-bearing system modifications have been investigated for reductions in transmitted dynamic force levels. The results obtained indicate both logical reasons for the existence of high noise levels at the bevel gear mesh frequencies and also the feasibility of reducing them, through design or redesign efforts, by reducing the dynamic force levels which are transmitted to the gearbox casing through the spiral bevel gear shaft bearings.

Examination of rolling-element bearing stiffness values, and resulting critical frequency maps, indicates that in the CH-47 forward rotor-drive gearbox, both input and output bevel-gear shafts are operating such that the bevel mesh frequency is at or near the shafts' third critical frequencies, which are bending critical frequencies. The following important results were obtained in the CH-47 gearbox studies:

1. With regard to that component of the gearbox noise spectrum which is due to vibrations of the gearbox housing at the bevel gear mesh frequency, noise reductions on the order of 3 to 4 db were predicted for the several bevel gear shaft geometries considered. Geometry optimization, carefully carried out, may be used to effect moderate changes in the relationship between mesh frequency and shaft lateral critical frequency, thus changing the shaft vibration mode shapes and bearing dynamic force levels and thereby the casing vibration and noise levels. The modifications considered are only representative rather than all inclusive, and other modifications yielding greater noise reductions will very likely be found as a result of a comprehensive study.

2. With regard to the same noise component as above, drastic noise changes were predicted as a result of relatively large modifications to the radial stiffnesses of the input shaft ball (thrust) bearing. Care must be exercised to determine the relationship of the mesh frequency to shaft lateral critical frequency prior to modifying the stiffness of this element, however, since calculations indicate that the lateral critical frequency is very sensitive to major changes in this radial stiffness (predictions ranged from a 9-db increase in noise level to a 15-db decrease in noise level for 50 percent and 100 percent radial stiffness reductions, respectively). Stiffness modifications of the magnitudes

considered may not be achievable through bearing redesign, but may possibly instead be obtained by changes in thrust bearing radial support configurations.

3. Specification of small percentage modifications (on the order of ten percent) in the radial stiffnesses of all the rolling-element bearings was not predicted to be an effective method for achieving large reductions in the noise produced at the bevel mesh frequency (although changes of 1 or 2 db may be achievable), primarily because changes of this magnitude will very likely be less than those needed to make major increases in the frequency separation between the mesh and lateral critical frequencies.

4. The addition of moderate amounts of viscous damping between the shaft and the casing near the input bevel gear location resulted in little or no calculated reduction in vibration levels of the input shaft.

The results discussed above are not additive. That is, the db reduction which may be achieved by applying more than one modification is not necessarily the sum of the calculated db reduction for each taken separately. The overall reduction will depend on the bearing radial dynamic forces, which in turn depend upon all of the elements which affect the dynamic characteristics of the shafts.

While no definitive measurements yet exist which can answer the question of the relative importance of the gearbox casing as a noise emitter compared to the aircraft structure, there are some preliminary indications that the gearbox casing may be the major source of noise at the bevel gear mesh frequency. Should this be confirmed, then the db reductions discussed above for the noise emitted by the casing would be very significant as far as the overall noise level at the bevel gear mesh frequency is concerned.

In the case of the UH-1D main rotor-drive gearbox, both input and output bevel-gear shafts are operating such that the bevel mesh frequency is at or near the shafts' second critical frequencies. For the input bevel gear shaft, this is a rigid-body mode, whereas it is a bending mode for the output bevel gear shaft.

The following important results were obtained in the UH-1D gearbox studies:

1. With regard to that component of the gearbox noise spectrum which is due to vibrations of the gearbox housing at the bevel gear mesh frequency, noise reductions on the order of 2 to 4 db were predicted for the several bevel gear shaft geometries considered, for the addition of a moderate amount of viscous damping between the shaft and casing near the input shaft roller bearing, and for the substitution of a material dynamically similar to titanium as the shaft material. These modifications, the results of which must not be considered additive, are generally effective because they increase the frequency separation between the mesh and lateral

critical frequencies. The modifications studied should be considered as representative rather than all inclusive.

2. With regard to the same noise component, drastic noise reductions are predicted as a result of relatively large changes in the radial stiffness of the roller and triplex ball bearings on the input bevel gear shaft. Such modifications are effective because they produce relatively large separations between mesh and critical frequencies. Care must be taken to determine the relationship of the mesh and critical frequencies prior to making such changes, since shifting the critical frequency the wrong way may drastically increase the noise level.

3. Specification of small percentage changes (on the order of ten percent) in the radial stiffnesses of all the rolling-element bearings was not predicted to be an effective method for achieving large reductions in the noise produced at the bevel mesh frequency, primarily because changes of this magnitude generally result in little additional separation between the mesh and lateral critical frequencies. Bearing support configuration changes, or changes to single bearing stiffnesses, may prove useful for this purpose, however. These and other configuration changes may exist for achieving this frequency separation. The ones considered herein were selected to illustrate the technique.

Apparently no definitive measurements exist for the UH-1D which can answer the question of the relative importance of the gearbox casing as a noise emitter at the bevel mesh frequency compared to the aircraft structure. There are strong indications, however, based upon the analysis of previous recordings and studies, for instance (7), and upon test cell measurements, that the gearbox casing is the major source of noise at the bevel gear mesh frequency. Eventual confirmation of this relative importance will cause the db reductions discussed above to be highly significant as far as the overall noise level at the bevel gear mesh frequency is concerned.

RING-GEAR MESH FREQUENCY GEARBOX CASING VIBRATION STUDIES

The ring-gear sections of the UH-1D and CH-47 gearbox casings have been analytically modeled for acoustic-frequency vibrations analyses. Thin-shell vibration studies have yielded shell-mode natural frequencies for each ring-gear section for various ring-gear structural-support conditions. Shell vibration response calculations have also been performed, utilizing as inputs the lower planetary planet-gear to ring-gear dynamic forces calculated in References 1 and 2. These calculations have yielded calculated casing vibration amplitudes (proportional to the noise levels generated directly by the ring-gear casing) and also force levels transmitted to the remainder of the gearbox casing (and thus reasonably proportional to those dynamic force levels transmitted to the airframe). Several ring-gear structural modifications have been investigated for reductions in vibration levels. The

results obtained significantly improve the understanding of the mechanisms by which acoustic-frequency vibration energy, produced as a result of gear mesh dynamics, is emitted from the gearbox as noise. Logical reasons are indicated for the existence of high levels of vibration, and thus noise, at the planetary mesh frequencies, and the feasibility of reducing these levels through design or redesign efforts has been established.

Examination of ring-gear casing calculated shell mode natural frequencies for the CH-47 (Figure 37) indicates that the natural frequencies are above both the upper and lower planetary mesh frequencies. The lowest calculated natural frequency (hoop circumferential mode, first axial mode) coincides with the third multiple of the lower planetary mesh frequency. Consideration of the effects of ring-gear casing end conditions upon the shell mode natural frequencies indicates that, for mountings more rigid than pinned ends (a situation which will likely be obtained in view of the relatively rigid ring-gear section ends), the natural frequencies will be considerably above the first three multiples of the two mesh frequencies. Such a result is significant, since it indicates that forced-response vibrations are present, rather than resonant vibrations. Force-response vibrations may be dealt with either by considerably stiffening the ring-gear structure, thereby permitting the structure to react the forces with resulting lower amplitudes, or by softening the local structure, thereby isolating the rest of the gearbox from the higher local vibrations in the area of the ring gear. In either case, little if any change may be expected in the transmitted force levels. Stiffening modifications have been analytically demonstrated to be effective in reducing vibration levels in the CH-47 ring gear.

In the UH-1D ring-gear casing, a different picture has emerged. Examination of calculated shell-mode natural frequencies (Figure 46) indicates that three circumferential modes at the second axial mode and four circumferential modes at the first axial mode fall within the frequency range of the second and third multiples of the lower planetary mesh frequency for the pinned-end casing condition. In particular, the second multiple of the lower planetary mesh frequency (four planets) falls very close to the two- and four-per-revolution circumferential modes, and the third multiple falls only slightly above the eight-per-revolution circumferential modes. This close correspondence and the likelihood that the pinned-end condition is approximated by the relatively thin wall of the UH-1D casing mean that the ring-gear vibrations are very likely of the resonant type. Resonant vibrations may be dealt with both by stiffening (or softening) and by the selective addition (or removal) of mass. Stiffening and the addition of mass have been analytically demonstrated to be effective in reducing vibration levels in the UH-1D ring gear. This result is particularly important in view of the likelihood, because of the isolation of the ring gear from the airframe, that whatever noise is emitted at the planetary mesh frequency or its higher multiples will very likely be emitted from the ring-gear casing itself.

The results of the acoustic power and sound pressure level calculations for

the two gearboxes are also significant and should be examined in detail. These calculations, which have been performed using as inputs the predicted casing vibration amplitudes, were done (without the use of empirical factors) by means of equations (Appendix III) based upon the physics of oscillating surfaces. The calculated noise levels, therefore, are anticipated to be very nearly those levels which would be recorded at the lower planetary mesh frequency by a microphone positioned near a vibrating ring-gear casing (other elements of the helicopter structure are vibrating also, but this calculation is only for the ring-gear casing). Comparison of the calculated noise levels with measured noise levels at the lower planetary mesh frequency will therefore provide a good indication of the relative amounts of mesh frequency energy emitted by the ring-gear housing compared to all other aircraft elements.

In the case of the CH-47, the nominal configuration ring-gear casing is predicted to radiate 1.3×10^{-5} watt at the lower planetary mesh frequency, equivalent to a sound pressure level of about 71 db at 1 foot from a point source. The CH-47 ring-gear casing as modified is predicted to radiate 9.6×10^{-7} watts, equivalent to a sound pressure level of about 60 db at 1 foot. The modification results, therefore, in a reduction in sound pressure level of 11 db at 1 foot, a considerable decrease. However, measured sound pressure levels on the order of 105 db have been observed (2, 3, 4) adjacent to the CH-47 forward rotor-drive gearbox at the lower planetary mesh frequency. Therefore, other, more powerful noise sources must exist. The modification, in which the ring-gear casing was stiffened, must not be discarded as useless, however, even though its apparent contribution to the overall noise level is small. For this is the only element which is being forced to vibrate at a frequency corresponding to a very high measured noise component. Reductions in vibration levels, such as those achieved by this modification, will result in lower amplitudes of vibrations being transmitted to the remainder of the aircraft structure. Thus, although the noise emitted by the CH-47 ring gear itself appears to be only a very small part of the overall noise levels experienced, and therefore, the 11 db reduction will be insignificant, the mechanical vibration levels transmitted to the rest of the structure, and therefore the overall noise levels, will be significantly reduced.

In the case of the UH-1D, the nominal configuration ring-gear casing is predicted to radiate 4.38×10^{-3} watt at the lower planetary mesh frequency, equivalent to a sound pressure level of about 97 db at 1 foot from a point source. The UH-1D ring-gear casing as modified is predicted to radiate 5.83×10^{-4} watt, equivalent to a sound pressure level of about 88 db at 1 foot. The modification results, therefore, in a reduction in sound pressure level of 9 db at 1 foot, a considerable decrease.

Measured sound pressure levels on the order of 105 db have been observed [1] adjacent to the UH-1D main gearbox at the lower planetary mesh frequency. Therefore, the ring-gear casing is probably the major source of noise at the lower planetary mesh frequency. The 8 db difference between the calculated and measured values of 97 and 105 db, respectively, should be examined with consideration of the following: (1) there are likely to be other areas of

the gearbox participating in the vibration at the lower planetary mesh frequency; (2) the calculations are based on a nonenclosed point source; and (3) the measured results are expressed in one-third-octave form and thus include some contribution from the third harmonic of the upper planetary mesh frequency. Proper accounting for each of these elements would tend to reduce the 8 db difference.

In any case, the calculated and measured UH-1D noise levels at the lower planetary mesh frequency are much closer than are similar values for the CH-47. Therefore, changes in noise level at this frequency, calculated for modifications to the ring-gear casing, will be highly significant in reducing the measured noise level in the helicopter at this frequency, since the ring-gear casing appears to be the major significant source of noise.

GEARBOX-AIRFRAME ISOLATION STUDIES

A reasonably general analytical model of the gearbox-to-airframe interface has been prepared, including dynamic elements representative of an acoustic-frequency isolator. The force and motion transmissibility characteristics of this model indicate that good isolation of the airframe from high-frequency vibrations will result (i.e., that force and motion transmissibility across the gearbox-airframe interfaces will be lowest) when the local gearbox and cirframe structures possess relatively high mechanical impedance characteristics and the isolator possesses relatively low mechanical impedance.

It appears possible to effectively isolate the airframe from the acoustic-frequency vibrations produced by the gearbox by tuning the isolators to the frequency range of about 200 to 500 Hz. Such isolators should be rigid enough to provide the static stiffness required for structural integrity, yet will provide for attenuation of vibrations at frequencies higher than about 1.5 times the isolator frequency.

IMPROVEMENTS TO HELICOPTER INTERNAL NOISE DATA BANK

Samples of acoustic data, in full octave and one-third-octave form, were discussed with and obtained from the Vertol Division - the Boeing Company for older versions of the CH-47 in several configurations. More recent data, together with narrow-band real-time reduction techniques, were also discussed. In addition, narrow-band, real-time data were also discussed with and obtained from the U.S. Army Aeromedical Research Laboratory, Fort Rucker, Alabama, for several CH-47C helicopter operating configurations. These data have proved very useful in further identifying the exact drive train components responsible for the noise levels measured inside operating CH-47 helicopters, and, perhaps more important, have indicated that only narrow-band data are suitable for use in machinery-noise reduction efforts of this type.

Samples of UH-1 interior acoustic data, in full-octave and narrow-band form

were discussed with an obtained from the Bell Helicopter Company, Fort Worth, Texas, for several aircraft configurations.

CONCLUSIONS AND RECOMMENDATIONS

The following conclusions are drawn as a result of the acoustic-frequency vibrations studies reported herein:

1. Consideration of gearbox-generated noise in terms of high-frequency mechanical vibration of gearbox internal components advances logical reasons for the existence of high noise levels at several gear mesh frequencies. Pursuing noise reduction via mechanical vibration reduction permits both the immediate application of existing analytical and experimental vibration methods to the problem, and perhaps more important, provides direction to the development of new technology required for the design of future quiet gearboxes.

2. With regard to noise components at the bevel gear mesh frequency, bevel shaft lateral natural frequencies are, in several cases, in close proximity to the bevel mesh frequency in both of the gearboxes studied. Shaft vibrations at these lateral natural frequencies apparently involve mode shapes in which the shaft bearings are not at nodal points. Hence, forces proportional to vibration amplitude and bearing stiffness are applied at the mesh frequency to the gearbox casing, producing vibrations and noise. Reduction of these force levels via redesign of bearings and shaft components, guided by vibration calculations, has been analytically demonstrated to be both feasible and practical.

3. With regard to noise components at the planet-to-ring-gear mesh frequencies, in the CH-47, the ring-gear-casing structural natural frequencies are well above the first three multiples of the mesh frequencies and forced-response rather than resonant-response vibrations are present. The CH-47 ring-gear casing probably acts more to transfer mechanical vibration energy to its surroundings rather than as a noise source, judging from the predicted casing vibration amplitude levels.

   In the case of the UH-1D ring-gear casing, on the other hand, several structural natural frequencies are apparently in close proximity to the first three multiples of the planet-to-ring-gear mesh frequencies. Thus, the UH-1D ring-gear structural vibrations are probably of the resonant-response type. Judging from predicted casing vibration amplitude levels, the UH-1D ring-gear casing is itself probably a significant noise source.

   Reduction of ring-gear-casing vibration levels via redesign of casing components, guided by vibration calculations, has been analytically demonstrated to be both feasible and practical.

4. The general analytical model developed for gearbox-to-airframe isolation analysis indicates that force and motion transmissibility across the gearbox-airframe interface will be lowest when the local gearbox and airframe structures possess relatively high mechanical impedance characteristics and the isolator possesses relatively low mechanical impedance. Isolators tuned to a frequency between the highest aircraft component structural natural frequencies and the lowest acoustic frequencies of interest should provide the best attenuation of gearbox noise components without adversely affecting structural integrity.

5. The survey of major organizations (U.S. Government agencies and helicopter airframe manufacturers) known to be active in the area of helicopter internal noise reduction has shown that a large amount of helicopter internal noise data and some acoustic-frequency vibration data exist. On the other hand, examination and discussion of existing data with aircraft manufacturer technical personnel indicate that this data may not have been put to the fullest use in determining the relative importance of the several paths by which acoustic frequency energy travels from its source to the ear.

The following recommendations are made:

1. Efforts should be undertaken, in helicopters in which noise is a problem, to determine as precisely as possible the routes by which internal noise components travel from their sources to the ear.

2. Efforts should be undertaken to assess, experimentally, the ability of existing gearbox hardware noise reduction technology to predict those quantities related to the acoustic characteristics of specific gearboxes. Where these existing techniques are not fully adequate, they should be improved and extended. Where adequate, they should be so documented, reduced to design or oriented form, and incorporated into the design process.

3. Efforts should be undertaken to develop and verify through tests the technology required for the prediction and reduction of aircraft structure-related internal noise components.

4. Efforts should be undertaken to assess the importance of aircraft systems other than the rotor-drive gearbox to helicopter internal noise levels. Where other systems, such as accessories, are found to be important noise contributors, noise-reduction efforts directed at these systems should be undertaken.

LITERATURE CITED

1. Laskin, I., Orcutt, F. K., and Shipley, E. E., ANALYSIS OF NOISE GENERATED BY UH-1 HELICOPTER TRANSMISSION, USAAVLABS Technical Report 68-41, U.S. Army Aviation Materiel Laboratories, Fort Eustis, Virginia, June, 1968, AD 675457.

2. Badgley, R. H., and Laskin, I., PROGRAM FOR HELICOPTER GEARBOX NOISE PREDICTION AND REDUCTION, USAAVLABS Technical Report 70-12, U.S. Army Aviation Materiel Laboratories, Fort Eustis, Va., March 1970, AD 869822.

3. Badgley, R. H., MECHANICAL ASPECTS OF GEAR-INDUCED NOISE IN COMPLETE POWER-TRAIN SYSTEMS, ASME Paper No. 70-WA/DGP-1, Presented at the ASME Winter Annual Meeting, December, 1970.

4. Camp, R. T., NOISE SPECTRA OF THE U. S. ARMY CH-47C HELICOPTER, USAARL Letter Report, U. S. Army Aeromedical Research Laboratory, Fort Rucker, Alabama, 17 October 1969, and subsequent unpublished communications.

5. Mechanical Technology Incorporated Staff, ROTOR-BEARING DYNAMICS DESIGN TECHNOLOGY - PART III: DESIGN HANDBOOK FOR FLUID FILM TYPE BEARINGS, MTI Report 65TR14, Prepared Under U. S. Air Force Contract AF 33(615)-1895 and also issued as Air Force Report AFAPL-TR-65-45, Part III, May, 1965.

6. Gray, D. E., Coordinating Editor, AMERICAN INSTITUTE OF PHYSICS HANDBOOK, Second Edition, McGraw-Hill Book Company, Inc., New York, 1963.

7. Camp, R. T., OVERALL AND OCTAVE-BAND NOISE ATTENUATION CHARACTERISTICS OF SOUNDPROOFING BLANKETS IN U.S. ARMY UH-1D HELICOPTERS, USAARU Letter Report, U. S. Army Aeromedical Research Unit, Fort Rucker, Alabama, 14 November 1968.

APPENDIX I
DYNAMIC RESPONSE CALCULATIONS OF THE UH-1D MAIN ROTOR-DRIVE GEARBOX RING-GEAR CASING

From Reference 1 and the drawings of the UH-1D, the following input data are obtained for dynamic response calculations.

UH-1D Lower Planetary

Number of Sun Gear Teeth = 57
Number of Planetary Gear Teeth = 31
Number of Ring-Gear Teeth = 119
Number of Planetary Gears = 4
Tooth Pressure Angle = 22°
Fundamental Frequencies of Dynamic Excitation = 1982 Hz
Tangential Dynamic Force at Planet - Ring Mesh = 73 lb
Ring-Gear Tooth Face Width = 0.8 in.
Ring-Gear Root Circle Radius = 7.15 in.

The four planetary gears were spaced equally around the ring gear as shown schematically in Figure 56. However, the dynamic forces on each planetary gear are not in phase. In other words, when one of the planetary gears, say, gear A, reaches its peak dynamic force, the rest of the planetary gears are only at some intermediate forces below the peak value. In fact, a simple layout of the gear teeth mesh would show that each planetary gear has a 90-degree phase difference from its neighboring gears. If gear A is used as a reference, then gear B is lagging A by 90 degrees, gear C is lagging A by 180 degrees, and gear D is lagging A by 270 degrees.

Let us concentrate on the dynamic forces existing on the ring gear by gear A. First, the dynamic force has a sinusoidal variation in time with a frequency ω. It also has a spatial distribution denoted by $p_A(\theta)$. Thus, the dynamic force of gear A on the ring gear is

$$P_A(\theta,t) = p_A(\theta) \cos \omega t \tag{22}$$

where $P_A(\theta)$ is the circumferential distribution of the dynamic force. Since we will be interested in calculating the casing dynamic response in the normal direction, the radial component of the tooth dynamic force is calculated.

$$\begin{aligned} \text{Radial Dynamic Force Amplitude} &= \text{Tangential Dynamic Force} \times \text{Tangent of Pressure Angle} \\ &= 73 \tan 22^{\circ} \\ &= 29.5 \text{ lb} \end{aligned} \tag{23}$$

Assume that this radial dynamic force is uniformly distributed across the face width and over one tooth spacing circumferentially. Let 2ℓ be the circumferential length of one tooth spacing.

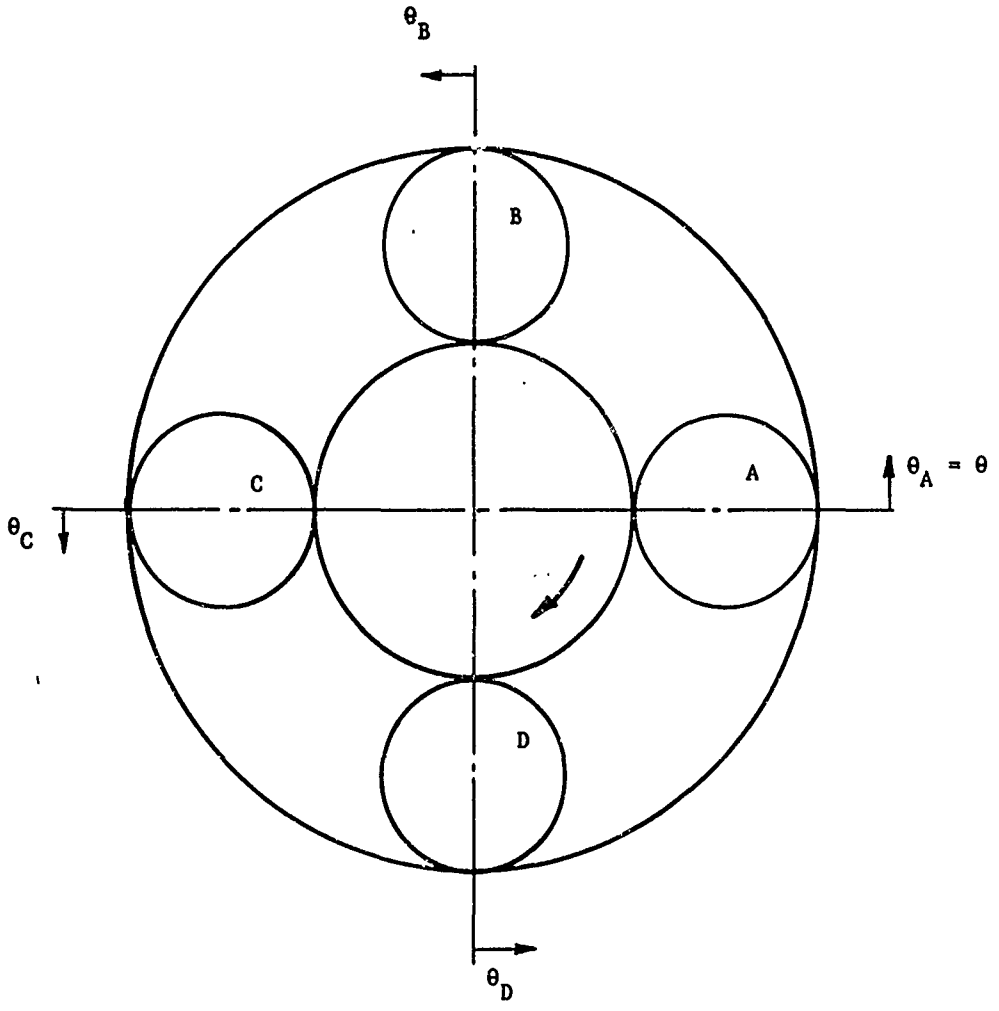

Figure 56. Schematic Diagram and Coordinate System for the UH-1D Lower Planetary Gears.

Then

$$2\ell = \frac{2\pi\ (7.15)}{119} = 0.377 \text{ in.} \tag{24}$$

The circumferential distribution of the radial dynamic force of one planetary gear is thus shown in the following sketch:

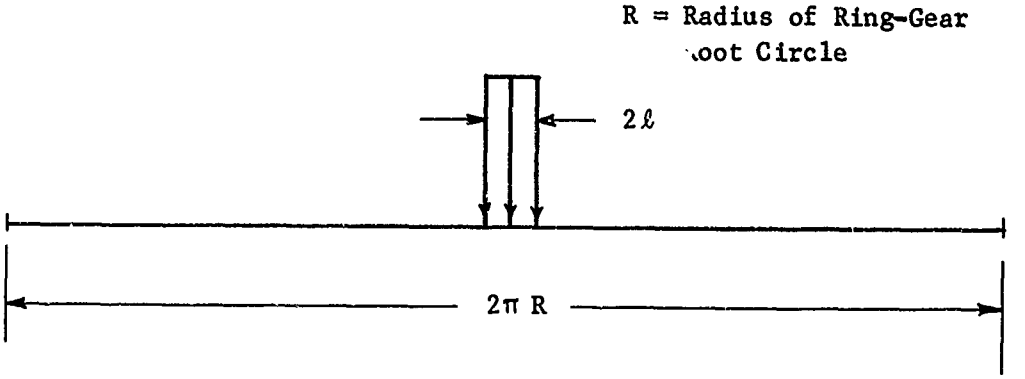

In order to facilitate a dynamic response analysis, this circumferential distribution is expressed in terms of a Fourier series.

In general, we can expand the periodic function f(x) depicted in the following diagram in Fourier series:

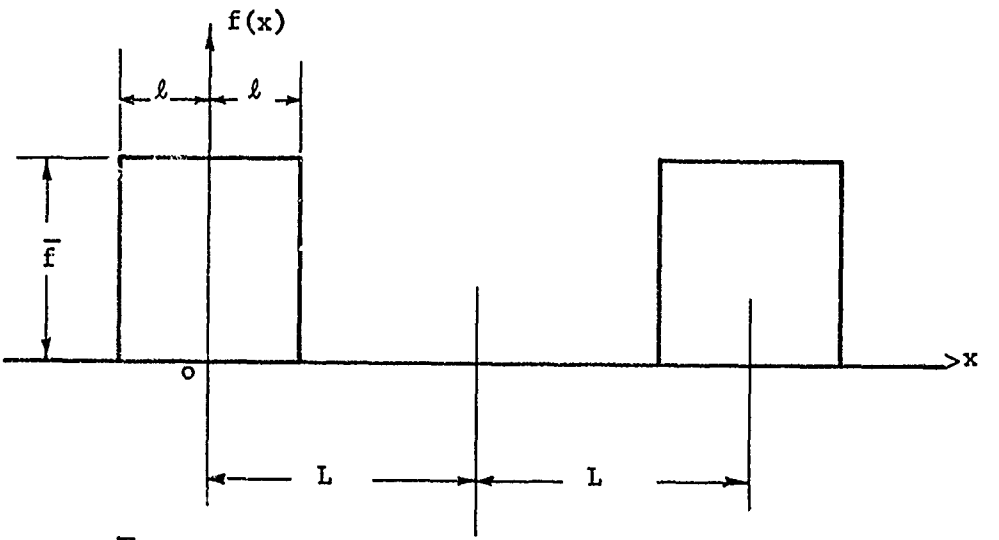

$$f(x) = \bar{f} \quad \text{for } -\ell < x < \ell$$
$$= o \quad \text{otherwise}$$

f(x) has a periodicity of 2L. Because of symmetry, f(x) can be expanded in a cosine Fourier series as follows:

$$f(x) = \frac{1}{2} a_o + \sum_{m=1}^{\infty} a_m \cos \frac{m\pi}{L} x \tag{25}$$

where

$$a_m = \frac{2}{L} \int_o^L f(x) \cos \frac{m\pi}{L} x \, dx$$

$$= \frac{2\bar{f}}{L} \int_o^{\ell} \cos \frac{m\pi}{L} x \, dx$$

$$= \frac{2\bar{f}}{m\pi} \sin \frac{m\pi\ell}{L} \tag{26}$$

Apply the above equations to the lower planetary of UH-1D, and replace L by πR, x by $R\theta$, and $\bar{f}$ by p_1 where p_1 is the radial dynamic force per unit area.

$$p_A(\theta) = \frac{1}{2} a_o + \sum_{m=1}^{\infty} a_m \cos m\theta \tag{27}$$

where

$$a_m = \frac{2p_1}{m\pi} \sin \frac{m\ell}{R} \tag{28}$$

Thus, the radial dynamic force of gear A is represented by Equations (22) and (27). The series in Equation (27) converges rather slowly. This may be anticipated because the radial dynamic force is confined to a relatively small region. However, in dealing with the present problem, the series will be cut off at m=10. This is hardly enough for the series approximation, as will be seen in the numerical computation. The justification to cut off the series at m=10 is explained in the following.

The goal of this analysis is to compute the dynamic response. The forcing frequency has a fixed value; for example, the fundamental frequency of the lower planetary is 1982 Hz. The significance of the m=11 term in Equation (27) is a forcing function to excite a mode with a circumferential wave number of 11. From Table I, it is estimated that the first-axial n=11 mode has a natural frequency of approximately 9000 Hz. This high frequency (9000 Hz) mode is hardly excited by the dynamic force with a frequency of 1982 Hz. Therefore, from the point of view of the dynamic response, the series of Equation (27) can be cut off at a high enough m and before the series converges.

In Equations (22) and (27), replace θ by θ_A where θ_A indicates the angular

coordinate associated with planetary gear A (see Figure 56).

$$P_A(\theta_A, t) = p_A(\theta_A) \cos \omega t \tag{29}$$

where

$$p_A(\theta_A) = \frac{1}{2} a_o + \sum_{m=1}^{10} a_m \cos m \theta_A \tag{30}$$

$$a_m = \frac{2p_1}{m\pi} \sin \frac{m\ell}{R} \tag{31}$$

Planetary Gear B

For planetary gear B, use the angular coordinate θ_B (see Figure 56) and let the phase lag of "B" relative to "A" be Ψ_B. Thus,

$$P_B(\theta_B, t) = p_B(\theta_B) \cos(\omega t - \Psi_B) \tag{32}$$

$$p_B(\theta_B) = \frac{1}{2} a_o + \sum_{m=1}^{10} a_m \cos m \theta_B \tag{33}$$

Planetary Gear C

$$P_C(\theta_C, t) = p_C(\theta_C) \cos(\omega t - \Psi_C) \tag{34}$$

$$p_C(\theta_C) = \frac{1}{2} a_o + \sum_{m=1}^{10} a_m \cos m \theta_C \tag{35}$$

Planetary Gear D

$$P_D(\theta_D, t) = p_D(\theta_D) \cos(\omega t - \Psi_D) \tag{36}$$

$$p_D(\theta_D) = \frac{1}{2} a_o + \sum_{m=1}^{10} a_m \cos m \theta_D \tag{37}$$

As mentioned earlier,

$$\Psi_B = 90° \tag{38}$$

$$\Psi_C = 180°$$

$$\Psi_D = 270°$$

From Figure 56,

$$\theta_A = \theta$$
$$\theta_B = \theta - 90°$$
$$\theta_C = \theta - 180° \qquad (39)$$
$$\theta_D = \theta - 270°$$

The following numerical values are computed.

Area on which the dynamic force acts = 2 ℓ x (gear face width)

$$= 0.377 \times 0.8 = 0.302 \text{ in.}^2$$

$$p_1 = \frac{\text{Radial Dynamic Force}}{\text{Area}} = \frac{29.5}{0.302} = 97.7 \text{ psi}$$

$$a_o = \frac{2p_1\ell}{\pi R} = \frac{97.7 \times 0.377}{\pi \times 7.15} = 1.64$$

$$a_1 = \frac{2p_1}{\pi} \sin \frac{\ell}{R} = \frac{2 \times 97.7}{\pi} \sin \frac{0.377}{2 \times 7.15} = 1.64$$

$$a_2 = a_3 = \ldots = a_9 = 1.64$$

$$a_{10} = 1.63$$

Now, knowing the Fourier coefficients a_o, a_1, a_2 and so on, the ring-gear dynamic response due to, say, planetary gear A, can be calculated. The dynamic forces as expressed by Equations (29) and (30) are used as input data to an MTI computer program . The computer program first calculates the dynamic response due to each Fourier component separately. The dynamic responses are then superimposed to yield the response due to gear A.

Let a general response function due to gear A be represented by

$$b_A(\theta_A, z) \cos \omega t \qquad \text{(from gear A)} \qquad (40)$$

where $b_A(\theta_A, z)$ is part of the print-out of the dynamic response program; for example, b_A could be the normal displacement amplitude W_A, or the azimuthal displacement amplitude or the like. Similarly, we have

$$b_B(\theta_B, z) \cos(\omega t - \Psi_B) \qquad \text{(from gear B)}$$
$$b_C(\theta_C, z) \cos(\omega t - \Psi_C) \qquad \text{(from gear C)} \qquad (41)$$
$$b_D(\theta_D, z) \cos(\omega t - \Psi_D) \qquad \text{(from gear D)}$$

The total of this general response function is the sum of the responses due to each individual gear. Thus, in terms of an amplitude $b(\theta, z)$ and a phase angle $\phi(\theta, z)$, the general response function is

$$b(\theta, z) \cos [\omega t + \phi(\theta,z)] = b_A(\theta_A, z) \cos \omega t + b_B(\theta_B, z) \cos (\omega t - \Psi_B)$$

$$+ b_C(\theta_C, z) \cos (\omega t - \Psi_C) + b_D(\theta_D, z) \cos (\omega t - \Psi_D) \quad (42)$$

Expanding Equation (42), then equating the cos ωt terms and equating the sin ωt terms,

$$b \cos \phi = b_A + b_B \cos \Psi_B + b_C \cos \Psi_C + b_D \cos \Psi_D \quad (43)$$

$$-b \sin \phi = b_B \sin \Psi_B + b_C \sin \Psi_C + b_D \sin \Psi_D \quad (44)$$

Squaring both sides and then adding,

$$b(\theta, z) = \Big\{ [b_A(\theta_A, z) + b_B(\theta_B, z) \cos \Psi_B + b_C(\theta_C, z) \cos \Psi_C + b_D(\theta_D, z) \cos \Psi_D]^2 + [b_B(\theta_B, z) \sin \Psi_B + b_C(\theta_C, z) \sin \Psi_C + b_D(\theta_D, z) \sin \Psi_D]^2 \Big\}^{\frac{1}{2}} \quad (45)$$

By taking the ratio of Equations (43) and (44),

$$\phi(\theta, z) = \text{Arc tan} \left[\frac{-\{b_B(\theta_B, z) \sin \Psi_B + b_C(\theta_C, z) \sin \Psi_C + b_D(\theta_D, z) \sin \Psi_D\}}{b_A(\theta_A, z) + b_B(\theta_B, z) \cos \Psi_B + b_C(\theta_C, z) \cos \Psi_C + b_D(\theta_D, z) \cos \Psi_D} \right] \quad (46)$$

The phase angle $\phi(\theta, z)$ is the phase advance relative to planetary gear A.

APPENDIX II
DYNAMIC RESPONSE CALCULATIONS OF THE CH-47 FORWARD ROTOR-DRIVE GEARBOX RING GEAR CASING

From Reference 2 and the drawings of the CH-47, the following input data are obtained for dynamic response calculations.

CH-47 Lower Planetary

Number of Sun Gear Teeth = 28
Number of Planetary Gear Teeth = 39
Number of Ring-Gear Teeth = 106
Number of Planetary Gears = 4
Tooth Pressure Angle = 25^{o}
Fundamental Frequency of Dynamic Excitation = 1482 Hz
Tangential Dynamic Force at Planet-Ring Mesh = 79.6 lb
Ring-Gear Tooth Face Width = 1.2 in.
Ring-Gear Root Circle Radius = 10.85 in.

The four planetary gears are not equally spaced around the ring gear as contrasted to the UH-1D arrangement. A schematic diagram of the lower planetary gears is shown in Figure 57. The angular locations of planetary gears A, C, B and D are respectively zero degrees, 91.343 degrees, 180 degrees and 271.343 degrees. Since the planet gears have an odd number of teeth, the sun-planet meshing and the planet-ring meshing are in phase (see Figure 41 of Reference 1). Furthermore, because the sun gear has an even number of teeth and the line connecting the centers of "A", sun and "B" is a straight line, the "sun-A" meshing and the "sun-B" meshing are also in phase. Therefore, it can be deduced that the "ring-A" meshing and the "ring-B" meshing are in phase (see Figure 57). Similarly, the "ring-C" meshing and "ring-D" meshing are also in phase. However, the phase relationship between the "ring-A" meshing and the "ring-C" meshing remains to be determined.

In Figure 58, the planetary gear "A" is at its peak dynamic (fundamental) load both at the "sun-A" meshing and the "ring-A" meshing. Next, consider the situation of the planetary gear "C". The sun gear has 28 teeth; each tooth takes an angular span of 360/28 = 12.87 degrees. Since the center-line of the sun-C gear is at an angular location of 91.343 degrees, the "sun-C" meshing is 1.343 degrees over the 90-degree point which is the peak load location. This 1.343 degrees is equivalent to 1.343 degrees/12.87 degrees = 0.1044 tooth space on the sun gear. Temporally, this means the "sun-C" meshing is 0.1044 x 360 degrees = 37.6 degrees from its peak loading at the fundamental frequency. As stated earlier, the "sun-C" and "ring-C" meshings are in phase. Therefore, the temporal phase difference between the "ring-A" meshing and the "ring-C" meshing is 37.6 degrees, with the latter lagging the former. At second harmonics, the temporal phase angle is doubled, and at third harmonics, tripled, and so on.

Referring to Figure 57, let the dynamic forces of gears A and B be

$$P_{AB}(\theta, t) = p_{AB}(\theta) \cos \omega t \qquad (47)$$

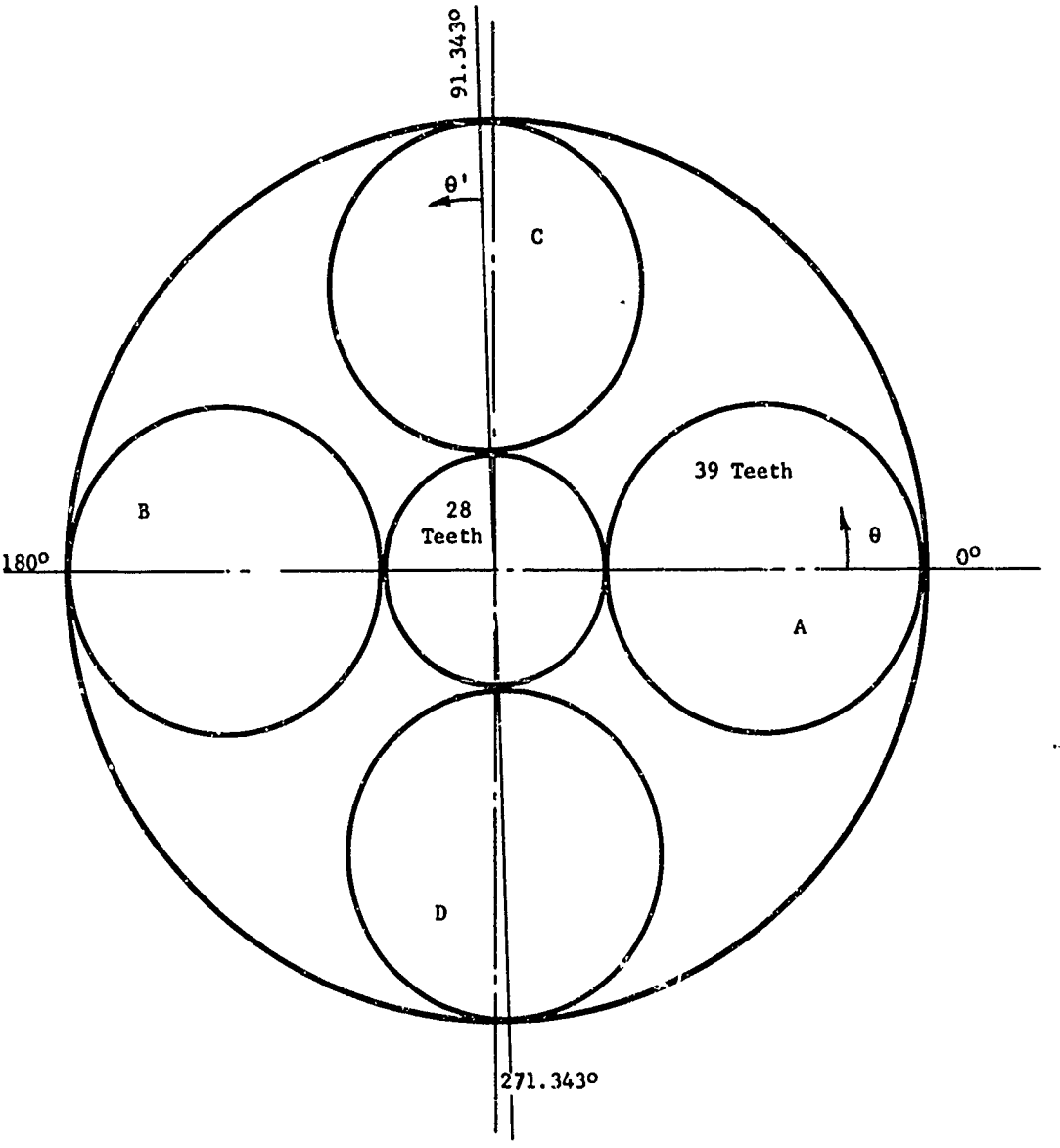

Figure 57. CH-47 Lower Planetary Gear Mesh Phasing Diagram.

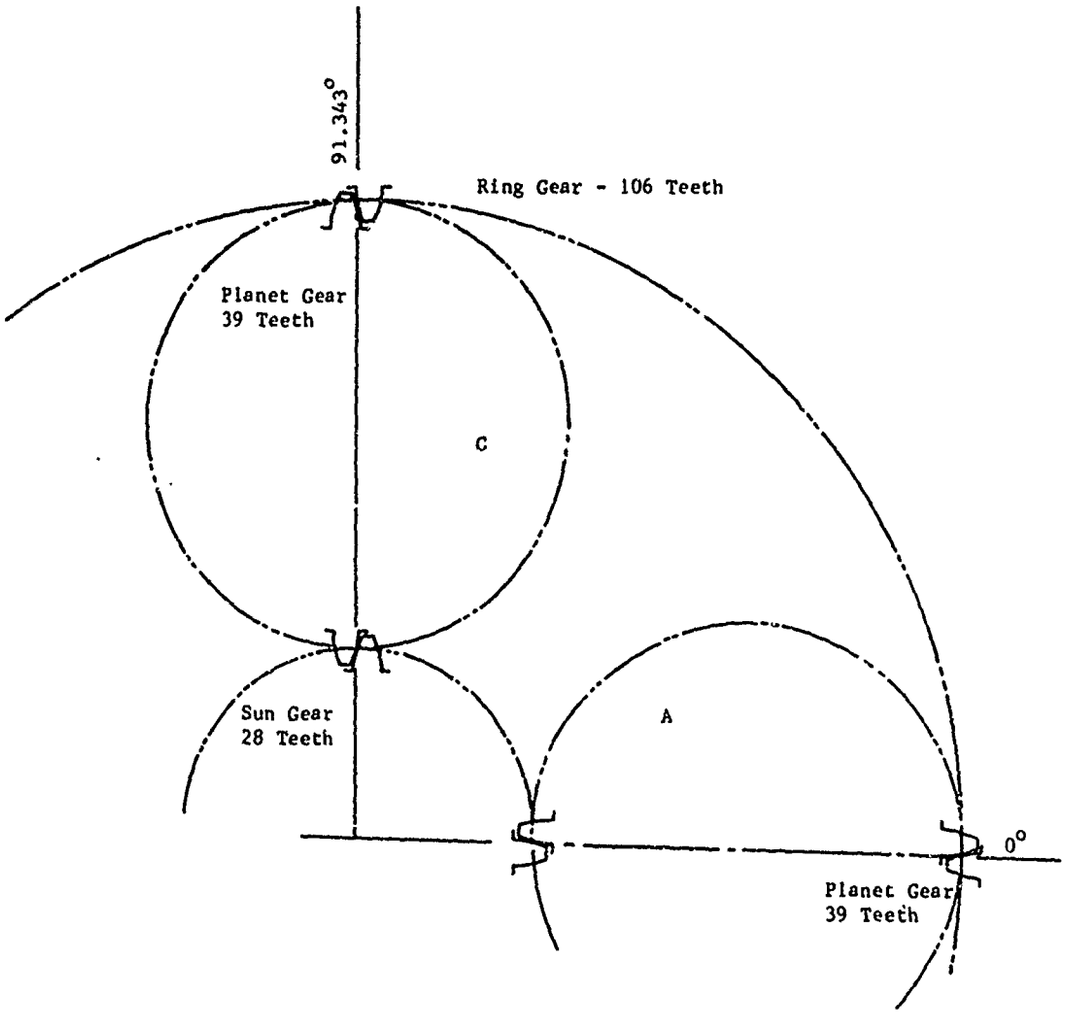

Figure 58. CH-47 Lower Planetary Gear Mesh Phasing Diagram Showing Gear-Tooth Positions.

where $p_{AB}(\theta)$ is the circumferential distribution of the dynamic force. The dynamic forces of gears A and B can be considered together and expressed in the form of Equation (47) because they are in phase. Similarly, for gears C and D,

$$P_{CD}(\theta', t) = p_{CD}(\theta') \cos(\omega t - \Psi) \qquad (48)$$

where $\omega = 1482$ Hz

$\Psi = 37.6°$

and θ' is shown in Figure (57).

The radial component of the tooth dynamic force is related to the tangential component by the tooth pressure angle.

Radial Dynamic Force Amplitude

= Tangential Dynamic Force x Tangent of Pressure Angle

= 79.6 tan 25° = 37.2 lb.

From the CH-47 gearbox assembly drawing, it is seen that one half of the gear face width is supported by the structure; the other half is not. For the analysis, the radial dynamic force is assumed to be distributed uniformly across one-half of the gear face width and over one tooth spacing circumferentially. Let 2ℓ = circumferential length of one tooth spacing. Then,

$$2\ell = \frac{2\pi\ (10.86)}{106} = 0.644 \text{ in.}$$

Thus, the dynamic radial pressure

$$p_1 = \frac{37.2}{0.6 \times 0.644} = 96.5 \text{ psi.}$$

The circumferential distribution of the dynamic radial pressure exerted by planetary gears "A" and "B" on the ring gear is shown in the following sketch.

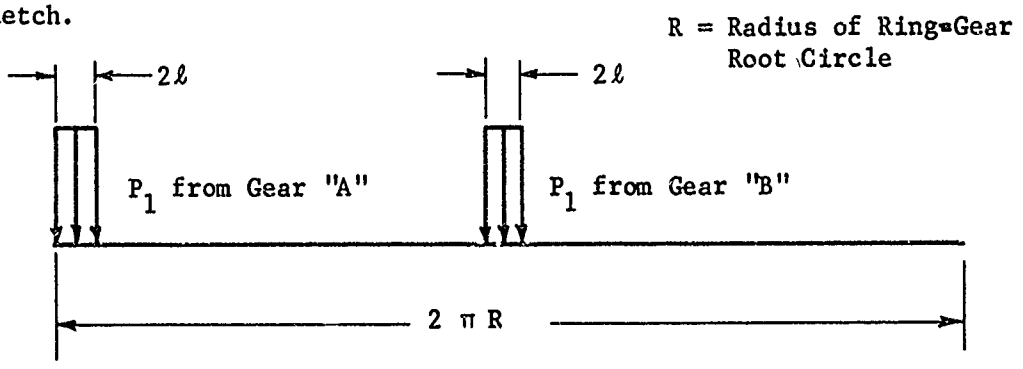

In order to facilitate a dynamic response analysis, the circumferential distribution is expressed in terms of a Fourier series. In this case the periodicity is πR, as can be seen from the preceding sketch.

Using Equations (25) and (26) and replacing L by $\pi R/2$, x by $R\theta$ and $\overline{f}$ by p_1, the following is obtained:

$$p_{AB}(\theta) = \frac{1}{2} a_o + \sum_{m=1}^{6} a_m \cos 2m\theta \tag{49}$$

where

$$a_m = \frac{2p_1}{m\pi} \sin 2m \frac{\ell}{R} \tag{50}$$

The series has been truncated at m = 6. The justification of so doing was given in Appendix I.

Similarly, for planetary gears C and D, the circumferential distribution of dynamic forces $p_{CD}(\theta')$ of Equation (48) can be expressed by

$$p_{CD}(\theta') = \frac{1}{2} a_o + \sum_{m=1}^{6} a_m \cos 2m\theta' \tag{51}$$

The a's are given by Equation (50).

From Figure 57,

$$\theta' = \theta - 91.343° \tag{52}$$

The following numerical values are computed:

$$a_o = \frac{2p_1}{\pi} \frac{2\ell}{R} = \frac{2 \times 96.5 \times 0.644}{\pi \times 10.86} = 3.65$$

$$a_1 = \frac{2 \times 96.5}{\pi} \sin \frac{0.644}{10.86} = 3.65$$

$$a_2 = 3.65$$

$$a_3 = 3.64$$

$$a_4 = 3.62$$

$$a_5 = 3.60$$

$$a_6 = 3.58$$

Now, knowing the Fourier coefficients a_o, a_1, a_2 ... a_6 and with ω = 1482 Hz, the dynamic response due to planetary gears A and B can be calculated. The dynamic forces as expressed by Equations (47) and (49) are used as input data to an MTI computer program. The computer program first calculates the dynamic response due to each Fourier component separately. The dynamic response due to gears "A" and "B" is then obtained by superimposing the responses of each individual component. The dynamic response due to gears "C" and "D" is obtained by the same procedure.

Let a general response function due to gears " A" and "B" be represented by

$$b_{AB}\ (\theta,\ z)\ \cos\ \omega t \qquad \text{(from gears "A" and "B")} \tag{53}$$

where b_{AB} (θ, z) is part of the print-out of the dynamic response program; for example, b_{AB} could be the normal displacement amplitude or the azimuthal (axial) displacement amplitude or the like.

Similarly, a general response function due to gears "C" and "D" can be written as

$$b_{CD}\ (\theta',\ z)\ \cos\ (\omega t - \Psi) \qquad \text{(from "C" and "D")} \tag{54}$$

The total of this general response function is the sum of the responses due to "A, B" and "C, D". Thus, in terms of an amplitude $b(\theta, z)$ and a temporal phase angle $\phi\ (\theta, z)$, the general response function is

$$b\ (\theta,\ z)\ \cos\ [\omega t + \phi\ (\theta,\ z)] = b_{AB}\ (\theta,\ z)\ \cos\omega t + b_{CD}\ (\theta',\ z)\ \cos\ (\omega t - \Psi)$$

Thus,
$$b(\theta,\ z) = \left\{[b_{AB}\ (\theta,\ z) + b_{CD}\ (\theta',\ z)\ \cos\ \Psi]^2 + [\ b_{CD}\ (\theta',\ z)\ \sin\ \Psi]^2\right\}^{\frac{1}{2}} \tag{55}$$

$$\phi\ (\theta,\ z) = \text{Arc tan}\left[\frac{-\ b_{CD}\ (\theta',\ z)\ \sin\ \Psi}{b_{AB}\ (\theta,\ z) + b_{CD}\ (\theta',\ z)\ \cos\ \Psi}\right] \tag{56}$$

The phase angle $\phi\ (\theta, z)$ is the temporal phase advance relative to planetary gear "A".

APPENDIX III
ACOUSTIC POWER GENERATED BY A VIBRATING SURFACE

A surface vibrating in a fluid medium emits sound. The acoustic power that is transferred to a medium by a vibrating surface depends on the physical characteristics of the medium, the oscillatory volume displacement of the fluid caused by the vibrating source, and the size and shape of the generator. The acoustic power generated by a vibrating surface can be expressed by (page 3-118 of Reference 6)

$$P = U^2 R_A \times 10^{-7} \text{ watts} \tag{57}$$

where U = rate of volume displacement of fluid (cc/sec)

R_A = acoustic radiation resistance seen by source (acoustic ohms)

Let the amplitude of the oscillatory displacement of an area element dA be W, and the frequency be ω throughout the area A at a particular mode. Then,

$$U = 2\pi \omega \iint_A W \, dA = 2\pi \omega \bar{W} A \tag{58}$$

where

$$\bar{W} = \frac{1}{A} \iint_A W \, dA \tag{59}$$

= Average displacement amplitude

The acoustic radiation resistance R_A depends on the size and shape of the generator. Two typical shapes are discussed in Reference 6: (1) pulsating sphere and (2) vibrating piston. In both cases,

$$R_A = K \frac{\rho C}{A} \quad \text{if } \frac{D}{\lambda} \geq 1 \tag{60}$$

where ρ = density of medium (gm/cc)

C = velocity of sound in medium (cm/sec)

D = diameter of sphere (or piston) (cm)

$\lambda = \frac{C}{\omega}$ = wave length (cm)

ω = frequency (Hz)

K = a numerical factor

The numerical factor K is equal to unity when $D/\lambda \geq 1$, i.e., in the high frequency range (see Figure 3i-1 of Reference 6). In the lower frequency range, K is less than 1. To make an estimate of the value of K at low frequency from the gearbox noise standpoint, take the fundamental frequency of the CH-47 upper planetary meshing, 406 Hz for example. The wave length

$\lambda = C/\omega$ is approximately 75 cm or 30 in. Suppose that the diameter of the ring gear is taken as D. Then, $D/\lambda = 22/30 = 0.73$. According to Figure 3i-1 of Reference 6, K = 0.85 for a spherical source, and K = 1 for a vibrating piston. It is therefore concluded that the value of K is not far from unity. For acoustic power computation, set

$$K = 1 \tag{61}$$

Using Equations (58), (60) and (61), Equation (57) can be written as

$$P = \omega^2 \bar{W}^2 \; A \; (2\pi)^2 \; \rho C \times 10^{-7} \tag{62}$$

where P = acoustic power (watt)

ω = frequency (Hz)

$\bar{W}$ = average displacement amplitude (cm)

A = area (cm^2)

ρ = density of medium (gm/cc)

C = velocity of sound in medium (cm/sec)

For helicopter noise, the medium is air, with $\rho = 0.00122$ gm/cc and C = 33,700 cm/sec. Thus,

$$P = 1.62 \times 10^{-4} \; \omega^2 \; \bar{W}^2 \; A \text{ (watt)} \tag{63}$$

Choose a reference acoustic power of 10^{-12} watt. Then a power level in db can be defined as

$$L_{power} = 10 \log_{10} \frac{P}{10^{-12}} \text{ (db)} \tag{64}$$

where L_{power} = power level (db)

P = acoustic power (watt)

For a point source, the power level is related to the sound pressure level measured at a distance r by

$$L_{power} = L_{s.p.} + 20 \log_{10} r + 11 \tag{65}$$

where L_{power} = power level (db)

$L_{s.p.}$ = sound pressure level (db)

r = distance from the source at which $L_{s.p.}$ is measured (meter)

The reference for the power level is 10^{-12} watt, and the reference for the sound pressure level is 0.0002 microbar.

At approximately r = 1 ft = 0.305 meter, Equation (65) reduces to

$$L_{power} \simeq L_{s.p.} \tag{66}$$

Thus,

$$L_{s.p.} \simeq L_{power} = 10 \log_{10} \frac{P}{10^{-12}} \quad (db) \tag{67}$$

Therefore, the sound pressure level measured at 1 foot from a point source is approximately equal to the power level, both in units of db. Equations (65), (66), and (67) are valid only for a point source. In applying Equations (65), (66), and (67) to the noise generated by ring-gear casings, a geometrical configuration factor should be introduced to take into account the casing geometry. However, this factor is neglected in the sound pressure level calculation for simplicity.

APPENDIX IV
SUMMARY OF EXISTING HELICOPTER INTERNAL ACOUSTIC DATA

During the investigations reported in References 1 and 2, it became apparent that detailed information would eventually be required to determine conclusively the exact sources, and their relative importances, of the noise found within operating UH-1D and CH-47 helicopters. Such a determination is considered essential to a clear understanding of the character of the internal noise, upon which depends the ultimate goal of achieving lower helicopter internal noise levels through drive train component design-level efforts. Helicopter internal noise is proving, as the more advanced real-time, narrow-band data reduction techniques are brought to bear upon it, to be composed of several very sharp noise spikes, located precisely at the known gearbox mesh frequencies and their higher multiples, superimposed upon generally acceptable background noise levels. For instance, narrow-band reductions of the CH-47 internal acoustic data presented in [4] indicate severe noise peaks which may reach sound pressure levels of 100 to 110 db superimposed upon background levels of generally 80 to 90 db.

When this portion of the investigation was formulated, several organizations were known to have extensive data records of internal noise levels measured in CH-47 and UH-1D helicopters. In order to prevent needless duplication, it was felt that future noise measurements should be conducted only after a survey had been made to determine the extent of existing data and, more important, the bandwidths used in its reduction. Thus, the Vertol Division - Boeing Company, Philadelphia, Pennsylvania; the Bell Helicopter Company, Fort Worth, Texas; and the U.S. Army Aeromedical Research Laboratory, Fort Rucker, Alabama, were contacted and visited to discuss the detail and type of existing data. It is believed that the data available at these organizations are the most complete and extensive available at the present time for the CH-47 and UH-1D helicopters.

A considerable amount of CH-47 internal noise data is available at the Vertol Division - Boeing Company. These data, which date back to the early 1960's, were recorded on magnetic tape, and exist for various aircraft configurations and operating conditions and for a considerable number of recording locations within the aircraft. Data reduction to date has been largely by full-octave and one-third-octave methods, although a limited amount has recently been reduced by real-time, narrow-band techniques. Considerable thought has obviously gone into the selection of data recording locations. While it is not immediately clear what percentage of this existing data will be directly useful in future noise reduction programs, it is felt that this extensive body of data and the experience of Vertol personnel must be considered as important sources of information during the planning and implementation of future CH-47 interior acoustic and vibration measurements.

With regard to UH-1 internal noise measurements, a considerable quantity of data is available at the Bell Helicopter Company, Fort Worth. These data, which also date back to the early 1960's, were entirely recorded on magnetic tape. They exist for various aircraft configurations and operating

conditions, and for a number of recording locations within the aircraft. Data reduction to date has apparently been primarily by the full-octave method, although a certain amount of data has been reduced by narrow-band analysis by means of tape loops. While it is not immediately clear how much of these existing data will be of direct use in future noise reduction programs, it is felt that these data and the experience of Bell Helicopter personnel must be considered as important sources of information during the planning and implementation of future UH-1D interior acoustic and vibration measurements.

In addition to the data discussed above, an important body of CH-47 and UH-1D interior acoustic data may also be found at the U.S. Army Aeromedical Research Laboratory, Fort Rucker, Alabama. These data, which have been recorded during recent years [4,7], are available on magnetic tape for various aircraft operating conditions and for several recording locations within the aircraft. Data reduction has been by octave-band analysis and, more recently, by the real-time, narrow-band technique with a filter bandwidth of 20 Hz. Four narrow-band spectra which were produced in a recent analysis by the author of Reference 4 are shown in Figures 59, 60, 61, and 62. These data were recorded along the centerline of a CH-47C helicopter, with the microphone held at about head height for a standing man. Station number denotes axial distance, in inches, aft of the nose of the aircraft. Superimposed by the authors above each of these figures is a diagram showing the mesh frequencies of the CH-47 forward rotor-drive gearbox for the operating conditions specified. Note the <u>precise</u> correspondence between each major noise peak and a known mesh frequency. It is felt that the detail shown in Figures 59-62 approaches that required in future acoustic technology development measurements. It should be stressed, however, that the noise data shown in these four figures are <u>not</u> to be interpreted as being representative of the acoustic levels which exist in all CH-47C helicopters. In addition, these data must not be construed as being the ultimate in terms of the amount of engineering information which may be extracted. Narrower bandwidths may be required, for example, to show the existence of side bands. These data are presented, however, to show the great increase in available information which results from narrow-band analysis. While octave-band, one-third-octave-band, and even one-tenth-octave-band measurements may be adequate for ear-protection purposes, they are decidedly inadequate for use in the development of noise-reduction technology.

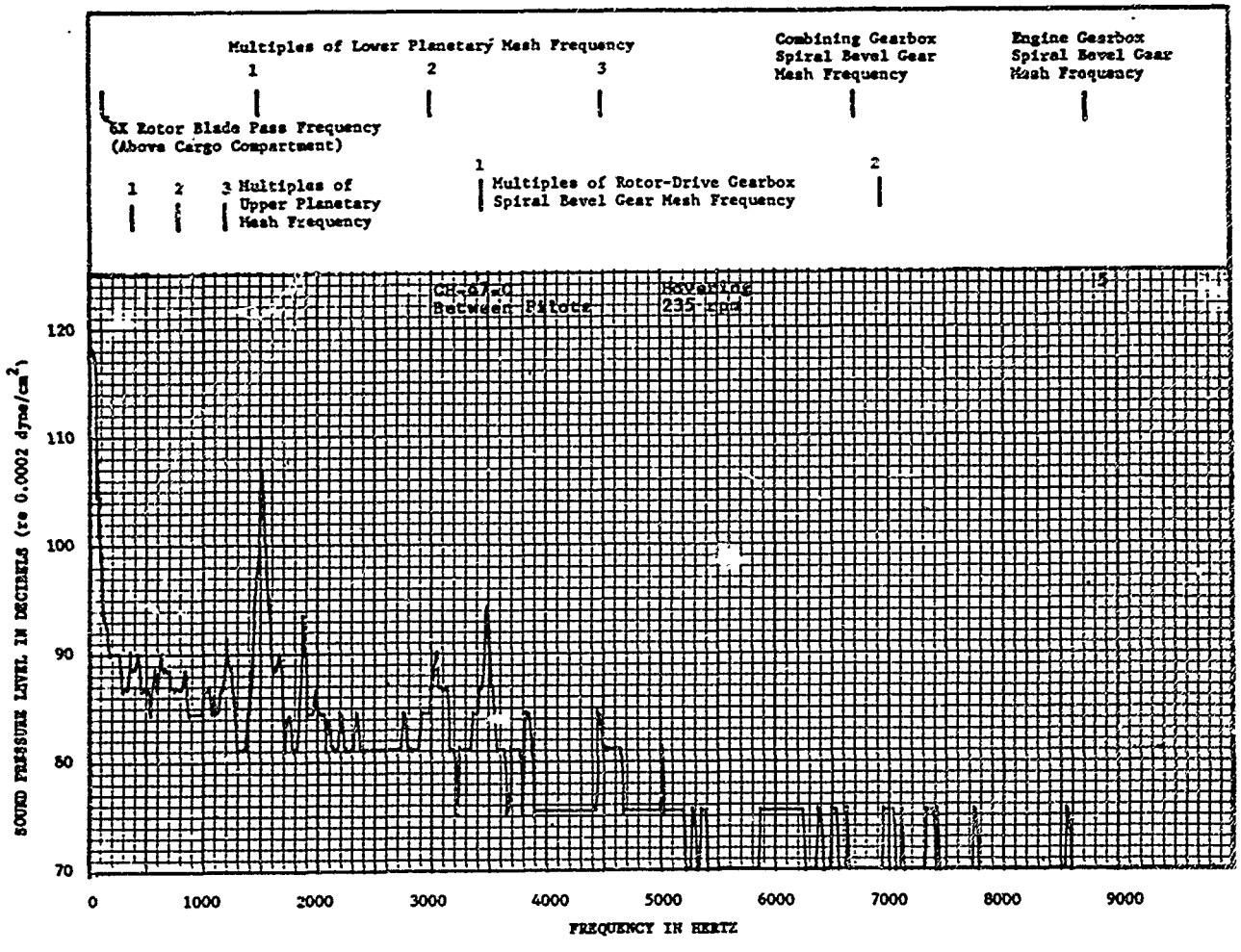

Figure 59. Measured Acoustic Spectrum Between Pilots in CH-47C Helicopter at Hover Condition With 235 RPM Rotor Speed (Courtesy of Mr. R. T. Camp, Jr., U.S. Army Aeromedical Research Laboratory - Ref. 4).

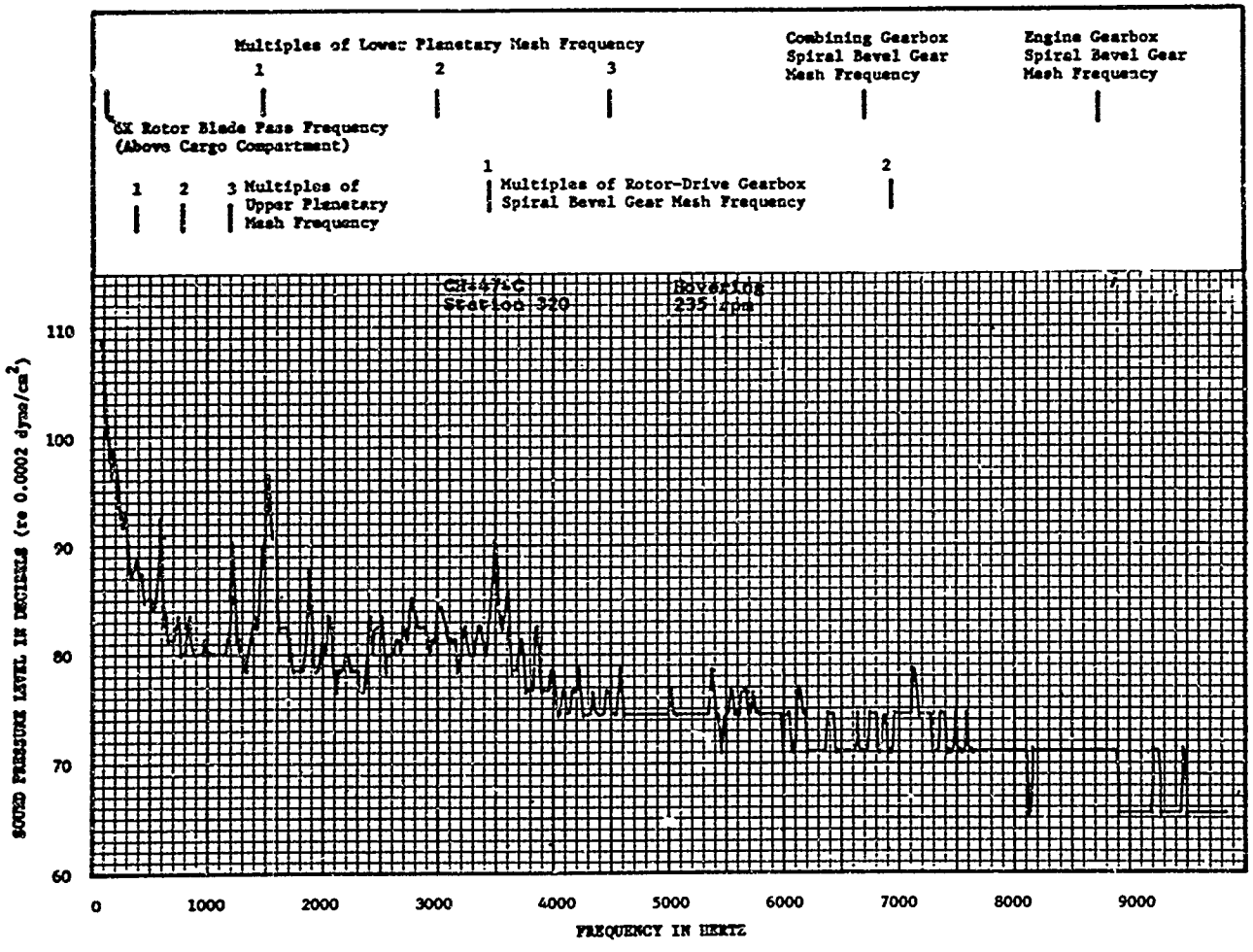

Figure 61. Measured Acoustic Spectrum at Station 320 in CH-47C Helicopter at Hover Condition With 235 RPM Rotor Speed (Courtesy Mr. R.T. Camp, Jr., U.S. Army Aeromedical Research Laboratory - Ref. 4).

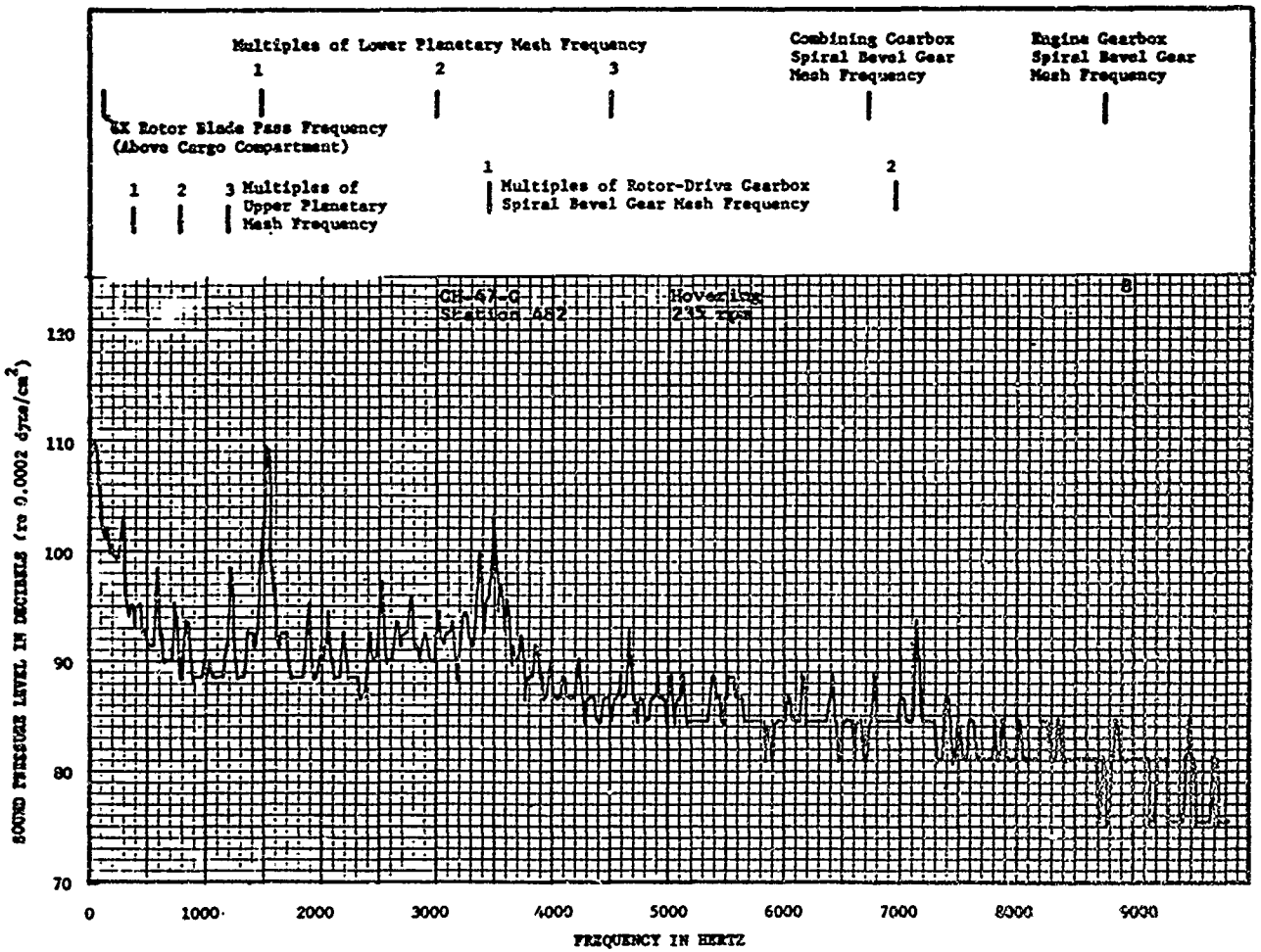

Figure 62. Measured Acoustic Spectrum at Station 482 in CH-47C Helicopter at Hover Condition With 235 RPM Rotor Speed (Courtesy Mr. R.T. Camp, Jr., U.S. Army Aeromedical Research Laboratory - Ref. 4).